

EVALUATION AND OPTIMISATION OF AIRFLOW DISTRIBUTION WITHIN A REFRIGERATED TRAILER

A thesis submitted for the degree of

Master of Engineering

By

LUGIEN A. JANSEN

B.Eng.

DEPARTMENT OF MECHANICAL AND INDUSTRIAL
ENGINEERING

GALWAY - MAYO INSTITUTE OF TECHNOLOGY, GALWAY,
IRELAND

Dr. P. Delassus
Head of Department



Dr. P. Delassus
Dr. J. Lohan
Dr. B.A. Regan
Supervisors

SUBMITTED TO THE GALWAY – MAYO INSTITUTE OF TECHNOLOGY,
GALWAY, IRELAND, SEPTEMBER 2006

Declaration

I declare that this thesis was composed by myself, that the work contained herein is my own except where explicitly stated otherwise in the text, and that this work has not been submitted for any other degree of professional qualification.

Galway 29th September 2006

A handwritten signature in black ink, appearing to read 'Lugien A. Jansen', written in a cursive style.

Lugien A. Jansen

Table of contents

I	LIST OF FIGURES	VI
II	LIST OF ABBREVIATIONS	XI
III	PREFACE	VI
IV	ACKNOWLEDGEMENTS	XIII
V	ABSTRACT	XIV
	CHAPTER 1 INTRODUCTION	15
	CHAPTER 2 LITERATURE REVIEW	20
2.1	MOBILE REFRIGERATION	20
2.2	THE REFRIGERATED TRAILER	22
2.3	EXPERIMENTAL FLUID DYNAMICS IN REFRIGERATED TRAILER	35
2.4	FLOW VELOCITY MEASUREMENT	38
2.5	ILLUMINATION TECHNIQUES	45
2.6	VISUALISATION	51
2.7	ACQUISITION AND IMAGING PROCESSING	56
2.8	AIR FLOW OPTIMISATION IN TRAILERS	65
	CHAPTER 3 DEVELOPMENT OF THE SCALED MODEL	70
3.1	SCALING DOWN OBJECTS	71
3.2	DEVELOPMENT OF THE SCALED TRAILER MODEL	82
3.3	THE PROPULSION SYSTEM	98
3.4	SPEED OF THE PUMP	103
3.5	SCALING THE CARGO	104
	CHAPTER 4 DEVELOPMENT OF MEASUREMENT EQUIPMENT	106
4.1	GENERAL	106
4.2	VISUAL ACQUISITION OF THE FLOW	107
4.3	FLOW VISUALISATION	115
4.4	ANALYSIS OF THE ACQUIRED DIGITAL IMAGES	122
4.5	CREATING THE PROGRAM	125
4.6	RESULTS OF THE PROGRAM	143
4.7	RECOMMENDATIONS ON THE SOFTWARE	144

CHAPTER 5 RESULTS OF EXPERIMENTAL AND NUMERICAL ANALYSIS	146
5.1 GENERAL	146
5.2 VISUAL FLOW ANALYSIS OF THE SIMULATION TANK	146
5.3 FLOW MEASUREMENTS	150
5.4 EFFECT OF LOADING/UNLOADING	155
5.5 COMPUTATIONAL FLUID DYNAMICS	160
5.6 ADDITIONAL WAYS TO IMPROVE THE AIR FLOW	166
CHAPTER 6 CONCLUSIONS AND RECOMMENDATIONS	168
6.1 CONCLUSIONS	168
6.2 RECOMMENDATIONS FOR FUTURE WORK	172
REFERENCE	168
BIBLIOGRAPHY	182
APPENDIX	187

“The farther backward you can look, the farther forwards you are likely to see”

(Sir Winston Leonard Spencer Churchill, 1874-1965)

I List of figures

Figure 2-1: Truck with the cargo space on a separate trailer chassis.....	23
Figure 2-2: Truck with the cargo space is part of the truck chassis.....	23
Figure 2-3: schematic representation of airflow around cargo [9].....	25
Figure 2-4: Cargo spacers used to allow for the air to flow around [].....	27
Figure 2-5: Heat transfer in a properly loaded refrigerated trailer [9].....	27
Figure 2-6: Heat transfer in an improperly loaded trailer [9].....	28
Figure 2-7 Heat transfer in a badly loaded refrigerated trailer [9].....	28
Figure 2-8: Schematic overview of dimensions inside a refrigerated trailer	31
Figure 2-9: 33-euro pallet configuration	32
Figure 2-10: 33-euro pallet configuration	32
Figure 2-11: 32-euro pallet configuration	32
Figure 2-12: 32-euro pallet configuration	32
Figure 2-13: 32-industrial pallet configuration	32
Figure 2-14: Ribbed floors to improve returning airflow	33
Figure 2-15: Categories based on Newton's law [].....	36
Figure 2-16: Schematic representation of a PIV/ PTV system	40
Figure 2-17: Schematic of a LDA system (source: Dantec Dynamics 1999).....	42
Figure 2-18: Schematic of a CTA system (source: Dantec dynamics).....	44
Figure 2-19: Schematic working of a pitot tube.....	45
Figure 2-20: Relative intensity distribution of a single laser beam	46
Figure 2-21: Relative intensity distribution of a single laser diode light sheet [30] ..	48
Figure 2-22: Relative intensity distribution of a laser light sheet [30]	49
Figure 2-23: Schematic layout of a hydrogen bubble generator.....	54
Figure 2-24: The two-frame PTV using the matching probability	62
Figure 2-25: Duct fitted to TK refrigeration unit	66

Figure 2-26: The end of the duct.....	66
Figure 2-27: A bulkhead fitted in a refrigerated unit.....	67
Figure 3-1: The effect of changing the length-scaling factor.....	74
Figure 3-2: The effects of changing the viscosity.....	76
Figure 3-3: General dimensions of a refrigerated trailer.....	82
Figure 3-4: The view is obstructed by the frame.....	84
Figure 3-5: The use of a false floor solves the problem of the lost view.....	85
Figure 3-6: The frame of the simulation rig.....	85
Figure 3-7: Part of the tank analysed with the use of FEA.....	86
Figure 3-8: Constrains and mesh of the FEA model.....	87
Figure 3-9: Von Misses stress on the FEA model.....	88
Figure 3-10: 3 Dimensional deformation of the frame.....	88
Figure 3-11: Displacement along the “top bar” of the frame.....	89
Figure 3-12: Schematic representation of the refraction of light.....	91
Figure 3-13: Constrains on the 12 mm perspex sheet.....	92
Figure 3-14: Deformation of the 12 mm perspex bottom plane.....	92
Figure 3-15: The water tank with the cargo attachment points.....	95
Figure 3-16: Photograph of the 1/5 scaled test rig of a refrigerated trailer.....	96
Figure 3-17: Cross-section of the water tank.....	96
Figure 3-18: Cross-section of the tank with cargo.....	97
Figure 3-19: Performance curve of Wilo BN80/160-7.5/2.....	99
Figure 3-20: Reference numbers in the propulsion system.....	100
Figure 3-21: Speed drive control box used to control the pump speed.....	103
Figure 3-22: Measured performance curve of the pump.....	104
Figure 4-1: Comparison of sensitivity of CMOS and CCD photonic sensors.....	108
Figure 4-2: Synchronisation between the camera and two laser pulses.....	110
Figure 4-3: Schematic representation of a camera.....	112
Figure 4-4: Geometry of the deformation of the image on the camera.....	112
Figure 4-5: The sinus curve of the power supply on 50 Hz.....	119
Figure 4-6: Flow visualisation with a Metal-Halide lamp.....	119
Figure 4-7: Metal-Halide lamp illuminating the particles in the tank.....	119
Figure 4-8: Histogram of intensity over an image.....	120
Figure 4-9: Tank set-up with the high-speed camera and optics.....	120

Figure 4-10: The 2mW laser used for initial laser tests	120
Figure 4-11: Laser diode	121
Figure 4-12: Nd:YAG laser.....	121
Figure 4-13: Original image Figure 4-14: Image enhanced by software	123
Figure 4-15: Some of the first successful PIV results in ideal circumstances	124
Figure 4-16: Frame of movie fragment used for developing the program.....	126
Figure 4-17: Result of the first calculation algorithm	127
Figure 4-18: Different intensities on every second line causing stripes	128
Figure 4-19: Frame after introduction of levelling algorithm.....	128
Figure 4-20: Schematic representation of equation 4-6	129
Figure 4-21: Schematic representation of equation 4-7	130
Figure 4-22: Explanation of the coordinate system and values V1 to V4	130
Figure 4-23: Averaging rules used to calculate corner values.	131
Figure 4-24: Original image.....	132
Figure 4-25: Re-created image.....	132
Figure 4-26: Original frame	133
Figure 4-27: Calculated background.....	133
Figure 4-28: 3D grey value plot original.....	133
Figure 4-29: 3D grey value plot calculated.....	133
Figure 4-30: Matrix used to identify the six positions	134
Figure 4-31 Possibility 1	134
Figure 4-32 Possibility 2	134
Figure 4-33 Possibility 3	134
Figure 4-34 Possibility 4	134
Figure 4-35 Possibility 5	134
Figure 4-36 Solution 1	134
Figure 4-37 Solution 2	134
Figure 4-38 Solution 3	134
Figure 4-39 Solution 4	134
Figure 4-40 Solution 5	134
Figure 4-41: Illustration of the method presented by S.J. Baek <i>et al.</i>	136
Figure 4-42: Preliminary Vector plot.....	138
Figure 4-43: The calibration grid as captured by the camera.....	139

Figure 4-44: Vector plot made over multiple frames.....	140
Figure 4-45: Vector plot of the whole trailer made over multiple frames	141
Figure 4-46: Example of vector plot	141
Figure 4-47: Velocity magnitude contour plot of a refrigerated trailer	142
Figure 4-48: Velocity magnitude contour plot of a refrigeration unit	142
Figure 5-1: Flow inside the tank (visual).....	147
Figure 5-2: Flow inside trailer, straight to the back (visual).....	147
Figure 5-3: Flow in a trailer with a refrigeration unit (top view).....	148
Figure 5-4: Vector plot of the front part of the trailer (vectors in m/s).....	151
Figure 5-5: Vector plot of the back part of the trailer (vectors in m/s).....	151
Figure 5-6: Distance the flow travels at 12.17 m/s	152
Figure 5-7: Distance the flow travels at 14.4 m/s	152
Figure 5-8: Distance the flow travels at 17.88 m/s.....	152
Figure 5-9: Distance the flow travels at 19.86 m/s	152
Figure 5-10: The estimated effect of air velocity.....	153
Figure 5-11: Measured values (red) versus simulation results (blue)(m/s)(front) ...	154
Figure 5-12: Measured values (red) versus simulation results (blue) (m/s)(back) ..	154
Figure 5-13: Cross-section of the simulation tank with the cargo restraints.....	156
Figure 5-14: shot of the flow beside the cargo with the velocity vectors plotted in.	157
Figure 5-15: Side view from the flow along the cross section of the trailer.....	158
Figure 5-16: Flow pattern as seen from the top of the trailer.....	158
Figure 5-17: Flow pattern with a bulkhead open on the top	159
Figure 5-18: Flow pattern with a bulkhead closed on the top.....	159
Figure 5-19: Vector plot of the velocity through the mid plane of the trailer.....	162
Figure 5-20: Path lines of the flow entering the trailer	163
Figure 5-21: Path lines indicating the flow returning to the refrigeration unit	164
Figure 5-22: Direction of the flow visualised in three different plans	165
Figure D-1: Tank with initial laser test set-up	D-1
Figure D-2: initial test run with air circulation	D-1
Figure D-3: Air bubbles circulating through the tank in initial test runs	D-1
Figure D-4:The attachment of the pump to the tank and the speed drive.....	D-1
Figure D-5: Simulation tank after the build is completed.....	D-2
Figure D-6: The simulation tank set-up	D-3

Figure D-7: A side view of the tank.....	D-3
Figure D-8: The height-speed camera.....	D-3
Figure D-9: The water pump assembly	D-3
Figure D-10: The controller for the laser as used in the project following up.....	D-3
Figure D-11: The back of the water tank	D-3
Figure D-12: The inside of the water tank	D-4
Figure D-13: Close-up of the bulkhead assembly	D-4
Figure D-14: The laser as used in the follow-up project.....	D-4

II List of Abbreviations

°C	Degrees Celsius	°C
°F	Degrees Fahrenheit	°F
A	Area	m ²
C _p	Thermal capacity	J/(kg°C)
F	Force	N
J	Joule	J
Nu	Nusselt number	h _a x/k
Pr	Prandtl number	C _p μ/k
Re	Reynolds number	ρVx/μ
t	Time	s
Δt	Time	s
u	Velocity	m/s
ν	Kinematic viscosity	m ² /s
W	Watt	J/s
φ	Shear strain	-
μ	Dynamic viscosity	kgm ⁻¹ s ⁻¹
τ	Shear stress	N/m ²

2-D Two-dimensional

3-D Three-dimensional

CFD Computation Fluid Dynamics

ELC Encapsulated Liquid Crystal

PIV Particle Image Velocimetry

PTV Particle Tracking Velocimetry

ID Inside diameter

OD Outside diameter

III Preface

This thesis contains original work, which has not been submitted or used for a degree at any other university,

The investigation was carried out in the Thermo King Research and Development Centre at the Galway production plant in Ireland and the Galway Mayo Institute of Technology, under the supervision of Dr. Patrick Delassus, Dr. Basil Regan and Dr. John Lohan.

This thesis mainly focuses on the development of a hydraulic test environment in order to show fluid simulations, which reflect airflow distribution in a refrigerated trailer. It includes early test results and recommendations to improve the airflow and to aid further research.

Lugien A. Jansen

June 2006

IV Acknowledgements

I would like to thank Dr. P. Delassus, Dr. B.A. Regan and Dr. J. Lohan, my supervisors, for their support, guidance, help and advice while this research was being conducted and this thesis being compiled. I would also like to thank Thermo King Europe Ltd, and all the divisions attached to Thermo king for the possibilities and opportunities to conduct this research and for making resources available to successfully conduct this work.

I would like to thank Thermo king for providing the co-funding for this project with Enterprise Ireland.

I would like to thank my parents for their support during this period of study. It would not have been possible to complete this thesis without this vital support.

V Abstract

Thermo King as a supplier of mobile refrigeration equipment is interested in more information about the airflow distribution inside a refrigerated trailer in various loading conditions to optimise the performance of the refrigeration units. A more efficient way and/or more uniform way of keeping the internal environment inside the refrigerated box at the required conditions will increase the quality of the cargo as well as causing less damage to the environment.

The objective of this project is to develop a testing environment that makes it possible to conduct airflow tests for the purpose of learning more about the internal airflow of a trailer. This test environment will be in the form of an hydraulic transparent test rig representing a scaled model of a refrigeration system. The test environment must be able to simulate multiple unit configurations in the form of different airflow volumes, and different configurations of air inlet and outlet positions. Different cargo configurations inside the trailer will be used to simulate different types of loads.

Secondly, advice and recommendations on the improvement of airflow as well as ideas for further research will be discussed. It is recommended that the project be continued by future researchers to obtain more extensive results from the simulation environment developed and created during this project. Real flow investigation and improvement in airflow distribution should be developed and tested to enable Thermo King to make a more efficient, competitive and more environmentally friendly refrigeration unit.

Chapter 1

Introduction

In the past most fruit and vegetables were sold canned, and fresh produce was only available during harvesting seasons. The transportation of fresh meat, eggs and vegetables involved the cooling of the cargo with dry ice and salt, this was only possible over short distances however. Malfunction of the truck meant the loss of the precious cargo, which was a regular occurrence.

This was changed after Frederick M. Jones invented a refrigeration unit that was small enough to fit on a trailer and that could stand the harsh conditions of the transportation. United States Thermo-Control Company was born, which was soon changed to “Thermo King”.

Mobile refrigeration had an immense impact on the food market. It was suddenly possible to transport fresh and frozen foods over distances of up to a thousand miles. This meant that fresh and frozen foods could be imported and exported to the country, and that they could be distributed to people everywhere on the continent. This was the reason that sprawling supermarkets soon replaced small stores, with a large variety of fresh foods and perishables, previously unavailable to most people.

Nowadays, according to research by the International Institute of Refrigeration (IIR, 1995), 47 million tonnes of perishable goods are exported each year. This includes transportation between different countries over long distances, of which 61% is transported by sea, 34% by land and 5% by air. Inter-continental transportation would far exceed this number, but there is no statistic data on this available. However, most of this type of transport would have been over land and especially road. A smaller part would have been transported by rail, rivers, and canals and also through the air.

Refrigeration is the process of lowering temperature and maintaining it for the purpose of chilling food or preserving temperature of sensitive goods. A refrigeration unit is used to create a temperature-controlled environment and therefore has the capability to retract heat from the controlled environment to maintain a tight temperature differentiation around the pre-described temperature (also called set point). Most refrigeration units have the possibility to heat the cargo as well as to cool it if necessary to deliver a total temperature controlled solution. Strict rules and recommendations apply to the variation of temperature and humidity of this environment, and there are different problems that can arise with the distribution of the air through the trailer.

The objectives of this project are to extend the knowledge accumulated from the mini-project already undertaken at Thermo King, USA [1], by;

1. Performing a more extensive literature review of airflow measurement and modelling techniques, air distribution systems and dynamic similarity,
2. Developing a method to simulate the airflow in a refrigerated trailer up to 16 m length through experimental or numerical analysis,
3. Validate and analyse the information acquired from the airflow simulations
4. Characterise the flow movement in the current trailer design as a function of different flow rates and cargo shape,
5. Identify different methods of improving the flow distribution and extract design guidelines to optimise flow distribution,

Simulation can be performed both theoretically and practically. This project focuses on the practical methods in the shape of a scaled model simulation, compared with real size trailer measurements. The reason for beginning with the practical application is that the theoretical application, usually in the form of “Computational Fluid Dynamics” (CFD), is very complicated, and the guarantee of a reliable result is small. Comparison between airflow measured values and CFD calculated flows performed in a cold store indicated a difference of 26% as reported in the paper “Analysis of the air flow in a cold store by means of computational fluid dynamics” [2]. Cemagref has conducted more numerical studies as published in the papers “Simplified modelling of air flows in refrigerated vehicles” [3] and “Numerical and

experimental study of airflow in a typical refrigerated truck configuration loaded with pallets” [4]. The system used modified algorithms to increase the accuracy of the CFD predictions and is validated with practical experiments to optimise simulation variables.

The aim of this project is to obtain some practical information about the flow regime. This will provide the opportunity to do a CFD model in a subsequent project using the test-rig data for validation.

Thermo King performed a thorough study with the use of computational fluid dynamics (CFD) on the effect of a chute in an empty and a loaded trailer. This analysis was performed with the expertise of the company Fluent Inc. in April 1999 and the publication called “Simulation of Air flow and Heat transfer in a Refrigerated Trailer” [5]. An addendum [6] was written in August of 1999. Fluent Inc. is the developer of the most widely used and best validated CFD software available. This project was conducted to optimise the design of a new air distribution “chute” and bulkhead.

Airflow distribution through a compartment is subject to research in areas other than refrigerated transport. Taking the example of an office, a scaled water model can be used which has the potential to determine the airflow in a real office. An example of this is published in the journal ‘Numerical Heat Transfer’ [7]. Ventilation flow was investigated with the use of numerical modelling, and validated with a 1/6 scale model of the test room. The parameters were determined according to Reynolds similitude. Quantitative analysis was performed with LDA equipment, and flow visualisation was obtained by injecting a fluorescent dye into the water stream. A rotating laser beam performed illumination. The conclusion after comparing the experimental results and numerical predictions is that the numerical results are sufficient for industrial purposes.

Problems arise however, with the measurement of the flow in a real-size (loaded) trailer due to dimensional restrictions. Measuring the airflow in a real-size trailer raises significant challenges. The main problem is that there is not much space in a refrigerated trailer for measurement equipment to be fitted. Furthermore due to the

size of the trailer it requires a significant amount of sensors to obtain detailed information. The sensors should not interfere with the flow. Suitable sensors for quantitative flow measurement are limited and expensive.

The development of a method to simulate the airflow in a controlled environment and the measurement of the airflow with the limited budget available are the two greatest challenges of the project.

The first of this thesis chapter on this thesis consists of an introduction. The second chapter of this thesis describes the background information on the topics related to all the aspects of this project in the form of a literature review. The literature review consists of a detailed description of the history of mobile refrigeration, progressing towards refrigerated trailers and the loading of different types of perishables in a trailer. It then describes current loading practice in the refrigerated transport market and the methods used to review and simulate those loading situations. The next section will do a thorough investigation in simulation practices, methods and the work done on simulations in a similar context. A review on methods to improve the airflow in refrigerated trailers is then conducted. The last part of this chapter will examine software suitable to be used in this project to aid in image recognition and flow calculation.

Chapter three focuses on the development of the test rig to conduct the airflow simulation. It will initially review the possibility and consequence of scaling the test object to determine the size of a simulation environment. A simulation medium is chosen after it is evaluated whether a fluid other than air could be used. After this evaluation the development of the simulation environment is reviewed. This part contains the main design considerations for the environment and the description of its development. The subsequent sections consider the simulation of the airflow through the simulation environment and the required velocity. This mainly consists of a review of the different propelling methods and the calculation of the required propelling speed for the different methods. The next section reviews the possibility of simulating cargo and the different methods and materials required to do so. It describes the challenges of shaping, assembling and attaching the cargo in the simulation environment. The final chapter examines the methods of running and

controlling the whole simulation and the need for an automated system with respect to performance, health and safety.

Chapter four describes the fluid flow analysis methods developed during the course of the project. The first section reviews methods of the visual analysis of the flow, providing detail on methods to capture the flow images and a review of high-speed cameras available for this challenge. The second section deals with the flow visualisation aspect of the analysis. There are different methods to visualise fluid flow, and this section reviews the most suitable methods for this project. A description of the analysis of the acquired images follows. This includes ways to deal with the images as well as the development of a suitable mathematical algorithm to analyse the images. The development of the program to conduct the analysis will then be described. This software code will analyse the images and visualise the results on the screen. The program consists of multiple modules, with some parts written in the mathematical analysis software, Matlab, and other written in the much faster programming language, Fortran. All the modules can be controlled from one script in Matlab. The final section consists of an overview and recommendations for future research.

The results of the experiments are discussed in chapter five. The chapter initially discusses the visual analysis of the flow. This analysis was carried out at a time when the analysis software was not yet functioning. This section describes the measurement of the flow using the flow analysis tools developed during this project on an empty trailer. The results are visualised and discussed with a view to being used in future projects. The validity of the experiments is established to ensure trustworthy results have been obtained. This confirmation takes the form of an airflow test performed in a refrigerated trailer equipped with a Thermo King refrigeration unit.

The final chapter consists of a general overview and conclusions drawn from the project. The development of the measurement system and the analysis of the airflow are discussed. The progresses achieved as a result of the project along with a general overview and conclusion are then presented.

The list of references and the appendices can be found at the end of the thesis.

Chapter 2

Literature Review

This chapter will describe the current state of art and the information published on the topic of airflow in a refrigerated trailer as well as fluid dynamics simulations, measurement methods and other background information relevant to this project.

2.1 *Mobile refrigeration*

2.1.1 Introduction to the history of refrigeration

Refrigeration is a process widely used to lower temperature in a closed environment and is nowadays found in anything from an air-conditioned car to a warehouse with frozen foods.

Refrigeration is a process in which heat is moved from one environment to another by means of a transportation medium, commonly called a refrigerant. An American working in Britain named Jacob Perkins discovered the cooling effect of certain liquids when they evaporate and invented the refrigeration cycle in 1834.

Not knowing about the invention of Jacob Perkins, John Harrison, a Scottish printer living in Australia, discovered the cooling effects also. He used ether to clean metal printing type and discovered the cooling effect of the substance while using it.

In 1862 Perkins started his first refrigeration company in a Brewery in Bendigo, Victoria in 1879; refrigeration did not come into homes on a large scale until refrigeration became electric in 1920.

It was, however, 1938 before the first mobile refrigeration unit was built [8]. There had been attempts to cool trucks in earlier times, but the unit usually fell apart due to the jarring and jolting of the truck as the first refrigeration units were very fragile and difficult to operate. The refrigeration units mainly ran on electrical power, which was not available on trucks. In 1938 however, Frederick McKinley Jones developed the

first working mobile refrigeration unit. His refrigeration unit became a great success, and it was patented. Joe Numero founded the '*United States Thermo-Control Company*', which soon became '*Thermo King*', which changed into the Thermo King Cooperation of today.

Mobile refrigeration opened the market for the transportation of perishable foods such as fruit, vegetables and meat. In the early days, most of these products were canned or alternatively, fresh produce was transported over short distances with the use of a lot of dry ice. A huge risk, however, was that the truck would break down during transport, the ice would melt and that the cargo would be spoiled. Other techniques for food preservation were drying, smoking, pickling or salting, but these techniques had the disadvantage of severely changing the appearance and taste of the food and only worked with specific types of food for a limited time period.

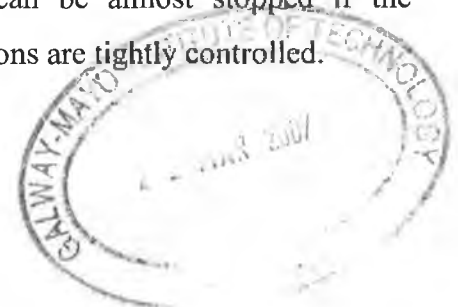
The invention of mobile refrigeration changed all of this. Grocers quickly realised the advantage of this invention where a fresher and greater variety of perishable foods became available everywhere. The market for mobile refrigeration was born.

2.1.2 Storing and moving perishable foods

Refrigeration used for the preservation of perishable commodities, particularly foodstuffs, is historically the most common application. Cooling or freezing foods slows the aging process of perishable foods and makes it possible to store them for longer.

From a commercial point of view the perishable food must be stored, transported and offered to the customers with minimal loss of quality and freshness. This requires the need for climate control systems that guarantee the optimal environmental conditions during the whole product cycle to ensure the quality of the food stays at the level acceptable to the public.

The quality of food worsens over time because of the ageing process of food caused by ripping, metabolic changes, moisture loss and aging due to bacterial activity. These unwanted processes are slowed down or can be almost stopped if the temperature is low enough and environmental conditions are tightly controlled.



Factors that are important during storage and transportation are:

- Temperature
- Relative humidity
- Air circulation
- Sanitation and air purification

It is important to stringently keep with the recommended temperature variations in order to guarantee quality during transportation. Damage from chilling or freezing should be prevented at all times.

Air circulating prevents hot or cold spots and hinders the build up of ethylene gas, which is a result of ripening of the produce, in the cargo. This project will focus on the air circulation around the product to improve the quality of refrigeration and reduces deterioration of the produce transported.

2.2 The refrigerated trailer

2.2.1 Transportation containers

There are different sizes of containers to move refrigerated cargo from one location to another. These include trailers, trucks and isolated sea containers. These various means of cargo transport need different kinds of refrigeration units to keep the internal environment temperature controlled. This project will mainly focus on the application of the trailer, even though truck and isolated sea containers are very similar to the internal configuration of a trailer.

A typical trailer can be considered as an independent chassis pulled by a truck as seen in Figure 2-1. The cargo area stretches the whole length of the body, and the trailer is isolated to prevent unnecessary energy losses. Refrigerated trailers usually have the refrigeration unit on the front of the trailer or in some cases fixed underneath the trailer.

The air is sucked out of the cargo compartment and goes through the evaporator inside the unit before it is blown back to the refrigeration unit, which is mounted on front. The main focus of this current project will be centred on this application.



Figure 2-1: Truck with the cargo space on a separate trailer chassis

Isolated sea containers have the same layout and roughly the same dimensions as trailers, whereas a refrigeration unit is mounted on the front of the container.

A truck may be considered as a single chassis where the cargo compartment and the truck are one vehicle as shown in Figure 2-2. In the case of a refrigerated truck the refrigeration unit is mounted in front of the isolated cargo space usually above the driver's cabin. In cases where the truck has a trailer the refrigeration unit is mounted under the chassis and is called an under-mount. A remote evaporator is used in the case of an under-mount, where the evaporator is attached to the unit, but the evaporator is completely inside the cargo compartment in the case of a unit mounted above the driver's cabin.



Figure 2-2: Truck with the cargo space is part of the truck chassis

The use of walls or different levels of loading can divide the cargo space into multiple sections so as to create multiple temperature-controlled environments that can be maintained at different temperatures.

2.2.2 Dimensions of a refrigerated trailer

Regulations concerning the dimensions of a trailer vary somewhat depending on the part of the world it is in. The external dimensions of European trailers are determined by European Union regulations and are the same for all trailers in operation today. In the European Union, the maximum length of a trailer must not exceed 14 metres whereas in the United States the regulation demands that it does not exceed 16 metres.

The project focuses on the European market. Although the outside dimensions are fixed, the inside dimensions of European trailers vary from manufacturer to manufacturer because the thickness of the wall and of the isolation foam vary.

Typical inside dimensions for European trailers are:

- Inside length: 13365 mm
- Inside width: 2495 mm
- Inside height: 2600 mm

The length of the trailer used in the United States ranges from 20 to 53 feet. The most commonly used trailer in the United States is the 14.63 m (48-foot) and 15.84 m (52 foot) trailer. The widths of these trailers are 2438.4 mm and 2590.8 mm respectively, which results in 114.3 mm to 254 mm less width in the internal dimension because of the isolation foam. The height is usually 2895 mm.

2.2.3 Airflow in a refrigerated trailer

The airflow through the trailer is schematically shown in Figure 2-3. The air is blown out of the refrigeration unit and circulated around the inside of the cargo after which it returns to the refrigeration unit to be recycled.

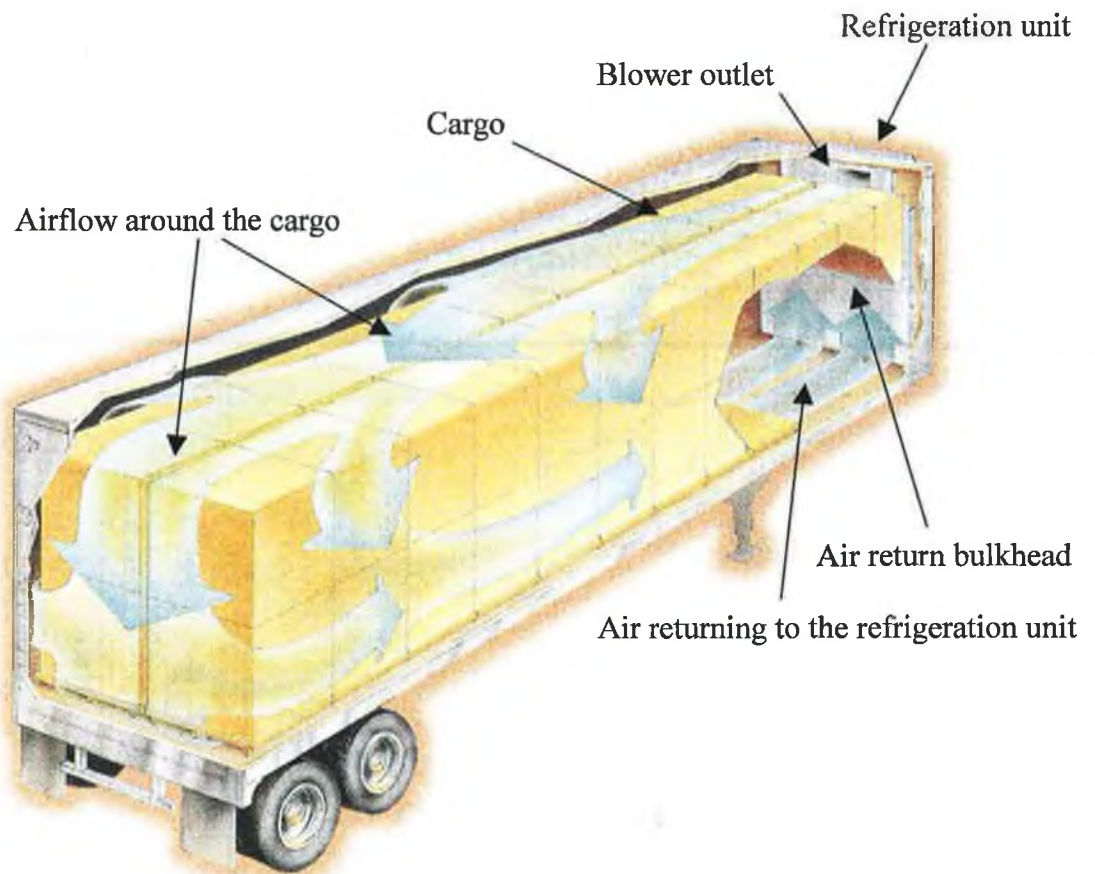


Figure 2-3: schematic representation of airflow around cargo [9]

The refrigeration unit provides the cold air (assuming cooling mode) and distributes this throughout the cargo area. The temperature of the return air is measured to control the performance of the unit. Most units have the option of operating at different speeds according to their cooling requirements. The air is forced over and partly through the cargo to return down along the back and then along the floor to the refrigeration unit where the heat is removed to the outside environment. In order to allow airflow around the back and to prevent pressure build-up or airflow stagnation, a gap of at least 4 cm should be maintained. A gap of 3 cm should permit approximately 20% of the air to flow along the sides of the cargo. This is needed to absorb the heat coming from the walls due to the thermal energy coming in from the outside environment.

The air is usually returned to the unit with the use of a bulkhead. This bulkhead has openings for the air at floor level, helping the airflow to go around the cargo. The bulkhead helps against any potential short-circuiting of the air and helps prevent the

airflow coming out from the unit outlet but flowing prematurely back into the inlet and thereafter to the evaporator.

2.2.4 Heat convection in refrigerated trailers

There are two types of convection that occur in refrigerated trailers. The first one is natural convection, which is the natural heat transfer between objects and a fluid: for example from the outside of the trailer, through the wall, to the inside. Another good example of natural convection is a radiator in a house.

The second type of convection is forced convection. This is convection caused by the airflow flowing through the trailer, as discussed above or, for example, the airflow around the trailer when the trailer is pulled along the road, or standing in a windy location.

Both types of convection are found in this application. Air circulation is not everywhere within the trailer; an example of this would be that there is no circulation inside the cargo boxes where there is no forced air movement.

2.2.5 Loaded trailers

Loading a trailer correctly is the most important factor with respect to the performance of the airflow. A badly loaded trailer will stagnate the flow to the back giving a short-circuit situation in which the air does not go to the back of the trailer, but rather takes the easiest path from the back to the front. That is why it is important that there is at least 4 cm of space between the back (doors) of the trailer and the cargo to leave a low resistance path for the air. At least 10 cm of space should be maintained for the incoming air at the top of the cargo for the same reason. In practice, however, a 30 cm gap is usually dictated and marked with a red line in the trailer, leaving the air-outlet unblocked.

To make sure that the 3 cm of space between the walls and the cargo and 4 cm space at the back is maintained during transport, spacers are put between the cargo and the wall. This can be seen in the schematic picture Figure 2-4.

More information can be found in paragraph 2.2.8, which focuses on loading patterns.

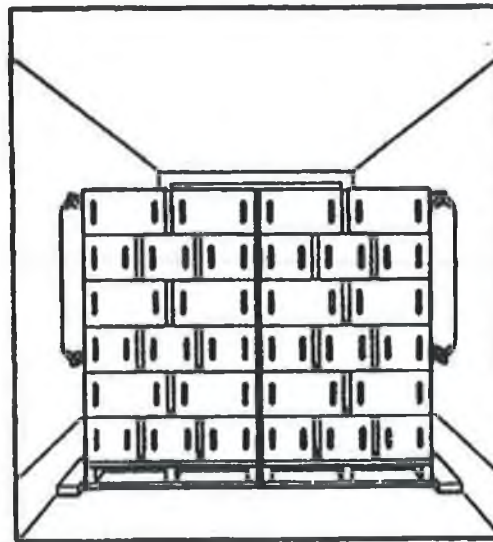


Figure 2-4: Cargo spacers used to allow for the air to flow around [9]

Figure 2-5 shows a correctly loaded trailer. The air coming from the refrigeration unit keeps the internal temperature in the cargo compartment steady, and all the heat that is comes from the hot ambient air is transported to the refrigeration unit and thus transported outside.

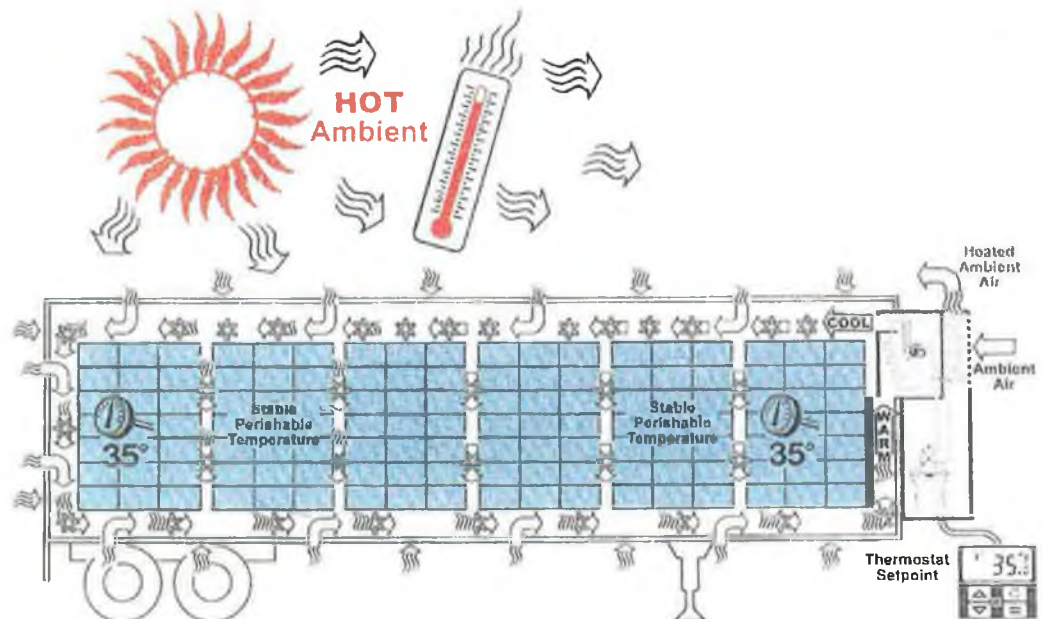


Figure 2-5: Heat transfer in a properly loaded refrigerated trailer [9]

Figure 2-6 however shows a unit where the air does not go to the back of the trailer due to a high flow resistance. The result is a short circuit flow, where the air does not travel to the back, but takes the way of the least resistance. The result is that the trailer is not properly cooled at the back, and that the heat coming from the cargo and from the outside ambient air is not transported out.

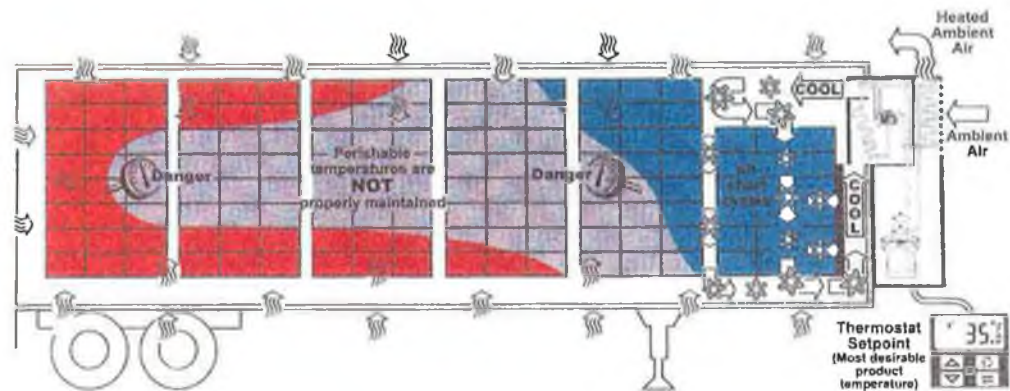


Figure 2-6: Heat transfer in an improperly loaded trailer [9]

Figure 2-7 gives a schematic view of a trailer where there is a lot of space above the cargo, and where there is not a lot of space at the back. Here the air takes a short cycle as well since it is the way of the least resistance; hence the back of the trailer heats up.

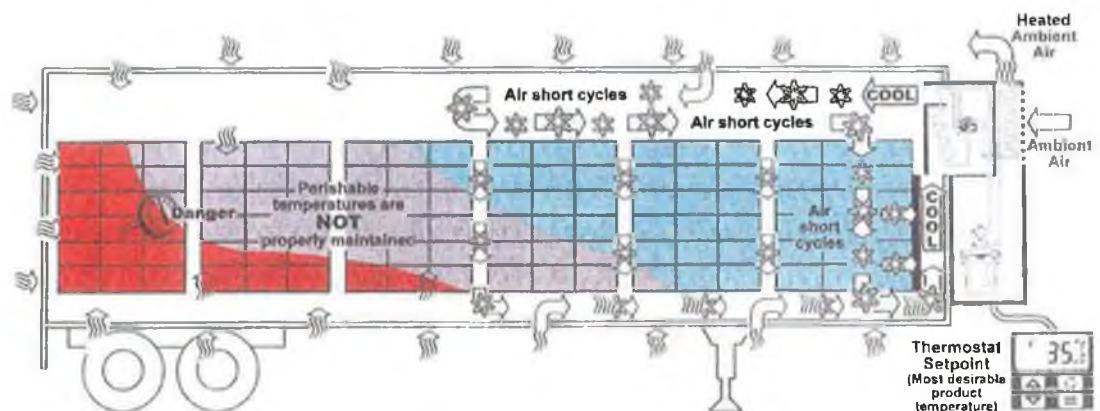


Figure 2-7 Heat transfer in a badly loaded refrigerated trailer [9]

The above figures give an example of correctly and incorrectly loaded trailers, indicating areas of research that could be further examined.

2.2.6 Publications on temperature distribution in cold stores

Papers have been published on the subject of temperature distribution in cold stores. These papers have proved very helpful on the topic of airflow distribution in temperature-controlled environments. One of the publications “Temperature monitoring and modelling of chilled food in the cold chain” [10] is a French-Czech research project investigating different stages of the cold chain in which temperature modelling and monitoring was compatible with calculated and measured values. Results of this study can be used to evaluate results acquired in this project.

The paper “Simulation and measurement on the full-load performance of a refrigeration system in a shipping container” [11] describes a mathematical model developed to simulate a refrigerated trailer. It is being compared with the results of a full size container in a temperature-controlled environment and results were validated. The airflow model used can be useful if mathematical or numerical modelling is employed in this project.

Different types of cargo have different demands for airflow. Frozen foods for example must be stored in closed boxes and do not need constant air circulation, where as fresh fruits and vegetables need constant air circulation to remove the heat of respiration. J. Moureh at al. [12][13][14] did a significant amount of research on local temperature differences in and around cargo piled on pallets in small containers or under isolation covers.

An example of research on the airflow system itself was published at the 20th IIR meeting, entitled “Air distribution design for controlled atmosphere in reefer cargo holds” [15]. This paper focuses on the challenge of providing proper air distribution in order to achieve uniform temperature conditioning throughout the cargo. The focus is on the effects of usage or non-usage of crating for air distribution, and the effects and orientation of pallets and equipment in order to influence the airflow at different airflow velocities. Tests were performed in a test rig with 18 pallets loaded with banana boxes. The conclusion was that the uniformity of the airflow distribution was poor in all the tests performed, even when airflow aids were added.

2.2.7 Cargo carriers

Pallets are the most common means of holding cargo. Pallets have the advantage of leaving space for the airflow to move under the cargo. In the absence of pallets a T-ribbed floor needs to be used, as illustrated in paragraph 2.2.9. Depending on the commodity and area of production, 75 to 90 percent of fresh fruit and vegetables are now placed on pallets and slip-sheets.

Different dimensions of pallets, however, are used throughout the world. Block-style 1200 x 1000 mm pallets are standard in European pallet pools and can be used for any exports to Europe. The Euro pallet, 1200 x 800 mm, is popular in some European countries. The popularity of the Euro pallet is increasing because it allows for a maximum of 33 pallets in a European trailer, which is the most efficient use of the available space. The 1200 x 1000 mm pallets will fill a European trailer with 26 pallets. This is also called the industrial pallet, as this pallet is commonly used in industrial applications.

The standard pallet in the US measures 1016 mm x 1219.2 (40 x 48 inches), whereas in Australia measures usually 1100 x 1100 mm.

A similar load carrier (used in Europe) is a roller cage. A roller cage is usually half the size of a euro pallet, i.e. 800 mm by 600 mm. Roller cages are widely used by supermarkets and distribution centres, as they are easy to move, and easy to combine with euro pallets. The advantage of a roller cage is that they are very useful for transporting single-packages, which are commonly seen in supermarkets. The sides of a roller cage are made of iron wire, which gives stability to the load.

This project will focus on the Euro pallet as the basis for the experiments since this type of pallet utilises the space in the trailer most efficiently, leaving less space for airflow, and gives a more realistic picture of the “worst-case” airflow scenario. Since the test will be in a test rig with a plain bottom, without a T-ribbed floor, the use of some kind of pallet representative is essential.

2.2.8 Loading patterns

Loading patterns are particular configurations in which the cargo is loaded into refrigerated trailers. Loading patterns enhance or restrict the airflow around the

cargo. These patterns only apply if the cargo holder has a designated size, and are not used in applications where random loading is employed.

One of the ways to compare different loading patterns is the use of the “slack” factor. This is a figure calculated from the trailer length, where all the space taken up is subtracted from it, resulting in the free space available. Typical figures for calculating the clearance between the pallets and front and rear wall are listed in Table 2-1:

Table 2-1: Dimensions of the inside of a loaded refrigerated trailer

Description	Dimension	Value [mm]
Box length	A	13418
Pallet load	B x number of rows	-X
Rear door w/ Hardware	C	-95
Rear door Air space	D	-75
Front wall	E	-100
Front wall Air Space	F	-75
Stack factor	G x number of rows	-X
Slack		X

(Representative dimensions can be found in Figure 2-8)

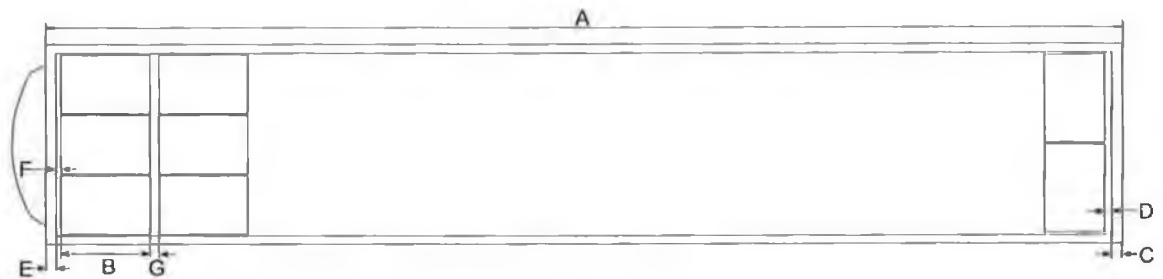


Figure 2-8: Schematic overview of dimensions inside a refrigerated trailer

A negative “slack” factor means that there is less than the recommended space around the cargo, i.e. the pattern does not fit the space around the cargo and will cut off the airflow. The slack factor should be zero or positive to guarantee proper airflow. To achieve this, the distance between pallets is lowered, and the cargo is usually stacked up to the front bulkhead so it will fit into the trailer.

Different configurations and their respective slack factors can be seen in the table below.

Table 2-2: Different loading configuration in refrigerated trailers

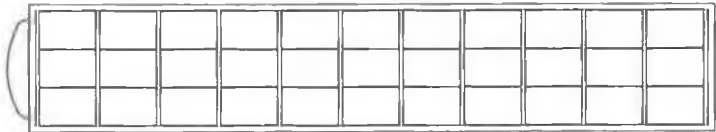



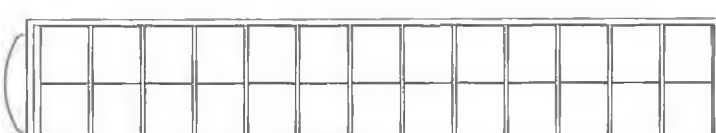
Load configuration	Slack factor	Schematic image
Configuration 1: 33-euro pallets	-347	
Figure 2-9: 33-euro pallet configuration		
Configuration 2: 33-euro pallets	-427	
Figure 2-10: 33-euro pallet configuration		
Configuration 3: 32 pallets	53	
Figure 2-11: 32-euro pallet configuration		
Configuration 4: 32-pallet	-47	
Figure 2-12: 32-euro pallet configuration		
Configuration 5: 32-pallet	-187	

Figure 2-13: 32-industrial pallet configuration

The above loading patterns give an idea of the space available in refrigerated trailers. Trailers are often overloaded, and it is possible that cargo haulers usually do

not adhere to stacking rules. This project intends to investigate the various loading configurations in order to estimate the results of negative stacking factors.

2.2.9 Trailer improvements

Improvements can be made to trailers to enhance the performance of the refrigeration unit. A good working refrigeration unit is important for the whole temperature control process and a good flow around the product is as important since the air is the medium through which the refrigeration unit works. The United States Department of Agriculture [16] published a handbook dealing with common refrigerated trailer design issues.

Improvements to the floor can be made inside the cargo space to improve the airflow returning to the unit and provide at least the 0.15 m² recommended area for the air to return to the unit (Figure 2-14). Different types of ribbed floors can be found. The T-rail floor, as seen in Figure 2-14, is one of these, but ordinary duct board floors are very common as well.

These ribs on the floor are necessary if no pallets are used, although this is not advisable since heat energy can be conducted straight from the floor into the cargo. Pallets help to improve the airflow if orientated in the right direction, but can arrest the airflow if incorrectly orientated. This will be further discussed in paragraph 2.2.7. The trailer should be kept clean so as to ensure a hygienic environment but also to prevent hotspots where ribs in the floor are blocked and airflow ceases.

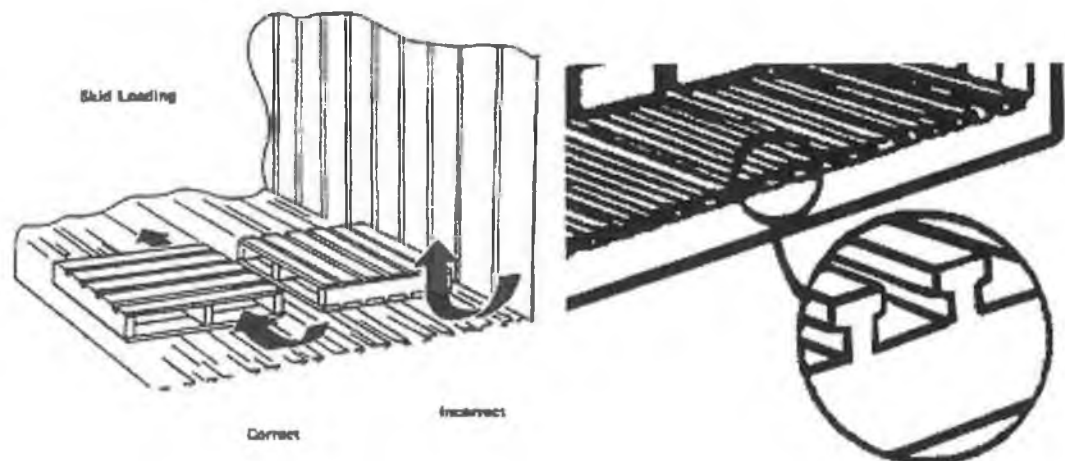


Figure 2-14: Ribbed floors to improve returning airflow

Ribbed walls are also a further help to stimulate the airflow along the side of the trailer, by preventing the walls from heating up the cargo. There should always be a gap of 3cm between the load and the cargo. This should allow at least 20% of the airflow to flow along the side of the trailer wall and to return to the refrigeration unit.

Another common improvement made to refrigerated trailers is a chute that guides the airflow from the host unit to the majority of the trailer. The rule is to have at least 1550 cm² of cross-sectional area to guide the air, ranging from 3 to 5 m from the back of the trailer according to guidelines issued by the NPLA/TRF [17].

These chutes are usually made of a flexible material, and have holes to let air escape as it travels along the length of the trailer. Thermo King claims that no chutes are needed. However, most transporters have them installed in their trailers to aid the airflow. The installation of chutes makes the precise loading of a trailer less important compared with a trailer loaded without this air guidance tool.

2.3 Experimental fluid dynamics in refrigerated trailer

This section examines more closely information on scaling models, Experimental Fluid Dynamics (EFD), flow simulation and flow visualisation.

The scaling of objects for the purpose of experiments is carried out to reduce the geometrical size of the original object. The advantage of a scaled model is that it is less costly on space and resources to build and operate. This involves the refrigeration trailer in the case of the current project.

2.3.1 Scaling similarity

Scaling of the original object is realised according to the rules of similarity [18,19]. The scaling factor (λ) will be different for different situations. In some cases models are scaled up to allow for better study of the area of interest, but in most cases, a scaled down version is used to reduce the size of the object, and to make analysis more cost effective.

Rules of similarity are mathematical rules that the model has to comply with. Euler in 1765 and Joseph Fourier in 1822 wrote first about this dimensional reasoning. There are different levels of similarity:

- Geometrical similarity, where the geometry is scaled according to the scaling factor (λ_l).
- Kinematic similarity, where similarity in time and geometry are satisfied.
- Dynamic similarity where the ratio of forces in the model to those in the original are the same.

An important phenomenon in fluid dynamics is turbulence. Turbulence can be described as a chaotic fluctuation state of a flow. This depends on flow factors such as the Reynolds number. It is therefore very important to try and accommodate as many of the simulation factors as possible to maintain as close a representation of turbulence in the scaled model as in the original model.

It is beyond the scope of this thesis to examine turbulent flow more fully. For further details refer to Tenneks & Lumley [20] or Hinze [21].

Because there is no free surface, the rule of keeping the original and prototype Reynolds number, Mach number and specific heat ratio correspondingly equal applies to this application. The Froude number is less important since this relation mainly includes the scaling of gravitational forces. However, it will be calculated as well to determine what the best scaling factor for the Froude number will be.

The fluid in the scaled model should be considered carefully to obtain an accurate representation of the flow with the best possible environment to carry out measurements and experiments. The known literature suggests that maintaining the Reynolds number should give a good representation of the flow.

2.3.2 Simulation medium

2.3.2.1 Fluids as simulation means

The simulation will be realized with a fluid as medium, which covers a liquid as well as a gas. The difference between a fluid and a solid is that a fluid lacks the ability to resist deformation [22,23]. Because of the lack of this ability, the fluid starts to move. A solid will deform when forces are applied, but does not have to move because it can resist the deformation force.

Fluids whose dynamic viscosity (μ) is constant are called Newtonian fluids. Different types of fluids can be seen in the figure below:

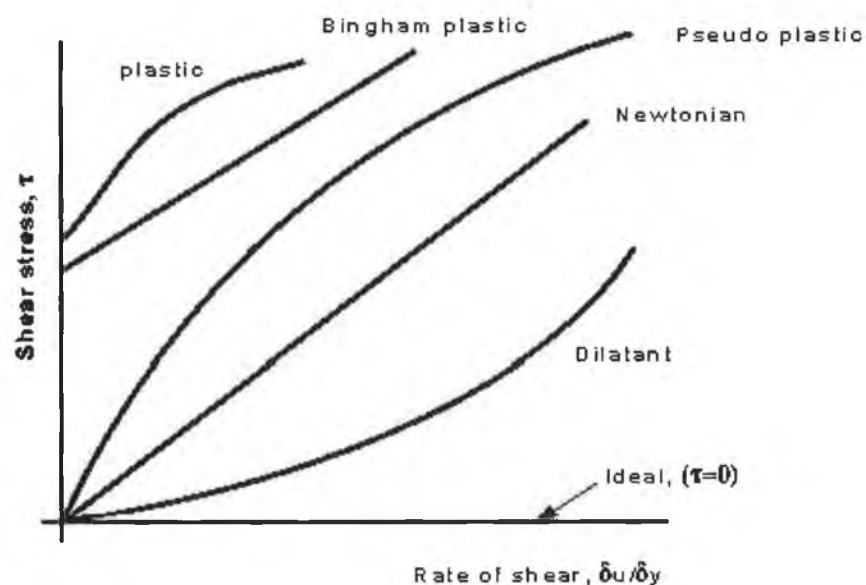


Figure 2-15: Categories based on Newton's law [24]

The properties that are the most important for experimentation, and which will be reviewed are the density and the viscosity.

2.3.2.2 Simulating using liquids versus gases

Gases and liquids have many common characteristics. However, there are a few important differences:

- A liquid is assumed as being incompressible, where a gas is easy to compress.
- A certain amount of liquid (mass of liquid) will occupy a given space, but a gas fills up all the space that is available to it.

A temperature change in a gas will have an effect on the momentum exchange between layers, and therefore change the viscosity. The effect of a change in the cohesive force is of minor importance as it is only very weak in gases. The viscosity is also liable to pressure changes, but this effect is not seen under normal conditions.

The temperature of the air inside the refrigerated trailer does not deviate significantly between leaving the outlet of the unit and returning to the inlet. The change in density in a refrigerated trailer caused by the change of temperature during steady operation will not be much, and can be neglected in the choice of a simulation medium.

The biggest difference between a gas and a liquid, which is of importance for the project, is the difference in the cohesion force and the difference in compressibility. The compressibility can be ignored however if the Mach number [18] is below one. This means that the compressibility of gases can be neglected if the velocity of the gas is below the speed of sound. This rule is defined for subsonic speeds ($0 < M < 1$) subjected to the restriction that the Mach number should not be too close to 1.

A possibility is the use of air as in the life size trailer in order to keep the simulation as close to reality as possible. The problem, however, will be that high air velocity is needed to maintain similarity of the Reynolds number in both the scaled model and the original trailer. The velocity without pressurising the tank will be around 100 m/s for a 1/5 model. Practical problems will arise in getting the air to flow at that speed and performing measurements simultaneously. This problem can be overcome by the

use of another gas medium and/or to pressurise the test rig to bring down the required simulation speed.

The problem with a gas is that it will occupy the whole space available as pointed out earlier, and an airtight rig would have to be built. Air can be obtained out of the atmosphere whereas other gases may not be so easily obtained and would incur greater expense. All of this shows the many complications that will arise in the use of air as a simulation medium. The pressurisation of the tank is too costly and also is not a feasible option. Calculations involved can be found in the next chapter.

Liquids are often used in simulation facilities as a substitute of a gas. The research facility of NASA [25] uses de-ionised water as fluid medium, where the University of Bremen [26] uses Bayer Baysilone M20 silicone oil. The reason for using silicon oil is the higher viscosity, which performs better in simulation. Different fluids will be reviewed in the next chapter about the building of the simulation rig.

2.4 *Flow velocity measurement*

An important part of this project is the measurement of the fluid flow, and the translation of this into usable information. Basic information and guidelines on laboratory measurement can be found in the “ASHREA Standard” [27].

The analysis of the flow means translating the physical flow data inside the test compartment into digital information that can be used for analysis purposes. The aim is to make this translation as accurate as possible, with a sufficient amount of data to facilitate interpretation.

The following measurement equipment is commonly used in fluid dynamics:

- Particle Image Velocimetry (PIV)
- Particle Tracking Velocimetry (PTV)
- Laser Doppler Anemometer (LDA)
- Constant Temperature Anemometer (CTA)
- kPitot tube
- Variable Area Metre
- Orifice Plate
- Venturi Metre

The PIV and PTV systems are very useful to visualise the flow field and to see the turbulent characteristics. PIV and PTV are evolving fast, and have taken over the flow visualisation market compared to the more conventional methods. LDA is a modern and very accurate method but has the disadvantage that it only measures at one point.

Constant Temperature Anemometer is a technique that gives good accuracy and reaction time in measuring flow speed but it differs from the above in that it is a contact measurement technique having the disadvantage that it will disturb the flow, which is also the same for the Pitot tube. The variable area metre, orifice plate and venturi metre are only suitable in pipes and are not suitable for external flow.

Another possibility to measure the flow speed is to regulate the raising of the water temperature and to look for temperature patterns. This involves a controlled simulation of the temperature of the water. It is hard however to record the data acquired by the temperature increase. A possibility is to put heat sensors all over the model, but this will not provide any information on the flow itself. Furthermore heat sensors for water are slow in response. They therefore require a higher accuracy in the temperature control of the water. The use of Encapsulated Liquid Crystals (ELC) is a possibility to monitor temperature change as well as fluid flow patterns, but it is costly and not suitable for high-speed flow. Infrared cameras are slow and are not sufficiently sensitive.

The following paragraphs will discuss some possibilities for the measurement commonly used in flow measurement applications, which would be suitable for the relatively high-speed flow simulation involved in this project.

2.4.1 Particle Image Velocimetry (PIV)

Particle Image Velocity is the most commonly used method in the flow analysis of two dimensional, or in recent years, three-dimensional flow field investigations. The PIV usually works with a digital camera and a pulsed laser light sheet. Particles in the water – for example powder with a mean diameter between 20 - 100 μm – are illuminated by a flash of a very thin laser light sheet that is produced by diffracting the laser beam with a cylindrical lens combined with a spherical lens. A typical set-up can be seen in Figure 2-16.

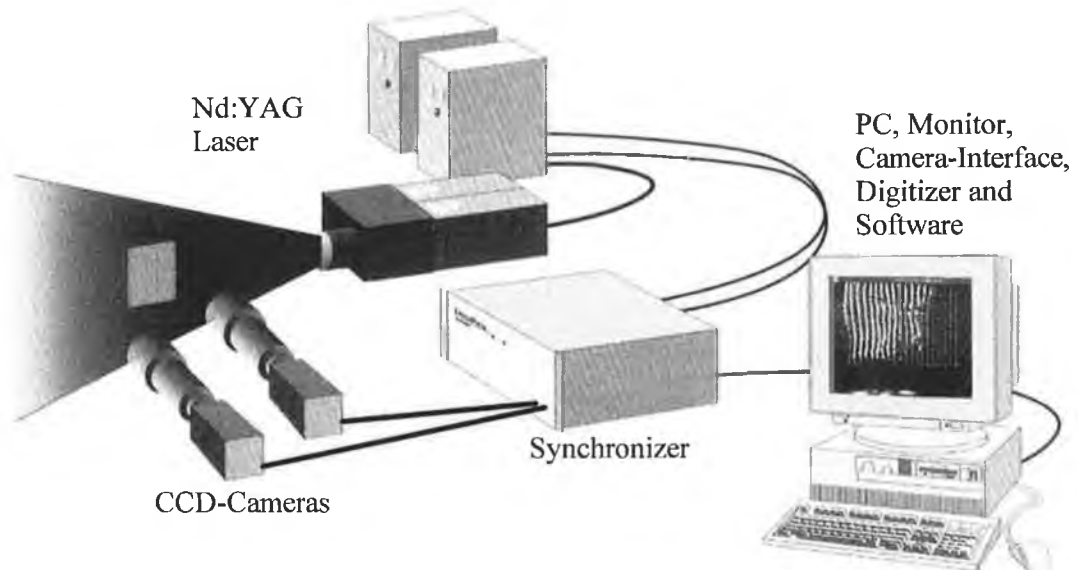


Figure 2-16: Schematic representation of a PIV/ PTV system

When the particles are illuminated by the laser flash an image is captured with the CCD camera and stored in the RAM of the host computer, shortly afterwards (2 ms in our case) the same procedure is repeated, usually, by a second laser.

With this pair of images of the illuminated particles and the known time step, it is possible to determine the velocity in the field of investigation by a correlation algorithm. Cross correlation works by seeking the physical space displacement between frames. PIV cross correlation correlates two images or one image in the case

of “double exposure where the two exposures are on the same frame, to get an average vector field. The total frame will be divided into very small interrogation windows on which the cross correlation will be performed resulting in velocity vectors. These vectors can then be summarized in vector plots. PIV has evolved hugely in the past few years, and the technology currently enables even three-dimensional measurements of flow.

2.4.2 Particle Tracking Velocimetry (PTV)

Particle Tracking Velocimetry (PTV) works very similar to PIV, however it tracks individual particle images in sub sequential frames. PTV starts with the locations of particles at successive times and optimises the association between these sets of locations, making use of historical information such as the previously identified velocities for the particles at the earlier times. PTV is developed to a level in which a sufficient number of velocity vectors can be measured with meaningful accuracy (Wernet and Pline 1993). Methods where PIV and PTV are combined to exploit the advantages of both those systems are examined at the moment.

PTV can be used as long as the centres of the tracing particles can be recognised. PIV systems use a denser seeded flow than PTV systems since the distance between particles has to be greater than the distance a particle travels in-between the two exposures/captures. The advantage of PTV is that it gives a resolute speed vector for a particle and not an average over the interrogation field.

2.4.3 Laser Doppler Anemometry (LDA)

A Laser Doppler Anemometer (LDA) measures the velocity at a point in a flow using laser light beams. It senses true velocity components, and measures that component in a sequence of near instantaneous samples. These characteristics offer several advantages. Unlike a Pitot an LDA does not disturb the flow being measured. It can be used in flows of unknown direction and it can give accurate measurements in unsteady and turbulent flows where the velocity is fluctuating with time.

The LDA uses a light beam emitted by a CW laser that is split in two. Usually a Bragg cell splits the beam in two by using a glass crystal with a vibrating piezon crystal attached to it. This works as an optical grid where the output consists of two beams of equal intensity with a frequency f_0 and is shifted with a frequency f_{shift} . The

probe focuses the two beams on the intersection point in the volume where measurement is performed. The laser light is modulated due to interference between the two laser beams and produces parallel planes of high light intensity. A schematic can be seen in Figure 2-17.

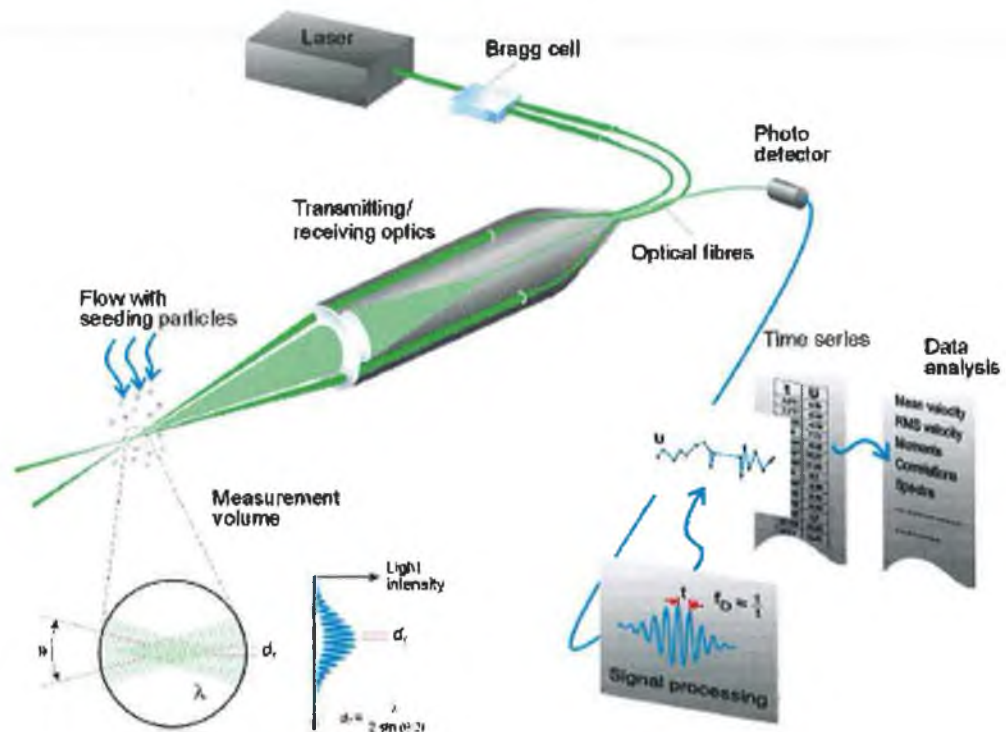


Figure 2-17: Schematic of a LDA system (source: Dantec Dynamics 1999)

Flow velocity information comes from light scattered by tiny “seeding” particles carried in the fluid as they move through the illuminated area. The scattered light contains a Doppler shift that is proportional to the velocity component perpendicular to the bisector of the two laser beams. This corresponds to the x-axis shown in the probe volume.

This scattered light is collected by a receiver lens and focused on a photo-detector. The fluctuating light intensity is converted into an electrical signal that is sinusoidal with a Gaussian envelope. This is due to the intensity profile of the laser beams. The distance a particle travels can be obtained by analysing the frequency of the scattered light. The speed can be calculated using the frequency and travelled distance.

LDA can perform measurements in a two-dimensional plane where two by two beams are used using a different wavelength of laser light. This second pair of beams is usually accommodated in the same optics as the first pair.

A third pair of laser beams can be added to calculate even three-dimensional measurements. In order to do this a further optical head must be added to the system.

The disadvantages of the LDA system are the high costs involved and the shortcoming of only measuring at one point instead of the whole flow field. The advantages are that it is fast and accurate in its measurement, and the information is obtained without interfering with the flow.

2.4.4 Constant Temperature Anemometry (CTA)

Constant Temperature Anemometry (CTA), also called hot wires, is another method of measurement. Hotwires work on the principle that is based on the cooling effect of a flow on a heated body. A servo amplifier keeps the resistance over the hot wire constant and also the temperature since the resistance of the wire changes when its temperature changes. The heat transfer between the medium and a cylindrical body can be calculated with equation 2-1

$$Q = (T_w - T_o)A_w h = A + BU^n; n \approx 0.5 \quad (2-1)$$

A_w the wire surface area and h the heat transfer coefficient merge into calibration constants A and B .

The air speed can now be calculated by measuring the voltage over the servo bridge since this represents the heat transfer. For this reason the hotwire is only suitable in a measurement environment with a constant temperature as a change in temperature would upset the calibration. The CTA system can schematically be seen in Figure 2-18.

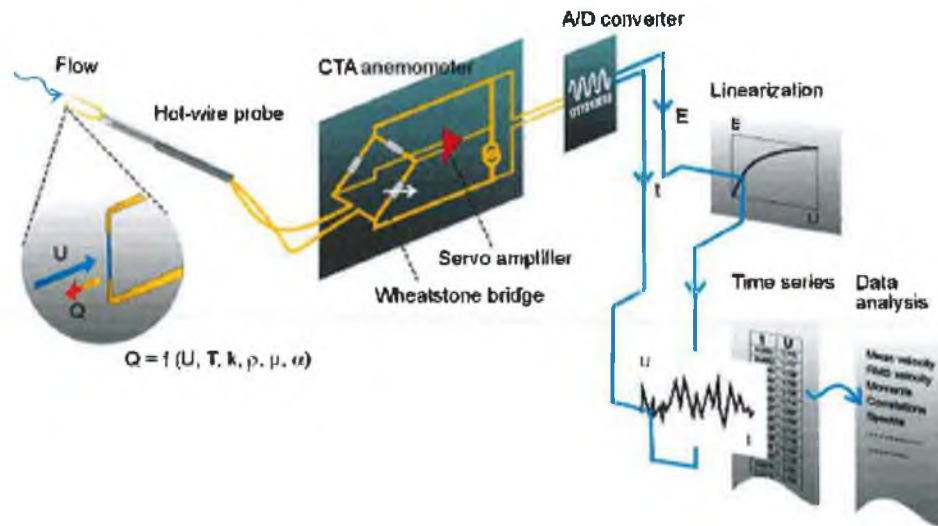


Figure 2-18: Schematic of a CTA system (source: Dantec dynamics)

Hotwires are available in a range of different configurations. The probe would be different depending on the media it is in contact with i.e. water, air. Probes that measure in one, two, and three velocity components are also available.

The main problem with hotwires in this application is that they can only endure up to 5 metres per second in a liquid with viscosity like water, and only up to 80-100 metres per second in air. Along with the fact that a hotwire is a measurement method, it measures with the use of contact. Due to the disturbance of the flow it is rendered unsuitable to use in this application. Practical information on CTA measurement can be found in the publication “How to measure turbulence with hot wire anemometers” [28].

2.4.5 Pitot tubes

The Pitot tube invented by Henri Pitot and modified to its modern form by Henry Darcy, is a velocity-measuring instrument used to measure fluid flow. The Pitot tube uses the difference in pressure between the tip of the tube and holes in the side of the tube. A schematic picture is displayed in Figure 2-19.

The holes at the side (P_s) are perpendicular to the airflow, which gives the static pressure. The total pressure, which constitutes the static pressure, and the dynamic pressure together is measured at the front of the tube (P_t). A pressure transducer measures the difference between the two pressures.

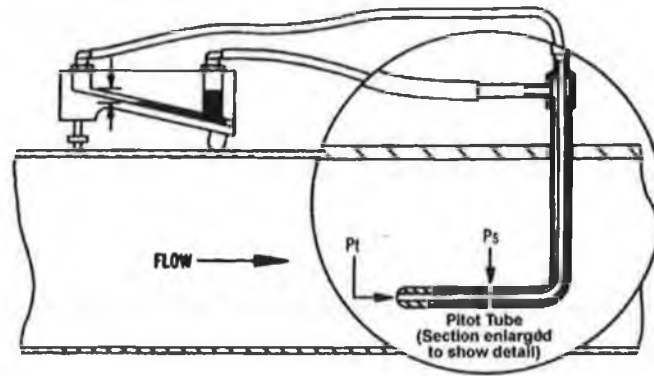


Figure 2-19: Schematic working of a pitot tube

The disadvantage of pitot tubes is that they interfere with the flow due to the fact that it is a contact measurement system. It is direction sensitive making it difficult to use in turbulent flows. There is, however, a great variation in velocity probes where probes measuring in three velocity dimensions are available.

Pitot tubes can be used until supersonic velocities (in a gas) are reached as the assumptions of Bernoulli's equation are violated in that state.

Pitot tubes are suitable to be used in the higher flow speeds as the pressure difference in low flow speeds will be minimal and make it difficult to produce an accurate measurement. Pitot tubes can be used for gases as well as liquids, but the disadvantage is that they disturb the flow.

2.5 Illumination techniques

A light sheet is a thin layer of highly intensive light, which is used to highlight a specific point in the flow. The light sheet is typically created in the visual spectrum, between wavelengths of 400 and 700 nm. It is also possible to make a light sheet in the non-visible spectrum, such as infrared or ultraviolet, as long as the flow can be captured. Once lit by the U.V. light, they seed the flow with particles, which emit light in the invisible spectrum.

The particles mentioned above are seeded in the flow to be examined. These particles are very small and as close to the density of the fluid as possible. This ensures that the particles follow the flow as accurately as possible. These particles usually have a transparent property so that the light, which illuminates them, is

scattered when it flows through the particles. This scattered light will be visible and can be optically recorded.

As a rule, high power lasers (argon, MD:YAG) are used to create the light sheet which delivers a sheet with a minor spread. The distribution will generally be a two-dimensional Gaussian distribution. The laser beam with a general diameter of approximately 1mm can be widened by means of a simple cylindrical lens.

This will result however in a high intensity region at the centre and a low intensity region at the edges of the light sheet (see Figure 2-20). A homogeneous light sheet is required due to the low scattering of light when passing through the tracer particles.

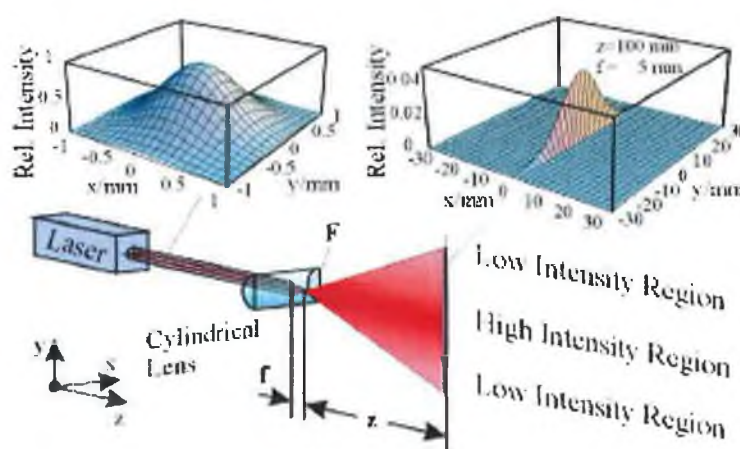


Figure 2-20: Relative intensity distribution of a single laser beam

The high-speed camera used in this project is not likely to be able to reach the high frame grabbing speeds needed for ‘frame-straddling’ as discussed in paragraph 4.2.2. This means that the light sheet probably needs a function to pulse the light and create “multi-exposure” frames if we want to have a small enough displacement between two exposures needed for cross correlation (PIV). Motion tracking (PTV) will be possible if the displacement compared to the density is low enough to identify particle paths. “Single exposure” on a high speed might be enough for this method.

A more affordable way to make a light sheet is to take a high intensity lamp (like a halogen lamp or a Xenon flash tube) and let the light go through a gap of a few millimetres generating a small sheet of light. This method is described by the ZARM [29] institute when visualising a flow seeded with particles. Aluminium particles in particular give a good visual result, which can be seen by the naked eye.

2.5.1 CW-lasers/Pulsed lasers

The high-speed camera used in this project is not likely to be able to reach the high frame grabbing speeds eliminating the possibility of using a Continuous Wave (CW) laser that is only suitable to operate in a continuous wave if PIV is to be utilised. Most lasers however have a function in which they can be pulsed when an analogue input is provided to regulate the laser output power.

When a pulsing laser is used with the relatively slow capture rate of the camera, “multi exposures” on one frame will occur. This may be helpful to do the required calculations on the flow field but may on the other hand result in an image that is too full of illuminated particles. A lower seeding rate on the flow may solve this problem but will make it unsuitable for PIV. If it is impossible to synchronise the laser and camera to a level where only “double exposure” occurs, it may be possible to give only a maximum of two pulses. Two pulses have to be given within the time of one frame to get a “double exposure” system. This will increase the need for a controller that has the possibility to fire two pulses and then wait for a prescribed time before releasing another two for the next frame.

The light sheet needs a typical pulse power of 12 mJ for water applications, as advised by a TSI Incorporate applications engineer who specialises in PIV systems. Some resources however use less power in their application. The repetition rate of the laser pulses has to be short, whereas typical systems use between 10 and 100 μs between two pulses. The duration of the pulse has to be shorter than 10% of the time between two pulses to prevent blurring.

A possibility with lasers as light sheet resources is that a second mirror is used at the end of the tank reflecting the light sheet back and giving extra illumination at the end of the light sheet. This produces a light sheet, which is too thick. This will be of use in the production of a more even light sheet. Therefore the reflected light will be most beneficial at the point where the light sheet is at its weakest. However, this will only work for light sheets with a very constant thickness as a diverging light sheet will expand especially after reflecting on the mirror. This leaves a light sheet which is too thick.

2.5.2 Multiple Laser diodes

Another way of making a light sheet is explained in the paper “Laser light sheet imaging of gas flow with laser diodes” [30]. Laser diodes can be used to generate an intensive light sheet with less effort and expense.

The light sheet needs to be pulsed as pointed out in paragraph 2.5.1 where CW-lasers are discussed. The preferred method however would be the use of the laser diode as opposed to the pulsing of the light sheet itself.

This high spread divergence, as the source of light will make it unsuitable to directly create a light sheet. The spread in the x-direction will be calumniated and the light divergence will be close to parallel when using a cylindrical lens putting the focus length behind the laser source (Figure 2-21).

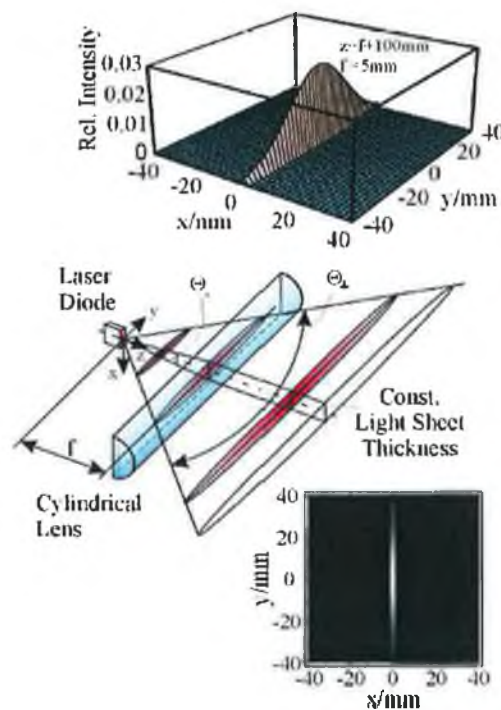


Figure 2-21: Relative intensity distribution of a single laser diode light sheet [30]

The thinness of the light sheet will follow out of the focus distance of the divergence angle.

One laser diode doesn't have the power of gas or solid state lasers, so multiple laser diodes have to be used to obtain the same optical power as the gas or solid state lasers.

The advantage of using multiple laser diodes is that a more uniform light sheet can be created when lining up more than one. The set-up as described in the paper “Laser light sheet imaging of gas flow with laser diodes” [30] is shown in Figure 2-22.

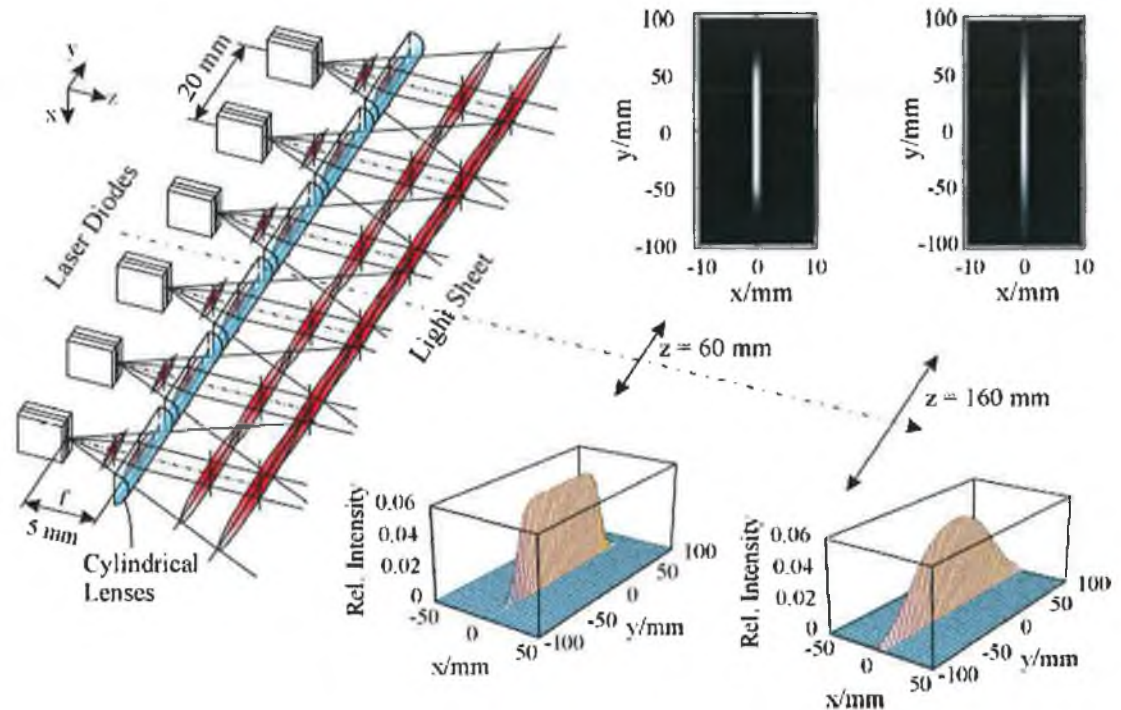


Figure 2-22: Relative intensity distribution of a laser light sheet [30]

This results in a light sheet that will give a more uniform illumination because the Gaussian intensity profiles of the laser diodes overlap. This results in higher efficiency since a limited area of the cross section of a single laser source can be used due to the Gaussian distribution. All of the cross section of the middle lasers in this set-up is utilised.

2.5.3 Xenon flash tube

Xenon flash tubes are used in applications where a bright flash is needed as used in small formats in photo camera.

The brightness of the flash is given in Joules (J), where the power can be calculated by multiplying the flash energy by the frequency of flashes. Small ‘do-it-yourself’ U-tubes typically go to 1 or 2 Joules per flash at a frequency of 10 Hz, giving a maximum of 10-20 W output. Bigger units, however, have a much higher flash energy. Water is usually used to ensure cooling of the units and to produce outputs of

250 W. A 25-Joule flash is typically used, although energy per flash can easily reach up to 350 Joules.

Typically two flashes are given within 100 μ s of each other, which creates problems with the high recharge time of the flash tube. One option is to make a light sheet mechanism that will have two flash tubes. These will be triggered with a small variable time delay to create the effect of two laser light sheets. The disadvantages of this system are however; that the flash interval will be long in duration, and also that the system will not be very flexible for different flow analysis.

2.5.4 Lasers light sheet resources

Light sheets are widely used in flow visualisation, and specifically in the PIV/PTV technique. These include commercially available light sheets such as TSI and Dantec, and also governmental institutes such as NASA [31].

Commercial light sheets usually use a Q-switched Nd:YAG laser which produces high energy light pulses of a short duration (5-10 nsec.). Maximum power output varies from 12 to 120 mJ per pulse for the recently-developed dual mini Nd:YAG lasers and up to 400 mJ per pulse for the larger versions of this type of laser. A pulse last for a 1 – 10 nsec, whereas a typical power output range of a Nd:YAG laser varies from 100 mJ to hundreds of Watts.

The light-sheet thickness should be adjusted to be approximately four times greater than the out-of-plane displacement of the seeding particles in order to optimise the PIV results. Since it is hard to know the out-of-plane distance at this stage of the project, a variable light sheet thickness might be appropriate.

The paper “Jet-Wall Interactions: Investigation into the effects of turbulent water jets within an enclosure” [32] used a 4W Argon Ion laser to visualise a water jet with the use of conventional 35 mm and 120 mm film and a CCD camera (12 bit Cooke Sensicam, 1280x1024 pixels). An ordinary light and strobe lights were also used but as the light intensity was too low a conventional camera was used.

The paper published by Kai-Uwe Graw et al [33] used a Nd:YAG laser (25 mJ per Pulse, 15 Hz), a laser pulse light arm, a laser pulse synchronizer, two high resolution and high frame-rate cross correlation CCD cameras (1K x 1K, 30 Hz frame rate) ,

high speed lenses (minimum illumination 1:1,4 and focal length $f=50\text{mm}$), two high speed camera interfaces, a multi channel digitiser and TSI Insight Stereo Ultra NT capture and analysis software. The fluid motion inside coastal waves was examined in this study.

The paper published by H. Meng [34] used an injection-seeded dual Nd:YAG laser (spectra physics PIV-400) which gives a 400 mJ pulse for 3D holographic PIV. This is a different method from conventional PIV with a holographic plate, three beams split from the one laser.

The University of Illinois [35] did early experiments with a Nd:YAG laser producing 70 mJ recorded on a 35-mm film in 1993. The lasers used were Continuum YG681C-10 Nd:YAG lasers with a maximum output of 550mJ/pulse at 532 nm wavelength and a 4-6 ns pulse. 70 mJ was used as well in the experiments in the paper "Video systems for PIV recording" [36].

A continuous wave light sheet of 16 W power output was used in the paper published by N. Tani [37] instead of a Nd:YAG laser in combination with a fibre optic PIV system. This will give a total power of 32 mJ over a 2000 μs shutter time.

A water tunnel experiment published by Kawaguchi et al [38] studied drag reduced channel flow. This water flow experiment utilises a double pulse MiniLaser-II 20 Hz laser from Newwave Research Co. Ltd. which gives a 25 mJ/pulse at a pulse rate of 20 Hz. The area illuminated is 40 mm x 34 mm.

Papers highlighted above show that a pulse used for water application at 25mJ or more is needed for the illumination. This 25 mJ is usually utilised however for a small area. A lot of applications use 70 mJ which is usually still only for a sheet length less than 100 mm. A recommendation will be to aim for at least 70 mJ in the light sheet up to 200 mJ every frame for a good result. This might turn out however to be very costly as lasers with these output capacities are very expensive to buy.

2.6 Visualisation

Techniques to visualise flow can be found in "Fluid flow visualisation" [39]. One method for generating flow visualisation in a water tunnel is to use a hot wire in the flow upstream of the model. Heating the wire generates a series of small hydrogen

bubbles along the length of the wire. These bubbles will reveal any vortices or wakes as they go around the model in one plane.

Another method is to use a dye in the water. This has the advantage of viewing all the flow around the model. The information can be acquired photographically with a 35mm camera or a digital video camera. The disadvantage is however, that the water will be saturated with the dye, and should be replaced. The flow is limited to lower speeds and has to be slightly laminar as well since the dye will spread too quickly in high turbulent flows.

Aluminium powder is an excellent way to visualise the flow if you use embedded particles. There should be some soap added to the water to reduce the surface tension of the water. The disadvantage is however that it is difficult to get the particles out of the flow again while simulating, and an increased wearing of the filters and pump is inevitable. A light sheet is needed to highlight the regions of interest since the aluminium is not injected at the point where visualisation is required. The water should be replaced or filtered often because the particles will accumulate.

A better suggestion might be to use seeding particles in the flow, which will reflect the light of a light sheet. These particles can be made out of a plastic, which causes less damage to the pumping system. Particles are available in different types, where some types illuminate a distinctive colour when lit with a certain wavelength. An example is the use of a UV-laser to illuminate where the particles will light up green when exposed to the light.

2.6.1 Particles

Seeding particles are the most commonly used method to visualise flow. There are different types of particles, varying from polymers, round shaped particles to glass spheres. Some react and emit light on a specific wavelength, where others only reflect the light. The required result of all the particles will be that they give a bright emission of light in the area exposed to the light sheet, which can be captured with the use of a CCD camera or conventional 35 mm camera.

Particles used for flow visualisation are for example Oil Particles Generator for air, Titanium Dioxide and spherical glass balls of approx. 30 μm – 50 μm for water. The task for all of these is the same: scatter and reflect the light so the camera can capture it.

ZARM [40] has done a study on the suitability of different seeding particles in a research project for “lid driven cavity flow” where Bayer Baysilone M20 silicone oil was used as a medium. The results of this research can be found in the appendix.

The use of Encapsulated Liquid Crystal (ELC) tracers is a method of capturing fluid flow as well as described in the paper ‘An Image Processing System for Real-Time 2-D and 3-D Tracking of TLC Particles’ [41]. ELC give the possibility to trace the movement of the fluid as well as the heat since they change in colour when the temperature changes. The sizes of the crystals are between 30-100 microns in diameter. This method can be used when temperature distribution as well as velocity has to be examined. This is not an issue in this project, however.

2.6.2 Hydrogen bubbles

It is possible to use a gas as a tracer in water. Gas bubbles in the water will scatter the light due to the diffraction of the light moving from the liquid to the gas.

The tank however should not be filled with gas since this will create a different boundary at the top. Also the difference in the density of the gas compared to the liquid will cause flow change problems.

A way to overcome this problem is to generate the air bubbles out of the air existing in the water. This method is called hydrogen bubble flow visualisation. Bubbles of air are generated by the principle of air expanding when it heats. Heating a thin wire inside the flow generates the bubbles, which will accurately follow the flow because of their small size. Figure 2-23 shows a schematic layout of a hydrogen bubble set-up as presented in a paper of K. Kerényi [42] et al.

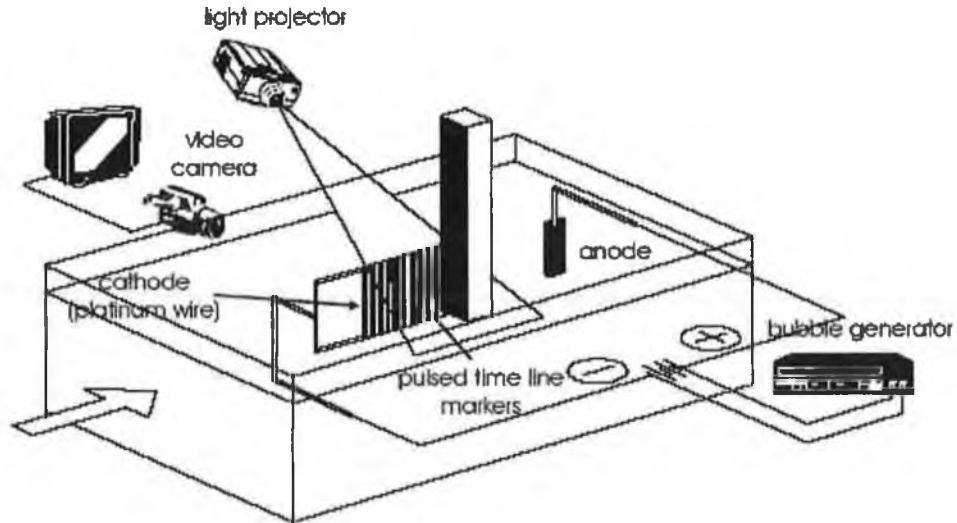


Figure 2-23: Schematic layout of a hydrogen bubble generator

The hydrogen bubble flow method is a clean way of generating visualisation in liquid flow. It is not suitable however for high velocity flows because the bubbles will be harder to create due to the higher cooling effect of the liquid passing the wire and they will also dissolve more rapidly because of the same reason.

2.6.3 Dye

The most used method in the past on the plane of liquid flow visualisation is the injection of a tracer dye into the water. The dye can be released from the object itself to see the flow on the body or can be injected in front of the object to see the flow around the object. Dye injection is a low cost method for flow visualisation. The disadvantage of this system however is that it may disturb the flow at the point where the dye is injected.

Dyes are available in different types and colours. Some dyes have a transparent colour only visible when exposed to UV light. These dyes can be used in combination with a light sheet to highlight certain areas of interest around the model.

The velocity of the water inside a water model should be between 0.0762 m/s and 0.1524 m/s to get good visualisation results according to NASA [43]. These are based on visualisations where a dye is used to colour the path of the fluid. Higher velocity will result in a higher turbulence mixing the fluid too much and inhibiting the view.

2.6.4 Oil

Oil visualisation is another method of visualisation where oil is painted on the surface of the test object. This technique is usually not used in liquid flow visualisations but in airflow simulation performed in wind tunnels. An example can be found in the paper “Visual Simulation of Experimental Oil-Flow Visualization by Spot Noise Images from Numerical Flow Simulation” [44].

This experimental flow visualisation technique represents the surface flow field with oil streaks. This technique requires a low flow velocity to prevent all the oil from being blown off or dripping off before the results can be acquired.

Oil flow patterns have been used for decades for visualisation of corner flows that are otherwise hard to access by non-intrusive optical measurement techniques. Colour pigments are mixed with oil and painted onto the surface of a model. During the test the oil will be blown away or evaporate leaving behind the colour. If a favourable mixture is chosen, the colour forms streak-like patterns on the surface of the model, which later will be interpreted by the researcher. Patterns are created due to the first pigments that stick to the surface which tend to accumulate more paint in a small wake behind them. These streaks visualise the direction of the flow close to the solid walls. Merzkirch [45] gives a more detailed description of this experimental visualisation technique.

Another way of visually representing the flow is the flow visualisation technique called *spot noise*, which is often seen in CFD visualisation. This technique uses small drops of oil carried by the simulation medium, which hits the model leaving a mark behind. It can be compared with small ink drops falling on a paper, where the ink leaves a small trace if the droplet hits it under an angle. Van Wijk et al. describes this technique in the book “Spot noise – texture synthesis for data visualisation” [46].

Those flow visualisation techniques are less suitable however for flow visualisation in simulations where liquid is used as the medium because the oil will not evaporate as in air and will leave no colour behind.

2.7 Acquisition and imaging processing

2.7.1 Available software packages

There are multiple possibilities in the detection of the fluid flow inside the simulation rig. The first thing to be decided is whether the software will be acquired from a supplier or if it will be developed during the project. Professional PIV and PTV systems are available on the market although they are highly expensive. A lot of the research is currently done on mathematical algorithm for PTV systems and can be found in papers and publications.

Initially, the decision was made to try to make custom software due to the fact that available PIV systems are too expensive to suit the budget of this project. The advantage of self-programming is that you can define with accuracy what you want to detect and adjust. It is also possible to customise exactly to the needs of the application and expand on the experience and know-how of the Galway Mayo Institute of Technology.

Two possible software packages available and identified that can help us with the writing of the software are Labview from National Instruments and Matlab from the Mathworks Inc. These programs have built-in algorithms useful for graphical analyses and are capable of doing the mathematical processing needed. It might however be worth looking at faster programming language such as C++ or the mathematical language Fortran to increase performance of the program.

2.7.2 Methods of analysis

Identifying and calculating motion is a sequence of actions. Information on the topic can be found in applications where motion tracking is important, for example where robots have to follow or grab objects [47,48,49]. This, however, implements tracking motion with the use of the same object in different frames, and not the proposed technique to calculate the speed by the travelled length of a particle with the use of a variation of the shutter time or by the distance between particles in two time intervals.

There are different ways of object tracing that can be used, as well as there are different traceable object and methods available. Different approaches are:

- Dye flow pattern tracing
- Particles position tracing (high shutter speed)
- Particle path tracing (low shutter time of camera)

With dye flow pattern tracing, the pattern of a dye injected in the flow will be followed as it moves along the camera. This method however may not work in the high-speed flow entering the water tank, but may be a good way of tracing the low-flow-speed regions. The disadvantage of using a dye tracer is that you only have one chance to capture the flow since it will spread through the water soon after it is released and not clearly identify the flow anymore. Another problem is saturation of the water in the tank involving purification of the water on a regular basis since multiple runs have to be carried out with the availability of only one image acquisition camera.

Another possibility is to put seeding particles in the flow. These particles can be traced with the use of the motion tracking software to be written. The camera used to capture the flow will have a high shutter speed to get a clear image of the flow. The points on the screen identifying the particles will be traced and a very high capturing speed is needed to make sure the particle does not move much between two frames. A pulsing light sheet can be of aid to obtain this short interval between two particle positions if the camera cannot acquire at a high enough speed.

The type of particles must be carefully chosen so they do not alter the flow, or give an erroneous idea of the flow due to weight or size. Seeding particles can be obtained in fluorescing form to highlight certain areas of the flow, although clear particles will probably work as well if a bright light sheet is used. The light sheet needs to have a considerable output of light because the shutter speed is short, letting only a small amount of light to the camera.

The third option is to capture seeding particles with a low shutter speed. If particles are big enough, and perfectly round of shape, frame captures with a low shutter speed will show a line where the particle moved during capture. Speed can be

calculated by measuring the length of the trace minus the diameter of the particle, knowing the shutter time. If this is executed in combination with the conventional tracking methods, a very high accuracy can be obtained since position of a particle can be predicted due to direction and speed of the image, checking the position on the next frame.

The most important factors in software for particle tracking velocimetry are the algorithms used in the image processing as explained in “Algorithm improvement in particle tracking velocimetry” [50]. Usually, the camera gives an 8-bit greyscale image delivered to the software. The first step is to modify and identify the different particles in the image. The second step is to use the algorithm to determine the motion between different frames. The first step is the most difficult step since the images from the camera are usually blurred and not perfectly sharp. If the frame is successfully analysed however, and accurate positions of the particles are produced, the second step will analyse this output to work out the motion. This is the most important step since this step has to deal with multiple points, and has to identify which point in one frame is the same in the next frame. Different algorithms and approaches can be taken in doing this, as described in the subsequent paragraphs.

Another technique is the technique used in particle image velocimetry. This method does not track individual particles, but looks at a small region of particles and uses cross correlation algorithms to determine the average speed of such a region. An example is given in a paper published by M.J. Molezzi and J.C. Dutton [51]

Both methods, PIV and PTV, will be examined and tested to find the best way of extracting the velocity from the captured data.

2.7.3 Methods to identify particles and analyse the flow

In the case of PTV, coordinates of the particle (centres) need to be extracted from the image. There are a methods to implement this as lined outlined below.

2.7.3.1 Image reconstruction

The image has to be reconstructed before coordinates can be extracted from the image as pointed out in ‘NASA’s Technical Paper 3416’ [52]. The recorded image suffers from perspective distortion. This effect has to be reviewed in our application.

The reason that the reconstruction of the image is important in the NASA wind tunnel is that the light sheet moves to acquire three-dimensional data by looking at sub sequential layers of the flow. Manual reconstruction or calibration might be a possibility in a two dimensional application, or in an application where multiple two dimensional planes are analysed sub sequentially.

This needs to be performed to relate physical distance to a certain amount of pixels on different cross sections of the tank. The further one moves away from the camera the bigger the area the camera acquires due to the perspective distortion. This means that a particle travelling the width of the camera region travels further at the other side of the tank than on the side closest to the camera.

A calibration grid could be a solution for this problem calibrating the camera on two identical meshes at the front and back of the tank and after detection interpolating the distortion at the distance of the light sheet. It can however just be a manual correction factor as well given to the software.

2.7.3.2 Basic particle detection

At least 90% of the processing, which is conventionally performed on frames containing particles, is concerned with performing threshold operations on the image to find the sections that relate to the particles.

Threshold is a technique that works on greyscale levels. A decision is made on which greyscale level the cut-off point will be. Every value above that will be identified as a particle, and every value lower will be ignored.

The location of the particles can be obtained after this. This process can be very easy if a particle corresponds with no more than one or a few pixels since the location can be extracted straight from the matrix. The centre has to be calculated if a particle represents a group of pixels.

This is the most straightforward method to extract the coordinates, but not the most advanced and accurate one because particles might get lost in the threshold screening process.

2.7.3.3 Extraction of Particle Coordinates Using CLEAN

The method CLEAN to extract particle coordinates from an image is described in an article written by M. Stellmacher and K. Obermayer [53]. This method replaces one of the cameras of a conventional stereo photo-grammetry system with a light

sheet. The reconstruction model consists of an object coordinate system transformation, the collinearity condition of photogrammetry and the equation of the light sheet plane.

Objects and their images are located with respect to an object (X, Y, Z) and an image (x, y, z) coordinate system. The two systems are related to each other by a transformation, where the orientations of the object systems are arbitrary.

The grey-scaled frame of the camera is convolved with the assumed shape of the images in order to extract the coordinates of the particles from an exposure. Then the location X of the maximum of the convolution of the images is determined and added to the particle list. The assumed shape is then scaled to the grey level of the image and subtracted so the particle is not in the resulting image. The resulting image is then lowered in grey level and this loop is repeated until the grey value falls below a given threshold.

This method gives a straightforward way to extract particles from an image. Other methods however are possible. A lot of programs, for example have built-in features to detect groups of pixels with a higher intensity value representing particles.

2.7.3.4 PIV

PIV was developed in the last two decades with the availability of the modern laser technologies and the availability of higher specification image acquisition systems. Previous problems with the spatial resolution are being solved with the availability of cameras with a higher resolution.

Although PIV has already been used for a while, pioneers like Kompenhans and Höcker [54,55] and Post et al. [56] have extended the PIV to high speed seeded flows. This high speed refers to high wind tunnel speed and although these high speeds are not investigated in this project it is good to keep those methods in mind for further applications.

The paper published by M.J. Molezzi and J.C. Dutton [57] describes a PIV system capable of capturing flows of Mach 0.4 up to Mach 0.5, which is equivalent to around 132 m/s to 166 m/s in air at room temperature and atmospheric pressure. The requirements needed to do this are a laser that gives pulses of only 4-6 ns and exposure intervals of 1 μ s or less. PIV systems usually use the Fast Fourier Transform (FFT) method.

Other references are the paper “Particle image velocimetry with optical flow” [58] and “An improved cross-correlation method for (digital) particle image velocimetry” [59].

2.7.3.5 PTV

Template extraction

A method used for PTV is template extraction. The motion is to be extracted from the frames with the use of a template representing the image to be tracked in the frame if the template extraction method is used. Different methods for applying the template extraction methods are:

1. *The Pixel Difference Method*
2. *The region Merging method*
3. *The histogram method*

Papers on these methods are “Particle tracking velocimetry using a discrete relaxation method” [60], “Synchronous Orthogonal Dynamic Programming for Particle Image Velocimetry” and “Synchronous Orthogonal Dynamic Programming for Particle Image Velocimetry” [61] and “Applying Feature Tracking to Particle Image Velocimetry” [62]

Two-frame PTV using match probability

The two-frame PTV using matching probability works as follows as described by S.J. Baek and S. J. Lee [63]:

1. *Maximum velocity.* The maximum velocity a particle can have is known. If this velocity (U_m) is taken over a frame interval Δt , a distance $U_m \Delta t$ between the two images can be travelled. This means that a particular particle can not travel beyond a present threshold T_m .
2. *Small velocity change.* The velocity of a particle will not change much in the small time interval Δt , since the particle has a finite mass.
3. *Common motion.* Multiple particles will move in one direction forming a region of point sharing a common motion ($=T_n$). This group of particles in a small region shows a pattern of similar movement.

4. *Consistent match.* Two points from one image generally do not match a single point from another image.

The small velocity change and the common motion heuristics can be combined into the quasi-rigidity condition ($=T_q$). The match probability algorithm is mainly based on maximum velocity and quasi-rigidity condition.

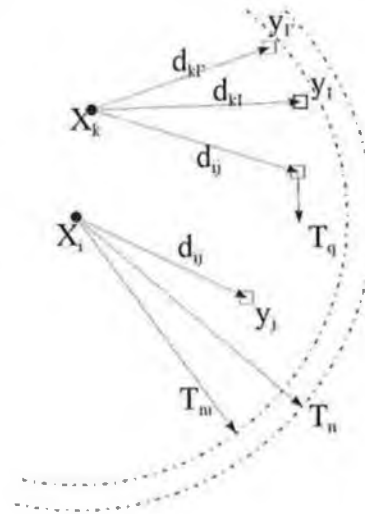


Figure 2-24: The two-frame PTV using the matching probability

If one looks at the two points x_i and y_i as seen in Figure 2-24, where x_i is in the first frame and y_i is the same point in the second frame. The point y_i has to be within the maximum displacement threshold T_m in respect to x_i . Neighbouring point x_k must have a similar movement as the point x_i according to the common motion rule, and within the neighbouring threshold to be seen as a neighbouring point.

The point x_i and y_i are neighbouring points if $|x_i - x_k| < T_n$.

The quasi-rigidity condition is applied to the neighbouring points with the displacement vector d_{ij} ($=y_j - x_i$) when the particles are in an area with the radius of T_q within the end of the vector d_{ij} . Particles have similar movement when they move within T_n in quasi-rigidity position in a time span Δt . The quasi-rigidity of the vector d_{kl} relatively to d_{ij} is represented as follows:

$$|d_{ij} - d_{kl}| < T_q \quad (2-2)$$

For updating the match probability, match probability of neighbouring points x_k are used to iteratively update the P_{ij} (interactive estimation of match probability) of x_i .

P_i^* represents the non-match probability that point x_i has no match within T_m . Each match probability is proportional to the neighbouring match probabilities, where the neighbouring match satisfies the quasi-rigidity condition. The iteration formula of

$$\tilde{P}_{ij}^{(n)} = A \cdot P_{ij}^{(n-1)} + B \cdot Q_{ij}^{(n-1)} \quad (2-3)$$

Is used to calculate the updated match probability for each object point $P_{ij}^{(n)}$.

Adaptive hybrid scheme

The adaptive hybrid method, as described by Hyoung-Bum Kim and Sang-Joon Lee [64] is an extension and enhancement of the two-frame PTV method as described above. The adaptive hybrid scheme enhances the original method, based on the match probability concept, where global match parameters are utilised. The adaptive hybrid scheme uses the PIV data to determine the local match parameters that are required for the particle-tracking algorithm.

The cross correlation method is used in conventional PIV systems. The FFT-based cross-correlation PIV method removes directional ambiguity and decreases the computation time required to extract velocity vectors. PIV however loses some spatial accuracy due to the limitations of a CCD camera and the restrictions when expanding to a three dimensional volumetric measurement from a two-dimensional plane.

Combining PIV and PTV gives PTV the flow data needed to enhance the analysis, where the disadvantages of the PIV system are overcome by the PTV tracking capabilities.

A tracking method based on deterministic annealing and alternative distance measurement

Another tracking method is found in the article 'A new particle tracking algorithm based on deterministic annealing and alternative distance measures' [65]. The new procedure is based on calculation algorithms for recognition of statical pattern proposed by Gold et al [66].

This method does not only look at the local velocity, but also at other local components of the flow field. It is based on a cost-function that measures the quality of the match between patterns and particles in sub-sequential frames as a function of an assumed set of flow field parameters. This cost-function is optimised with relation to particle correspondence and flow field parameters using a maximum entropy approach and deterministic annealing. This leads to an estimate for the flow field parameters that is robust against missing particles and other sources of noise. This particle matching method is based on works previously submitted by Gold et al [67, 68, 69] and Rangarajan [70] et al.

Holographic particle image velocimetry

Holographic PIV (or HPIV) is an emerging method as described in the article “Tracking turbulence with holographic particle image velocimetry” [71] and “A new algorithm for the interrogation of 3D holographic PTV data based on deterministic annealing and expectation minimization optimisation” [72]. This method gives instantaneous 3D flow field information. HPIV seems to be the best solution for 3D velocimetry and particulate flow diagnostic tools. Most fluid visualisation techniques do not give full detail in the turbulent, and often multiphase flows. The lack of such capability slows the understanding and control of these flows significantly.

Summary

This project will first of all start with a hybrid consisting of a simple version of the two-frame PTV analysis with match probability. The algorithm will however initially be without the common motion and consistent match rules in combination with the template extraction method to decide on the centre of a group of particles identified in the image.

The method can then be extended with the more sophisticated algorithm of the common motion and consistent match algorithms to identify any erroneous vectors.

2.8 Air flow optimisation in trailers

2.8.1 Methods to improve airflow

Work has been conducted on air improvement methods, and some of these methods are already used in current refrigerated transports. Examples are chutes (paragraph 2.8.2) to guide the airflow to the back of the trailer and a bulkhead (paragraph 2.8.3) to prevent “short cycling” of the air, and to secure a return air path. This protects the unit from the cargo been piled up to the front. Other possibilities to be investigated are nozzles and vanes.

Thermo King has performed a thorough study with the use of computational fluid dynamics (CFD) on the effect of a chute in an empty and a loaded trailer with the expertise of the company Fluent Inc. in April 1999 called “Simulation of Air flow and Heat transfer in a Refrigerated Trailer” [73], with an “Addendum” [74] in August of 1999.

The reports addressed the airflow inside a refrigerated trailer equipped with a Thermo King SB-III refrigeration unit equipped with a prototype air delivery chute and a Thermo King prototype air return bulkhead. The aim of the report was to:

1. Optimise the new air chute design
2. Determine the correct amount of air that discharges from the side of the chute, and to determine the size and quantity of the holes discharging the air.
3. Optimise the design of the bulkhead at the front of the trailer
4. Determine the optimum airflow rate for a refrigerated compartment to maintain a temperature variation of 5° or less within the compartment.

The first report examines two cases, where in the first case an unloaded trailer was studied and in the second case a loaded trailer with solid wall pallets was studied. In addition, a loaded trailer with pallets with open sidewalls was studied in the second report.

Chutes and ducts are commonly seen in the refrigerated transport sector. Approximately 90% of all trailers have a chute fitted to guide the airflow to the back. A bulkhead is essential in all loaded conditions since it prevents the cargo from being

stacked up to the front wall. The refrigeration unit would not receive any air at all when there is no bulkhead arrangement. Some trailers have a bulkhead integrated in the front wall of the trailer.

The next paragraphs explain various airflow distributions related topics that have to be examined as possible airflow improvement methods.

2.8.2 Ducts/chutes

Most refrigerated trailers use chutes to improve the airflow throughout the trailer. The figure below shows an experimental duct fitted in combination with a Thermo King refrigeration unit.



Figure 2-25: Duct fitted to TK refrigeration unit



Figure 2-26: The end of the duct

Guidelines for “duct designs” [75] are given in the ASHREA Handbook of 1993. The paragraphs give useful information on all the aspects of commercial or industrial duct design e.g. the best shape, static and dynamic friction losses and so forth. These formulas can be reviewed if a duct has to be designed for the refrigeration unit.

It is important as well to determine how many holes a duct requires to bleed off air when progressing along the length of the trailer. This is needed to cool the areas between the shipments and to dispose of the heat conduction of the walls as discussed in chapter 2.2.3. The amount of air that bleeds off out of the chute should be as uniform as possible over the length of the trailer.

2.8.3 Bulkhead

The bulkhead has three main functions as described earlier:

- Providing an air channel for the returning air to the unit
- Provide a structural base for the cargo to be stocked on to
- Prevent short-circuiting of the air blown in the trailer.



Figure 2-27: A bulkhead fitted in a refrigerated unit

The first function of a bulkhead is to provide an air channel. It also prevents the cargo from being stacked to the front of the trailer in a way that would block the return air from flowing back to the unit. It is essential that this return air would be unrestricted.

The structural base ties in with the previous function where the bulkhead prevents the cargo from being stacked too much to the front of the unit. The bulkhead needs to have a good structural strength because the cargo is stacked against it, and it has to endure a high pressure in different transportation situations.

The third function is to prevent air from short-circuiting from the refrigeration unit to the inlet of the unit. How often this happens is not exactly known, but is most likely to occur when the air blown into the unit is blocked and slowed down

significantly. This may happen when there is for example not enough floor clearance between the cargo and the unit, or not enough clearance between the cargo and the trailer resulting in a high static pressure. This high static pressure causes the flow to return to the refrigeration unit taking the way of the least resistance where slowing down and turning around causes less resistance than flowing around the cargo.

The bulkhead has to be easy to remove in case of maintenance to the refrigeration unit or when cleaning has to be done.

2.8.4 Airflow distribution in a room in a contained environment

Information on airflow distribution in refrigerated trailers is scarce, as there are not many companies doing research on this topic. A very similar application where a lot of research is done is in the field of air-conditioning and air distribution in for example offices. Basic information about the diffusion of air into a room can be found in the ASHREA Handbook, Fundamental [76].

Different air delivery methods can be identified when looking at methods of room air distribution [76]. Those types are mixing systems, displacement systems and local systems.

The system that is the object of this thesis is a mixing system since it is stated that a mixing system has to supply airspeeds much higher than in the occupied zone in normal conditions. When the air enters the room it mixes with the ambient air, which will reduce the air velocity and equalizes the temperature. The outlet is always positioned at the top of the refrigerated room, with the returning air coming from the bottom. The formulas found in the ASHREA fundamentals can be used when calculating the performance of a jet in a room. This however does not take into account any obstructions, and assumes a free flow. This calculation can be used to calculate the theoretical performance of the air coming from the refrigeration unit flowing into the refrigerated area. Nozzles could be added to the diffuser, improving airflow.

Another factor that is important in the refrigerated trailer is the use of the Coanda effect. The Coanda effect is an observable fact where the air is aimed to a corner in the trailer and sticks more or less to the surface. This helps the flow to reach the back

of the trailer and is a method Thermo King uses to make sure air will flow to the back of the trailer.

More information can be found in the paper “Air distribution design for controlled atmosphere in reefer cargo holds” [77]. A numerical approach to design air diffusers is given in the paper “Evaluation of CFD-modelling methods for air diffusers” [78].

2.8.5 Laminar elements and vanes

Laminar elements placed in the nozzle where the fluid comes into the trailer will smoothen the flow and lower the loss caused by internal friction. The Reynolds number will be lower, and you have less turbulent (so more laminar) flow. This increases the distance the flow travels in a positive way.

Vanes are fundamentally laminar elements, although usually designed to guide the fluid in a particular direction. Vanes affect grille performance if their depth is at least equal to the distance between the vanes, and a vane ratio above two has little or no additional effect. A ratio between 1 and 2 should be maintained [76].

If the ratio is less than uniform, effective control of the air stream discharge from the grill by means of the vanes is impossible.

The spread of a grill with straight vanes aiming forward is between 14 to 25°, depending on the type of outlet, duct approach and discharge velocity.

A grill with diverging vanes with an increasing angular deflection from the centreline to a maximum of 45° at the sides will reach a spread of about 60°, but reduces the throw considerably. The quantity of the discharged fluid for a given upstream pressure decreases with increased diverging vanes.

If it is needed to get a better throw, converging vanes can be used (vanes with decreasing angular deflection from the centreline). This results in approximately the same spread as with straight vanes, but has a slightly higher-pressure loss.

One can increase the throw as well by guiding the air along the ceiling, and increasing the adherence and lowering the drop.

Chapter 3

Development of the scaled model

The development, design and prototyping of a scaled model of the refrigerated trailer to perform the fluid dynamic experiments are reviewed in this chapter. Considering the size of a full trailer (2.5 x 2.5 x 13.5m) and the cost associated with such a trailer, the use of a scaled trailer model suits the purposes of this thesis. The scaled model facilitates various tests and creates more opportunities to perform advanced measurement on the flow including flow field measurement and pressure measurement.

Furthermore measurements performed in a real size trailer are more difficult to carry out since the measurement equipment will most likely interfere with the airflow. The scaled model of the refrigerated trailer will be developed so the measurement equipment can be situated outside the test rig, and will have little or no interference with the flow. A scaled model will have an additional advantage that it may be cheaper to facilitate the various tests which will modify and improve the air delivery system.

There are rules in scaling down real size models to smaller test objects. These rules have to do with the physics of fluid dynamics. Most rules can be summarized under the title 'Scaling similarity'. This will be reviewed in paragraph 3.1. The advantage that exists with the changing of the size of the object is that the fluid used to perform the experiments can be changed as well. Different fluids have different properties so one can choose the most suitable one to use in the simulation.

The design and development of the test rig will be discussed in paragraph 3.2, different needs and solutions will be outlined in order to make the design philosophy clear. This will include a short summary of the choice of materials, structural considerations and safety issues.

Paragraph 3.3 reviews the different methods to simulate the flow inside the scaled model of a refrigerated trailer and the selection requirement, where paragraph 3.4 reviews the speed settings for the pump which is selected for the propulsion system.

The scaling of the cargo inside the refrigerated trailer is dealt with in paragraph 3.5, where different aspects of the cargo choice will be reviewed. The simulation of the cargo will be important to obtain information on the airflow in real size trailers.

3.1 Scaling down objects

3.1.1 General scaling similarity

The next formula represents the rule of dynamic similarity without free surfaces as found in the literature [23] and applicable to this project:

$$\frac{F_m}{F_o} = \frac{M_m a_m}{M_o a_o} = \frac{\rho_m L_m^3}{\rho_o L_o^3} \times \frac{\lambda_L}{\lambda_T^2} = \lambda_o \lambda_L^2 \left(\frac{\lambda_L}{\lambda_T} \right)^2 = \lambda_o \lambda_L^2 \lambda_u^2 \quad (3-1)$$

Wherein:

- F = force
- L = Length (distance)
- M = Mass
- λ = Scaling factor (λ_L = length scaling factor, $\lambda_o = \lambda_T$ = time scaling factor)
- ρ = Density

One approach would be to maintain an identical Reynolds number between the real size refrigerated trailer and the scaled model. This will result in equation 3-2:

$$\frac{\rho_m u_m l_m}{\mu_m} = \frac{\rho_o u_o l_o}{\mu_o} = Re \quad (3-2)$$

With:

- ρ = Density
- u = Velocity
- l = Characteristic length
- μ = Dynamic viscosity

The similarity in Froude number is of lesser importance than the similarity in the Reynolds number, and not of real importance in our simulation model. It may be better however to try to accommodate them both.

The Froude number is:

$$Fr = \frac{U^2}{g \cdot L} \quad (3-3)$$

When equalising similarities in the Froude number,

$$\frac{U_m^2}{g \cdot L_m} = \frac{U_o^2}{g \cdot L_o} \quad (3-4)$$

$$U_m = U_o \sqrt{\frac{L_m}{L_o}} \quad (3-5)$$

The required simulation velocity is only dependent on the square route of the length scale factor.

It is evident that the problem is that a lower simulation speed is needed for similarity in the Froude and a higher simulation speed for similarity in the Reynolds number in order to get a realistic simulation. A possibility, however is that a fluid configuration exists which can be used at the needed flow speed to accomplish similarity in the Froude number, and comes close to the Reynolds number as well appearing in the original.

Additional formulas can be important when scaling the moving objects such as the fans in the refrigeration unit, and they can be found in the literature [79].

3.1.2 Pressure similarity

The pressure coefficient used in similarity simulations is expressed as C_p . The following formulas describe the scaling factor used for dynamic scaling similarity with pressure readings in the scaled model. The same method as the scaling of the size is used were the pressure coefficient in the model and original refrigerated trailer is kept the same:

$$C_p = \frac{\Delta p}{\frac{1}{2} \rho u^2} \quad (3-6)$$

$$(C_p)_m = (C_p)_o \quad (3-7)$$

$$\frac{\Delta p_m}{\frac{1}{2} \rho_m u_m^2} = \frac{\Delta p_o}{\frac{1}{2} \rho_o u_o^2} \quad (3-8)$$

$$\Delta p_m = \Delta p_o \frac{\rho_m}{\rho_o} \left(\frac{u_m}{u_o} \right)^2 \quad (3-9)$$

Using the formula for similarity:

$$\frac{\rho_m u_m l_m}{\mu_m} = \frac{\rho_o u_o l_o}{\mu_o} = \text{Re} \quad (3-10)$$

The formula for the kinematic viscosity (ν) is:

$$\nu = \frac{\mu}{\rho} \quad (3-11)$$

$$\frac{u_m}{u_o} = \frac{\nu_m l_o}{\nu_o l_m} \quad (3-12)$$

Combining them, we can use the following equation to calculate the pressure difference in the scaled model:

$$\Delta p_m = \Delta p_o \frac{\rho_m}{\rho_o} \left(\frac{\nu_m}{\nu_o} \right)^2 \left(\frac{l_o}{l_m} \right)^2 \quad (3-13)$$

The pressure scale factor (λ_p) can be calculated when the parameters below are known, which for a water model are:

$$\nu_o = 1.44 \times 10^{-5} \text{ m}^2\text{s}^{-1}$$

$$\nu_m = 1.14 \times 10^{-6} \text{ m}^2\text{s}^{-1}$$

$$\rho_o = 1.23 \text{ kgm}^{-3}$$

$$\rho_m = 998 \text{ kgm}^{-3}$$

This makes the pressure scale factor $\lambda_p = 127$.

This means that when the pressure loss over the full size trailer is a typical value of 500 Pa, the pressure loss in the scaled model would be 63500 Pa.

3.1.3 Scaling the size

The variables in the scaling factor equation are the velocity, the viscosity and the size of the model. This paragraph will look at the effect of changing the size of the model on the required velocity in a scaled refrigerated trailer.

The following graph shows the effect of changing the size of the simulation rig on the simulation speed:

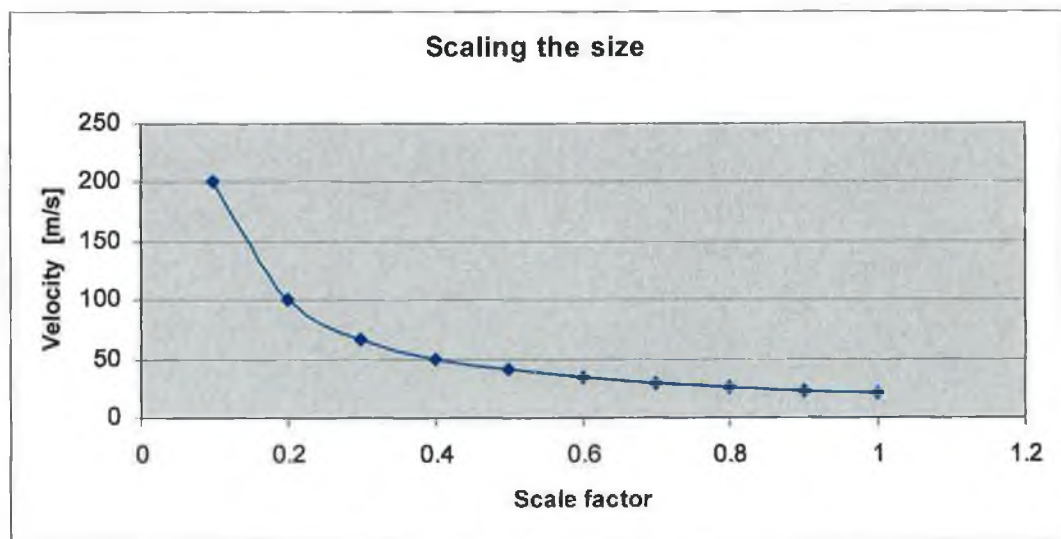


Figure 3-1: The effect of changing the length-scaling factor

A possibility is to use air as a simulation medium in the experiments. With air as the medium the formula will be as follows because $\rho_m = \rho_o$ and $\mu_m = \mu_o$.

$$u_m = \frac{u_o l_o}{l_m} \quad (3-14)$$

Thermo King currently uses a fan system to distribute the air with a maximum of 25 m/s, which will mean that the maximum simulation air speed will be 75 m/s based on a 1/3 model.

This speed does not reach the critical Mach speed yet, so simulation is still possible at this speed considering the airflow as incompressible, but the simulation by itself

would be very difficult to undertake since an enormous amount of air would have to be transported.

The reason for this high velocity is that the time scale is very high due to the scaling factor, and measurement, visualisation and generation of such airflow would prove difficult and hence very costly. A 1/3 model is very large as well and a smaller model is preferable, which obviously will even increase the velocity. Another problem will be that the operation velocity approaches the critical Mach number as explained later on.

Flow visualisation is practically impossible at velocity over 100 metres per second and measurements can only be accomplished with very specialised and expensive equipment. Standard non-contact measurement equipment is not capable of measuring those high velocities, and contact measurement techniques suitable for those speeds are too big in order to withstand the forces involved and hence interfere too much with the flow.

Two methods will be illustrated to reduce the simulation flow velocity as described. The possibilities are the use of a compressed gas, or the use of another fluid to replace the air as used in the original refrigerated trailer.

3.1.4 Changing the kinematic viscosity

The following graph shows the effect of changing the kinematic viscosity of the fluid against the simulation speed:

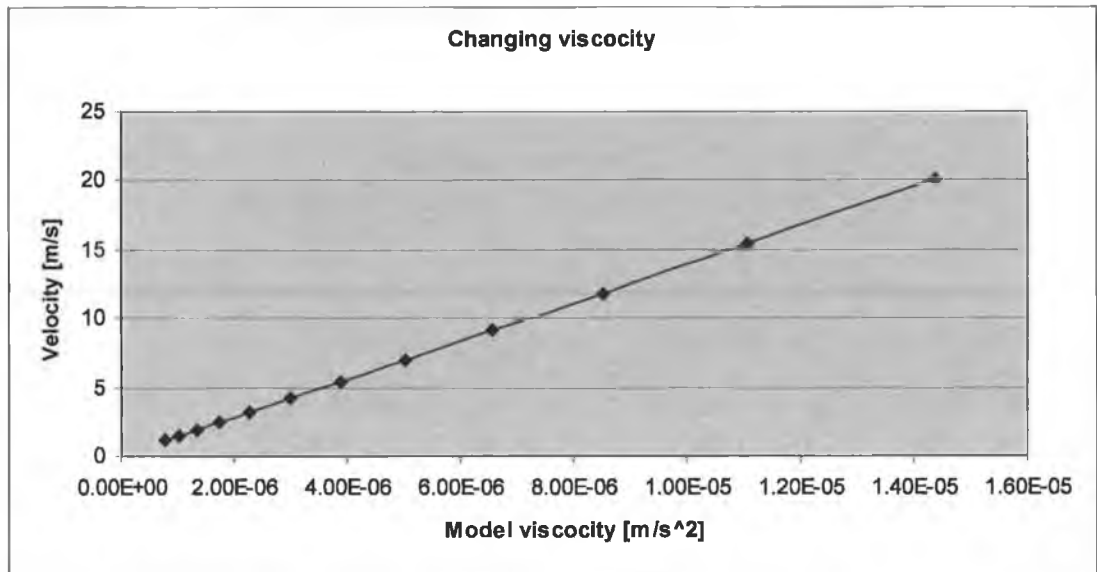


Figure 3-2: The effects of changing the viscosity

This graph shows that with a low kinematic viscosity the required simulation speed goes down. The viscosity of the model is shown on the x-axis of the graph showing the required simulation speed against the kinematic viscosity of air. The kinematic viscosity of water would be around $1.44 \cdot 10^{-6} \text{ m/s}^2$.

Modifying the density

It is possible to compress air to artificially increase the air density and bring down the maximum air velocity required while scaling down the refrigerated trailer.

Calculation starts with similarity in Reynolds number as explained in section 3-2. Equation 3-15 can be used for relating pressure, density and temperature with an ideal gas:

$$p = \rho RT \quad (3-15)$$

In which:

P = the pressure

ρ = density

R = gas constant (286 J/kg/K°)

T = temperature

We use the next equation to reflect the pressure change in the model to the pressure of the original:

$$\frac{P_m}{P_o} = \frac{\rho_m RT}{\rho_o RT} \quad (3-16)$$

We can make the following formula assuming x represents the times atmospheric pressure and a constant temperature is maintained:

$$\frac{x \cdot P_o}{P_o} = \frac{\rho_m}{\rho_o} \quad (3-17)$$

With a constant temperature, $p_o = x p_m$ and the knowledge that the value of μ (dynamic viscosity) does not change much with the change of pressure we get:

$$u_m = u_o \frac{\rho_o l_o}{x \rho_o l_m} \quad (3-18)$$

This means that every bar of pressured air will give the same amount of reduction ratio of the maximum required air velocity compared with the simulated air velocity calculated above.

In the 1/3 model situation, a model that is pressurized with 5 bar of pressure will require a simulation speed of 15 m/s.

Modifying density and dynamic viscosity

There is a problem when using air as the simulation medium in combination with scaling the refrigerated trailer because it is physically impossible to get the flow speed and the Reynolds number in the right proportion, without very high pressure inside the scaled model of a refrigerated trailer.

For example CO₂ can be used if we pressurize the model. CO₂ is the probably the best and safest option with gas as a simulation medium.

$$\frac{p}{RT} = \rho \quad (3-19)$$

$$\frac{p\lambda^{1.5}}{\mu_m RT} = \frac{\rho_o}{\mu_o} \quad (3-20)$$

$$p = \frac{\rho_o \mu_m RT}{\mu_o \lambda^{1.5}} \quad (3-21)$$

For a scaling factor of 0.2 however, it means that the chamber should be pressurized up to 6.3 bars. When using a 1/3 model, the pressure needed to be 3 bar to get dynamic similarity in velocity and Reynolds number.

Practically this is too high and not appropriate to build in a simple model, since the test rig will have a square cross section which typically cannot stand much pressure.

Changing the viscosity

Another possibility is to use another fluid. Initially, equality in Froude number and Reynolds number is maintained although the former is not as important as the Reynolds number, but will give a good initial idea of the required scaling parameters.

We will use equal Froude numbers given equations in 3-3, 3-4 and 3-5.

$$U_m = \sqrt{\frac{U_o^2 \cdot L_m}{L_o}} = U_o \lambda^{0.5} \quad (3-22)$$

We take $\frac{L_m}{L_o} = \lambda$ as the (length) scaling factor, with 3-2:

$$\frac{\rho_m \lambda^{1.5}}{\mu_m} = \frac{\rho_o}{\mu_o} \quad (3-23)$$

$$v_m = \lambda^{1.5} \cdot v_o \quad (3-24)$$

When we calculate the required static viscosity, this will mean that:

$$l_o = 1$$

$$l_m = 1/3$$

$$v_o = 1.44 \times 10^{-5} \text{ m}^2\text{s}^{-1}$$

The required kinematic viscosity (v) will then be $8.3 \times 10^{-5} \text{ m}^2\text{s}^{-1}$.

The nearest (practically usable) gas that can be used is CO_2 ($v \approx 8.1 \cdot 10^{-6} \text{ m}^2\text{s}^{-1}$) this will give a needed scaling factor of $\lambda = 0.681$.

Lowering the kinematic viscosity by using a liquid

Another option is using a liquid like water as testing medium and hence significantly lowering the kinematic viscosity. Liquids can replace air in fluid applications as long as the velocity of the air is lower than 1/3 of the Mach number and the fluid under investigation can be regarded as incompressible.

We take the air reference at 20°C, and the dynamic viscosity of water round about 15°C (laboratory temperature):

$$\rho_{\text{air}} = 1.23 \text{ kgm}^{-3}$$

$$\rho_{\text{water}} = 998 \text{ kgm}^{-3}$$

$$\mu_{\text{air}} = 1.78 \times 10^{-5} \text{ kgm}^{-1}\text{s}^{-1}$$

$$\mu_{\text{water}} = 1.14 \times 10^{-3} \text{ kgm}^{-1}\text{s}^{-1}$$

This results in the formula for the velocity of water:

$$u_m = \frac{\mu_o \rho_o u_o l_o}{\mu_m \rho_m l_m} = u_o \frac{1.14 \times 10^{-3} \cdot 1.23 \cdot l_o}{1.78 \times 10^{-5} \cdot 998 \cdot l_m} = 0.0789 \cdot u_o \cdot \frac{l_o}{l_m} \quad (3-25)$$

This means that the use of water will reduce the needed water velocity on the model by a factor of 12.67 if you compare it with the same situation simulating with air (and a 1/3 model). The result is 5.92 m/s if we use the discharge velocity of 25 m/s in

the life size trailer and water in a scaled model of one to three.

When including the Froude number as well in the calculation, the scale factor can be calculated with the formula used in the calculation of the gases:

$$\lambda = \left(\frac{v_m}{v_o} \right)^{\frac{1}{1.5}} \quad (3-26)$$

$$\begin{aligned} \text{With } l_o &= 1 \\ v_o &= 1.44 \times 10^{-5} \text{ m}^2\text{s}^{-1} \\ v_m &= 1.14 \times 10^{-6} \text{ m}^2\text{s}^{-1} \end{aligned}$$

The required scaling factor $\lambda=0.184$ if water is used (1:5.4) to satisfy the Reynolds and Froude number.

Other possible liquids are [80]:

1. Kerosene	($v \approx 2.3 \cdot 10^{-6} \text{ m}^2\text{s}^{-1}$)	$\lambda = 0.294 \text{ kg m}^{-1}\text{s}^{-1}$
2. Ethanol	($v \approx 1.5 \cdot 10^{-6} \text{ m}^2\text{s}^{-1}$)	$\lambda = 0.221 \text{ kg m}^{-1}\text{s}^{-1}$
3. Water	($v \approx 1.1 \cdot 10^{-6} \text{ m}^2\text{s}^{-1}$)	$\lambda = 0.184 \text{ kg m}^{-1}\text{s}^{-1}$
4. Bayer Baysilone M20 silicone oil	($v \approx 2.2 \cdot 10^{-5} \text{ m}^2\text{s}^{-1}$)	$\lambda = 1.335 \text{ kg m}^{-1}\text{s}^{-1}$

3.1.5 Decision on the size

To get the Froude number right we need to compromise with the Reynolds number. It is open for discussion however if the exact similarity of the Reynolds number is required in scaling the model. An appropriate model flow condition can be reached when the C_p number becomes independent of the Reynolds number and therefore a change in the Reynolds number would not give large differences in the model results. This is the case when the flow is fully turbulent.

The size of the model should be big enough to enable one to make accurate measurements and small enough to monitor. This means that it should not be bigger than necessary to make it easier to fit in a workshop, and limit the amount of fluid needed for the simulations (in case of a fluid other than air) but the measurement instruments must be able to measure the flow without disturbing it. The effects of the scaling factor on the required flow rate is that it more or less stays the same with a

changing scaling factor since the flow has to speed up with a smaller model, but will be smaller in area. This means however that the velocity of the fluid must be higher with a smaller scale which raises significant challenges.

The decision on the scale factor will be made keeping in mind the feasibility of the test rig to be built and operated in a workshop. After the above factors have been reviewed, a final scaling factor of 1/5 is chosen which gives a model of reasonable size, i.e. small enough to measure, big enough to house instruments and create an accurate representation of the trailer and the components that are connected to it.

3.1.6 The final choice of the simulation medium

The most obvious choice for a simulation medium will be a liquid, resulting from the calculations in the previous chapters if a scaled model is to be used. A liquid is the best choice because a gas like air requires a very high simulation velocity (100 m s^{-1}), which is not feasible under normal ambient pressure, and presents problems for measurement equipment as well. Compressing the gas can reduce the required velocity, but it is almost impossible to make an affordable test rig that can operate under the required pressure in which measurements can be taken.

3.1.7 Conclusion

The simulation fluid chosen is water. This can be justified by looking at the differences between fluids and gases and the scaling similarity rules. The main difference in properties between a fluid and a gas is the compressibility of a gas compared to a fluid. This as explained above does not have any affect on the scaled refrigerated trailer simulation model. The main reason to use a fluid is the much lower simulation velocity due to the much lower kinematic density, which gives much more flexibility to the visualisation and measurement of the flow.

The effects of changing simulating temperatures are considered but effects in the refrigerated trailer are minimal with a maximum temperature variation being between 2.5-5°C under normal circumstances.

3.2 Development of the scaled trailer model

3.2.1 The general dimensions

An average trailer has inside dimensions of 2495 X 2600 millimetres, although 2400 X 2400 millimetres is a commonly used dimension since the pallets are 1200 X 1000 millimetres or 1200 X 800 millimetres. One will use 2450 X 2600 millimetres in our scaled model, since this gives one some clearance at the walls and is the average height for the trailer. The length for European trailers is almost 14 metres, but a scaled model of the refrigerated trailer will be designed equivalent to a 16 metre, which will leave opportunities in the use of this extra space.



Figure 3-3: General dimensions of a refrigerated trailer

The refrigeration unit is mounted on front of the trailer (as can be seen in Figure 3-3). There is a hole in the front wall for this with the dimensions of round about 1700 X 1100 mm. The position of the hole is 105 mm from the top of the trailer and positioned in the middle. The resulting dimensions can be found in the following table:

Table 3-1: Scaled refrigerated trailer dimensions using a scaling factor of 1/5 for the key peripheral dimensions shown in Figure 3-3

Dimension (ref. Figure 3-3).	Original [mm]	Scaled model [mm]
A – Trailer width	2450	490
B – Trailer height	2600	520
C – Trailer length	16000	3200
D – Cut-out width	1700	340
E – Cut-out height	1100	220

3.2.2 Design specification

The specifications applicable to the scaled model of the refrigerated trailer are:

- The simulation rig has to be stiff
- The simulation rig has to be portable
- Ergonomics must be facilitated
- The windows have to be designed to sustain the pressures occurring during testing and transport
- The windows have to be transparent to facilitate adequate recording of the fluid flow

3.2.2.1 The frame

Basic requirements

The simulation area of the tank should be at a suitable height to facilitate observation of the simulation running in a comfortable position, while it is still possible to reach into it in order to adjust simulation properties like the cargo, for example. In summary, this means that the bottom of the simulation area will equal 0.9 metres, and the top approximately 1.5-metres.

A decision must be made on how to support the glass while taking into account the amount of steel that might block the view inside the tank. This support was along each edge but this had a negative impact of reducing visual access to flow fields within the tank. The support must not block the view of the boundary layer at the top

and bottom of the model. The tank should be designed to permit an unobstructed view of all important sections inside the tank (see Figure 3-4).

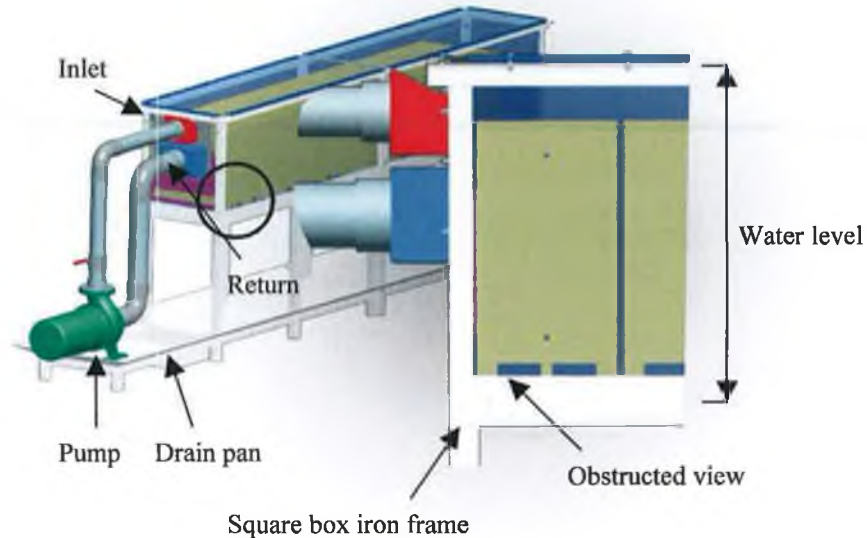


Figure 3-4: The view is obstructed by the frame

As a bulkhead is mounted which obstructs the view, the design at the front of the trailer is not of crucial importance. The bottom and top are important as the boundary layer and all the flow occurs there, as well as at the sides. The back is important as well, although in case of a European trailer, a glass plate is mounted near the end of the tank, which gives excellent view.

This suggests that we should focus on a clear view at the sides, bottom and top of the tank. There is only a little space in between the simulated cargo and the walls (approximately 10 mm) and about 60 mm at the top, making it very hard to give support to the glass as the prevention to obstruct the view on those areas. A possible solution is to mount a double bottom and top in the tank, to bring up the bottom, lower the top so it is not restricted at all by the frame. This would make it easier to design the frame and make decisions on the material since one can make the double bottom as thin or thick as one would need it. (see Figure 3-5).



Figure 3-5: The use of a false floor solves the problem of the lost view

Frame design

The frame is constructed of steel, consisting of 40 mm x 40 mm square frame that constrains the glass and gives strength and stiffness to the water tank. This frame is placed on legs so that a comfortable observation height is achieved for flow visualisation. Right angle irons of 40 mm x 40 mm are used to support the glass. Box profiles give the basic structure. The structure was designated to be stiff enough to withstand the weight and pressure of the water as predicted by numerical analysis.



Figure 3-6: The frame of the simulation rig

Strain/stress analysis of the main body of the tank

The stiffness of the model was analysed to ensure that the frame was stiff enough for the pressure caused by the water in the tank. The finite element package used was Pro/Mechanica from Parametric Technologies Corporation.



Figure 3-7: Part of the tank analysed with the use of FEA

The FEA model evaluates half of the tank without the legs (see Figure 3-7). The model is constrained on the positions where the legs are located (indicated in yellow in Figure 3-8). The force of the water in a full tank is uniformly applied to the beams at the bottom. The force applied to the sides' supports is linear progressive (an example indicated in red in Figure 3-8). The maximum force at the bottom decreases linear to zero force at the top. There is a mirror-constrain on the middle of the frame where it would be connected to the other half. The model was converted to shells because of the length/thickness ratio. This significantly reduces the amount of elements required to mesh the model.

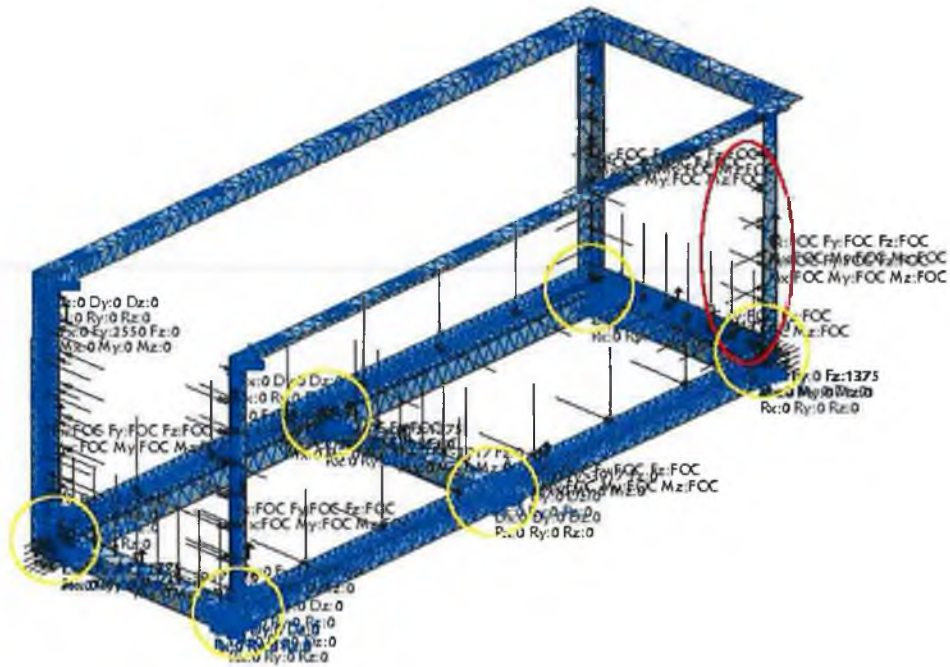


Figure 3-8: Constrains and mesh of the FEA model

The force is calculated using the volume of the water, which is 1600 mm x 500 mm x 520 mm, and by multiplying by the density of water, which is 998.23 kg/m³ at 20°C. This result is then multiplied by the gravitational force, which results in Newtons.

The material used for the beam is steel. The material properties are taken out of the material library of PTC Mechanical, which can be reviewed in Table 3-2.

Table 3-2: Material properties of steel

Material: Steel				
	Density	Young's modulus	Poisson's ratio	Shear Stiffness
	7.827·10 ⁻⁹ [tonne/mm ³]	199948 [N/mm ²]	0.27	78719.7 [N/mm ²]

Pro/Mechanica, automatically generates the mesh while only using rectangular elements. A total of 23793 elements and 11442 nodes were created. The representation below shows the stress in the frame. Figure 3-9 below shows a graphical representation up to 120 Mpa, which is the yield strength of steel with a 1.5 safety margin.

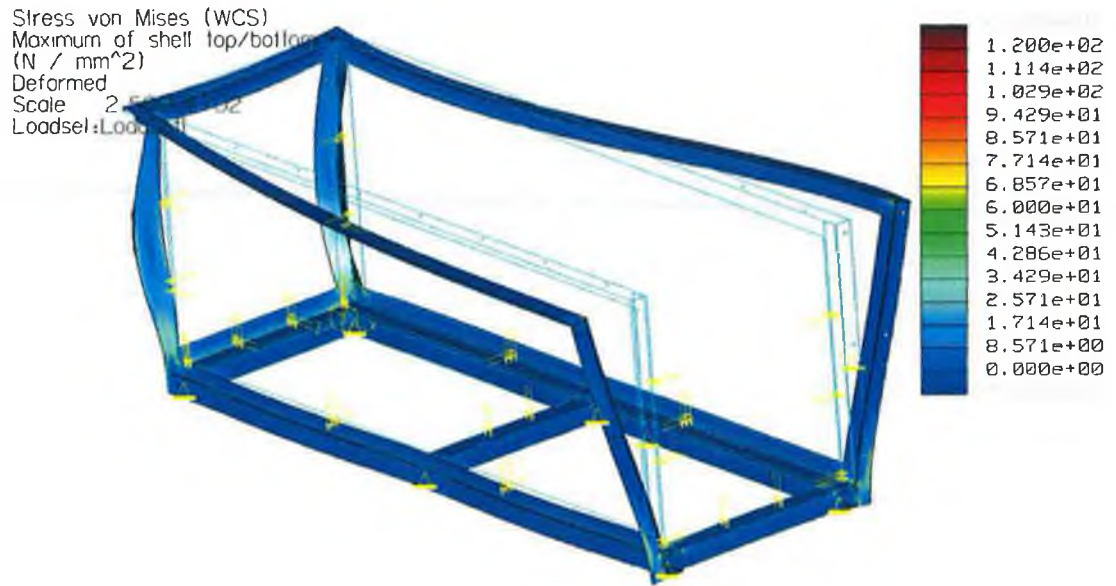


Figure 3-9: Von Misses stress on the FEA model

The picture below shows a graphical representation of the displacement of the frame. The red indicates the displacement while the blue indicates no displacement. The displacement as seen in both pictures is magnified 256 times.

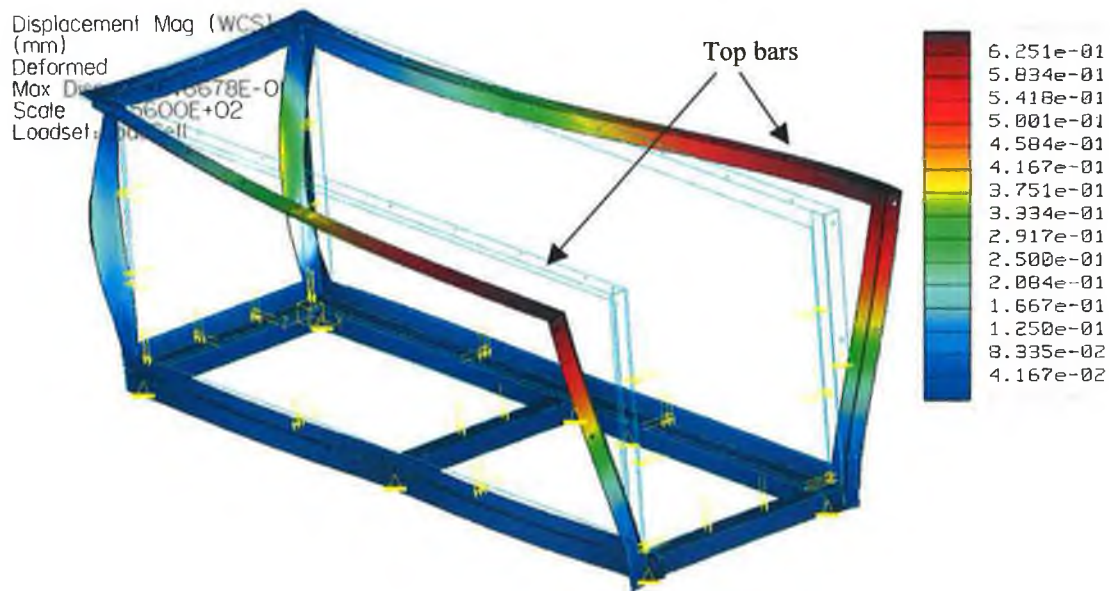


Figure 3-10: 3 Dimensional deformation of the frame

The graph presented in Figure 3-11 identifies the displacement of the beams at the top of the frame along the length of the first section, measured from the back. This analysis is important for the sealing of the tank and the deformation of the glass.

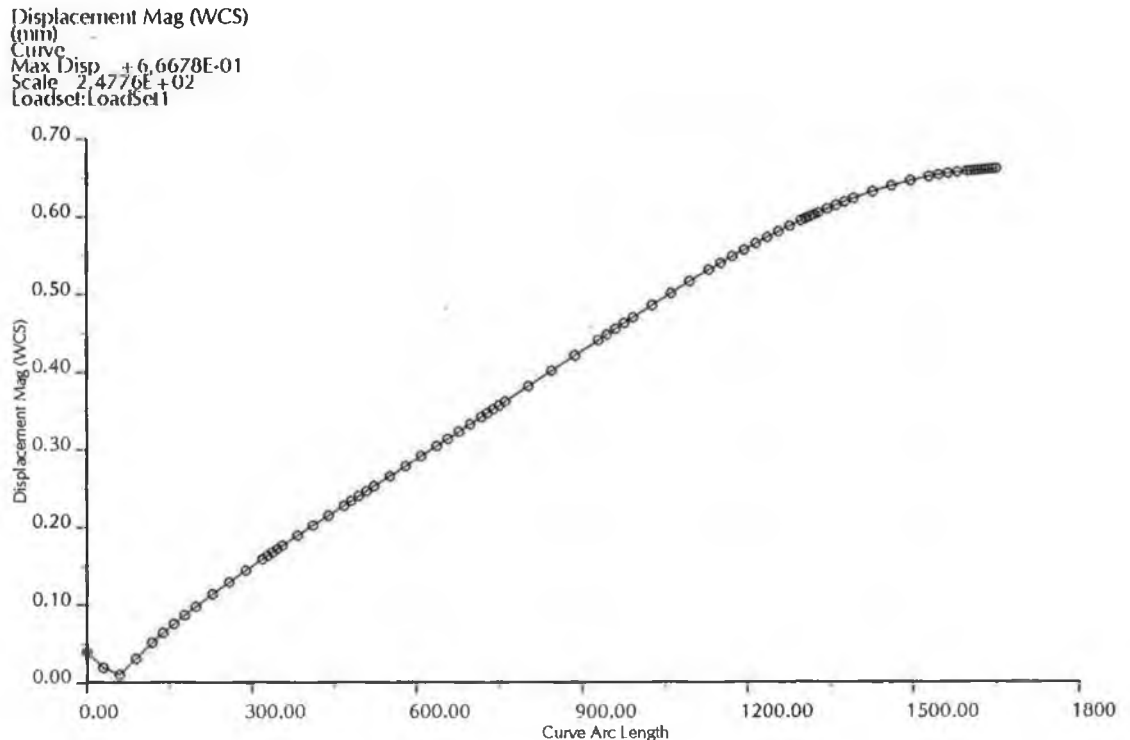


Figure 3-11: Displacement along the “top bar” of the frame

The maximum displacement experienced is 0.7 mm, which is not an issue for the sealing considering the gradual deformation over about 1600 mm of one half of the tank. The second half of the tank is constructed in the same manner as the part analysed. This results in the same result set.

The conclusion drawn out of the FEA is that the frame is over-designed. This is required however since too much of a deformation will give considerable problems with the sealing of the glass.

Surface treatment

The frame will be pre-treated in the Thermo King factory to prevent it from rust and afterwards painted black in the dip tanks used for the frames of the refrigeration units. The smaller sheet metal parts will be pre-treated and afterwards powder coated. The colour used will be black as it is the colour available in the dip tanks as

well as in the powder paint facility. This will also prevent reflections when acquiring the flow data while using a digital camera.

3.2.2.2 Material selection for side panels

Choice of material

There are different materials that can be used for the sides, front, back and bottom of the tank. The most obvious, easy to get and affordable materials are:

- Glass
- Polycarbonate
- Acrylate

All of the above materials have their own advantages and disadvantages.

Assembling glass and perspex sheets

All sheets of acrylate and glass will be placed on top of silicon sealant to make a good seal with the frame and the inside will be sealed as well preventing the water from leaking out between the beams. Sealing inside the tank is insufficient since any displacement of the glass will rip the sealant off the surface of the glass causing the water to pour out of the tank.

The connections between the different pieces of acrylate are made with Acryfix 107. This glues the different sheets seamlessly together. This is especially suitable for assembling the top cover.

Refraction of light

Important factors in the choice of materials are the visual preferences. One of them is the breaking index of the light, as one needs the deformation of the image to be as small as possible.

The absolute refractive index is the ratio of the velocity of light in a vacuum to that in a specified medium (v_{medium}).

$$\text{Absolute R.I.} = \frac{3 \cdot 10^8}{v_{\text{medium}}} \quad (3-27)$$

Table 3-3: Refraction index of light for different materials

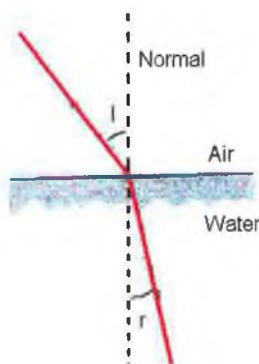
	Refraction index
Water	1.33
Glass	1.51
Perspex	1.49

To calculate the breaking index for substances other than air the two refraction indexes are divided by each other.

The breaking from air to glass/acrylate is described by:

$$\frac{\sin l}{\sin r} = n \quad (3-28)$$

In which n is the refractive index, l is the angle of entrance, and r is the angle of exit. These are measured from the normal to the glass/acrylate surface.

**Figure 3-12: Schematic representation of the refraction of light**

The deformation will be calculated according to the angle at which the light enters the camera lens. A default lens has an angle of 70° , resulting in $l = 35^\circ$.

Table 3-4: Comparison of light breaking indices of glass and perspex

Material	R.I.	Angle r in glass	R.I.	Angle r in water
Glass	1.51	23.18	0.881	20.42
Perspex	1.49	23.49	0.893	20.97

The refraction index of glass and perspex are almost the same. There is not much difference in the angle of the light when passing through them. This eliminates problems of different refractions when viewing through different planes.

Strain/stress analysis

The stiffness of the material is reviewed with the finite element software package *Mechanica* from PTC software. This determines the maximum displacement of the material under the given water pressure. The graphical result set of the bottom panel made out of perspex is shown as an example in Figure 3-14. The area that was constrained in the model is indicated in red in Figure 3-13. The model was meshed using rectangle elements. A total of 1963 elements and 1068 nodes were created.

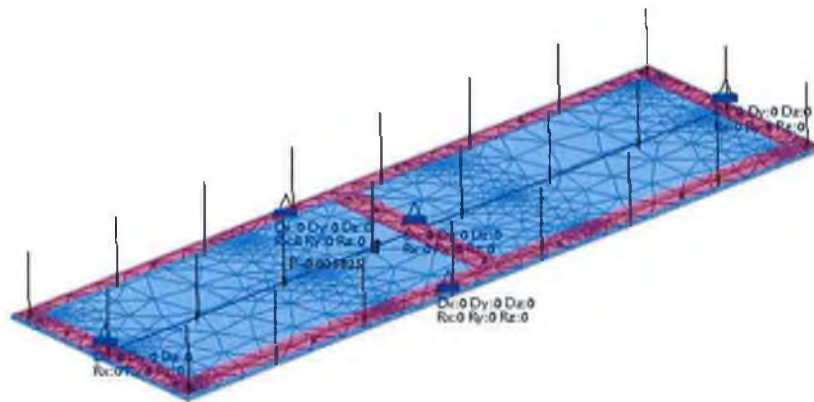


Figure 3-13: Constrains on the 12 mm perspex sheet

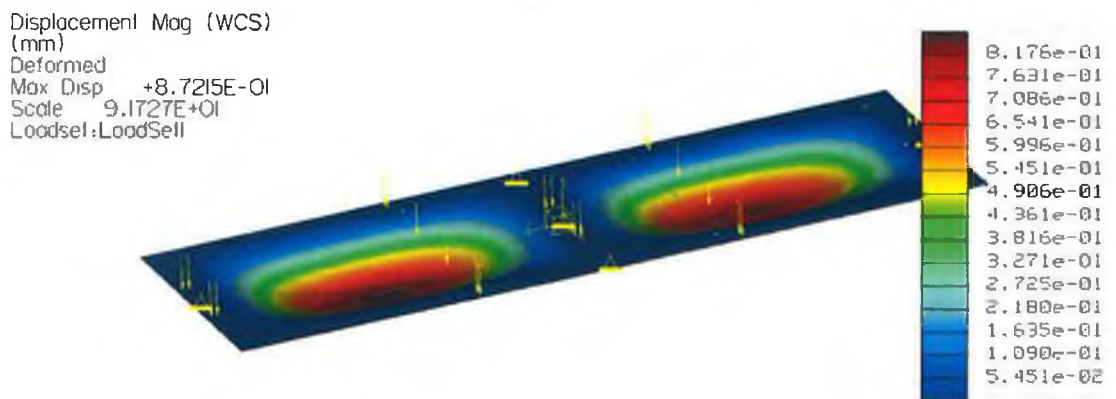


Figure 3-14: Deformation of the 12 mm perspex bottom plane

The material specifications as used in the analysis are as followed:

Table 3-5: Material properties of glass, perspex and polycarbonate

Material: Glass			
	Density	Young's modulus	Poisson's ratio
	$2.458 \cdot 10^{-9}$ [tonne/mm ³]	68935 [N/mm ²]	0.3
Material: Polycarbonate			
	Density	Young's modulus	Poisson's ratio
	$1.2 \cdot 10^{-9}$ [tonne/mm ³]	2300 [N/mm ²]	0.38
Material: Perspex			
	Density	Young's modulus	Poisson's ratio
	$1.19 \cdot 10^{-9}$ [tonne/mm ³]	3210 [N/mm ²]	0.3

Two situations will be tested. One situation will represent the maximum pressure of the water over the whole surface. The second situation will represent the increasing pressure over the height of the tank. The following tables show the results of the calculations:

Sidewalls:

Table 3-6: Deflection of the sidewall with polycarbonate and acrylate

Polycarbonate	8 mm	12 mm	Acrylate	8 mm	12 mm
Uniform pressure	5.79 mm	1.80 mm	Uniform pressure	4.46 mm	1.401 mm
Incremental pressure	2.91 mm	0.94 mm	Incremental pressure	2.24 mm	0.719 mm

Table 3-7: Deflection of sidewalls of glass

Glass	8 mm	12 mm
Uniform pressure	0.21 mm	X
Incremental pressure	0.11 mm	X

Front/back wall:**Table 3-8: Deflection of the front and back wall with acrylate**

Acrylate	8 mm	12 mm
Uniform pressure	1.58 mm	0.496 mm
Incremental pressure	0.839 mm	0.256 mm

Bottom:**Table 3-9: Deflection of bottom plane for acrylate and glass**

Acrylate	8 mm	12 mm	Glass	8 mm	12 mm
Uniform pressure	3.21 mm	0.87 mm	Uniform pressure	0.162 mm	X

Final choice

Glass will be used for the sides of the tank; the bottom, front and back will use 12 mm perspex, giving more flexibility to the design. The top will be made of two sheets with intersections of 4 mm. These will be assembled to form the hollow top cover.

3.2.3 Overall Weight of the scaled model

The water inside the tank will make up the overall weight of the model. The frame and the glass will weigh 98 kg. The tank is filled with $0.520 \times 0.500 \times 3.200 = 0.832 \text{ m}^3$ water. This results in $0.832 \times 998 = 830 \text{ kg}$ when the model is filled. Efforts were made to ensure that the tank was positioned on an even floor to avoid unnecessary stresses on the tank walls and frame.

3.2.4 Attachment of the load

The attachment of the simulated load is a significant challenge. It is imperative that all the blocks are restrained. A solid method of restraining the cargo is essential. Creating holes through the tank in order to attach the cargo should be avoided where possible.

Two basic types of loading will initially be tested which will be a full trailer load of 32- and 33-euro pallets. For time and budgeting purposes it is preferable that the

same restraining methods should be used for the 32-euro pallet configuration as for the 33-euro configuration.

Figure 3-15 shows a schematic picture with the restraining system in the tank.

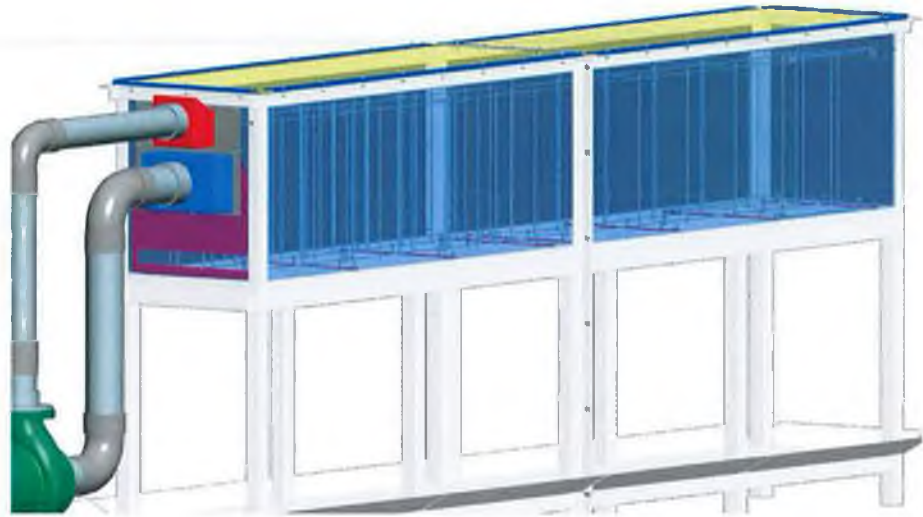


Figure 3-15: The water tank with the cargo attachment points

The system consists of stainless steel sheet metal strips and stainless steel bars which are linked up together restraining the cargo to one block.

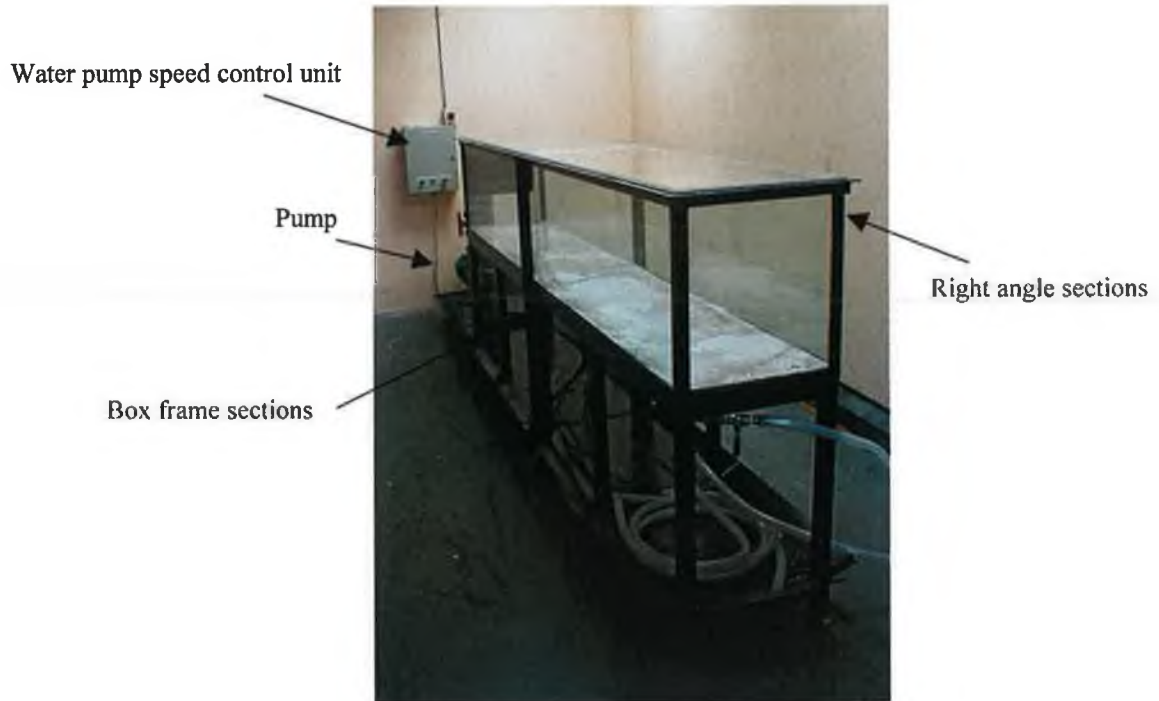


Figure 3-16: Photograph of the 1/5 scaled test rig of a refrigerated trailer

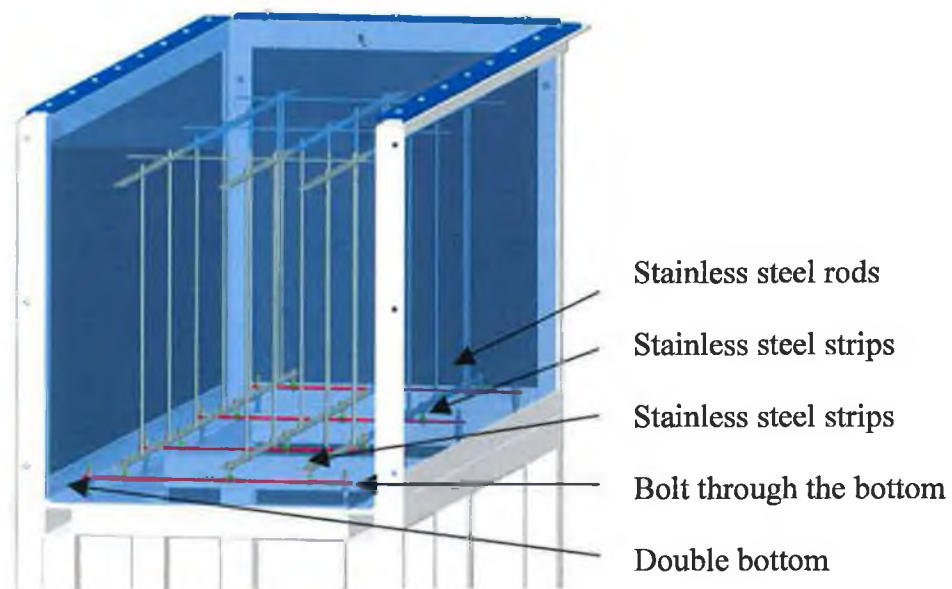


Figure 3-17: Cross-section of the water tank

The double bottom is attached to the floor with bolts. These same bolts are used to attach the red stainless strips as seen in Figure 3-17. These red strips are then connected to strips, which stretch the length and breadth of the unit. The cargo

blocks are mounted on these strips. Stainless steel rods through the block connect a similar mesh of strips on top of the cargo. All the blocks connected together form one solid assembly giving it stability and stiffness as Figure 3-18 shows.

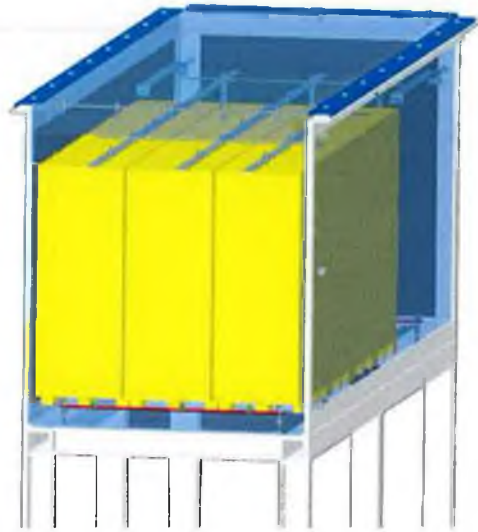


Figure 3-18: Cross-section of the tank with cargo

The next step is calculating the force on the cargo blocks if the complete water flow were to hit the cargo at full speed. The force can be calculated using equation 3-29 [81]:

$$F = \rho A u^2 \quad (3-29)$$

With:

F = force [N]

ρ = density [kg/m^3]

u = speed [m/s]

The area of the outlet is 96 x 36 mm. The density for water is 998 kgm^{-3} and the maximum simulation speed is 10 m/s. The maximum resulting force produced by the pump propelling the water is 345 N. This results in 345 N hitting the block at approximately 0.442 m from the bottom. The resulting momentum is $345 \times 0.442 = 152.5 \text{ Nm}$.

The width of the pallet is 160 mm. Therefore the required force needed to keep the block down in the most extreme conditions will result in 953 N.

Although it will never occur in a practical situation, the restraining system should be able to handle this force. The system of restraining however, will easily deal with this force since all the connections are linked up and form a matrix distributing the force to the bolts in the floor of the test rig.

3.2.5 Simulation of the different units

As previously mentioned, the aim is to design the test rig so it can simulate multiple layouts of air inlets in refrigerated trailers and trucks. This means that there must be an easy system to replace one layout with another one in order to carry out different tests.

The possibility to test truck units as well as trailer units is accomplished by exchanging the sheet metal parts on the front of the unit representing the refrigeration unit. The connection between sheet metal and the pipes will be accomplished by so called tank connectors that can be screwed together and sealed with the use of a rubber gasket.

3.3 *The propulsion system*

The decision has been made to use a water pump to circulate the flow around the tank instead of a scaled down version of the original fans used in refrigerated trailers. The main reason for this is the complexity and scaling issues arising from scaling the fans and the disputable improvement that would be achieved.

There are a variety of pumps available which are suitable for this application.

3.3.1 Basic pump selection

The pump must be capable of giving the maximum amount of flow needed to perform the simulation but should also be suitable to give a regulated flow as well. Regulation was initially to be accomplished with the use of a globe valve in the water supply pipe. This would mean that the pressure/head curve should not be too flat in light of the fact that regulation and stabilisation of the flow might be a problem.

Initial tests showed however that the regulation with the use of the globe valve was inconvenient even though the pump with the steepest curve possible was selected. The biggest problem was the occurrence of a cavity due to the pressure drop over the

globe valve, which resulted in a high quantity of bubbles in the tank. This possibly caused an oscillating effect and the pump started to oscillate the flow. The decision was made to purchase a speed drive to regulate the frequency of the pump giving a steady, less violent flow.

The performance curve of the pump chosen is displayed in Figure 3-19.

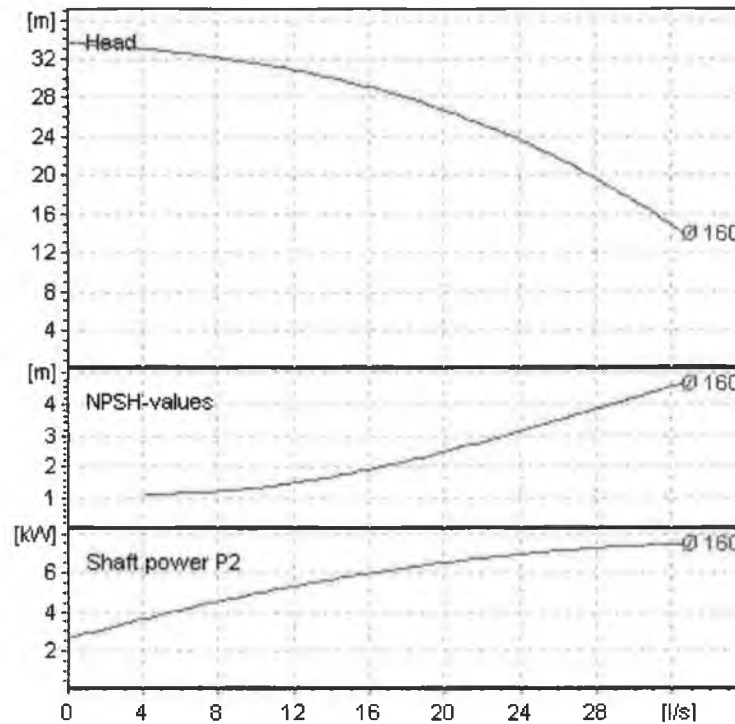


Figure 3-19: Performance curve of Wilo BN80/160-7.5/2

3.3.2 Pressure loss calculation

In order to simulate a flow of 20 m/s at the outlet in the scaled trailer the pump has to provide 86.4 m³/h of water. The loss in the pipes connected to the pump and the loss of the water flowing through the tank can be calculated with use of the formulas given in chapter 3 and chapter 10 of the 3rd edition of Fluid Mechanics [81].

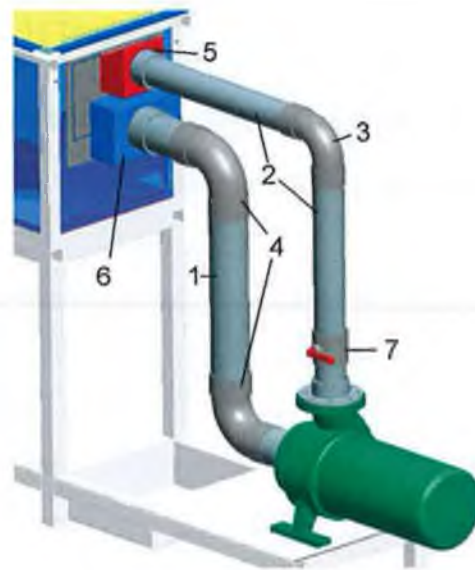


Figure 3-20: Reference numbers in the propulsion system

The reference numbers used below are taken from Figure 3-20. The pipe from the tank to the pump [1] has a 76.2 mm diameter and the pipe from the pump to the tank [2] is 63.5 mm.

The flow velocity in the pipe of 63.5 mm is:

$$V = \frac{24.1 \cdot 10^{-3} \text{ m}^3/\text{s}}{\frac{1}{4} \cdot (715 \cdot 10^{-3} \text{ m})^2 \cdot \pi} = 6.025 \text{ m/s} \quad (3-30)$$

The flow velocity in the pipe of 76.2 mm is:

$$V = \frac{24.1 \cdot 10^{-3} \text{ m}^3/\text{s}}{\frac{1}{4} \cdot (93 \cdot 10^{-3} \text{ m})^2 \cdot \pi} = 3.561 \text{ m/s} \quad (3-31)$$

3.3.2.1 Pressure loss in the corners

Equation 3-32 and equation 3-33 represent the calculation of the loss due to the corners in the pipes. The K factor for a 90° bend in a pipe is 0.9. The 63.5 mm pipe [2] has one bend [3] and the 76.2 mm pipe [1] has two bends [4].

$$h_b = \frac{0.9 \cdot V^2}{2 \cdot g} = 1.665 \text{ m} \quad (3-32)$$

$$h_b = \frac{0.9 \cdot V^2}{2 \cdot g} = 0.582 \text{ m} \quad (3-33)$$

$$\Sigma H_{b1} = 1.665 \cdot 1 = 1.665 \text{ m}$$

$$h_{ex2} = \frac{K_e \cdot V_i^2}{2g} = 0.323m \quad (3-37)$$

3.3.2.5 Head loss from expansion into tank

The expansion in the water tank [6] causes some losses also which are calculated with Equation 3-38. This is caused by the contraction from the pipe to the tank.

$$h_{E3} = \frac{V^2}{2g} = 1.850m \quad (3-38)$$

3.3.2.6 Head loss from tank back to pipe

Equation 3-39 calculates the loss of the flow from the tank to the return pipe [5].

$$A_1 = 480 \times 80 \text{ mm (estimated)}$$

$$A_2 = 250 \times 40 \text{ mm}$$

$$h_{E4} = \frac{V^2}{2g} \left(\frac{A_2}{A_1} - 1 \right)^2 = 0.353m \quad (3-39)$$

3.3.2.7 Head loss of the globe valve

The head loss of the globe valve [7] is calculated with equation 3-40 where the K-value for the globe valve is $K_e=10$. This is however a very high figure and might not be realistic since the valve is not closed and should not give too much resistance when in an open position.

$$h_{glb} = \frac{K_e \cdot V_i^2}{2g} = 18.50m \quad (3-40)$$

3.3.2.8 Total head loss

The total head loss in the piping system without the globe valve is:

$$\Sigma h_l = \Sigma H_{b1} + \Sigma H_{b2} + h_f + h_N + h_{ex1} + h_{ex2} + h_{E3} + h_{E4} \quad (3-41)$$

$$\Sigma h_l = 7.48m \quad (3-42)$$

The estimated loss inside the tank is 6 metres. The estimated loss is calculated by converting the typical pressure loss in a real trailer to the scaled model. The total will then be round the 13.48 metres, which should not give any problems when checking the pump performance curve as illustrated in Figure 3-19.

The globe valve is not taken into account as it is not used in the final design since a speed drive will regulate the pump speed and so the flow volume to prevent cavitations occurring.

3.3.3 Pipes and fittings

The velocity in the suction pipe should not exceed four (6 at max) feet/sec so as to prevent cavitations. This is exceeded however where we are up to 3.6 m/s (11.8 ft/s). Cavitation can be a problem when entering the tank and gives visualisation disturbances in the form of air bubbles. This is exactly as seen in the high-speed simulations, although it is hard to determine if the air comes from cavity in the pipe/pump system or air that is sucked in the tank along the sides.

3.4 Speed of the pump

The speed of the pump is controlled by a speed drive to be able to accurately regulate the velocity at which the water will enter the tank. Measurements of the performance of the pump results in the performance curve as seen in Figure 3-22. A different measurement is carried out when a bulkhead is installed since this gives a significant increase in pressure drop.



Figure 3-21: Speed drive control box used to control the pump speed

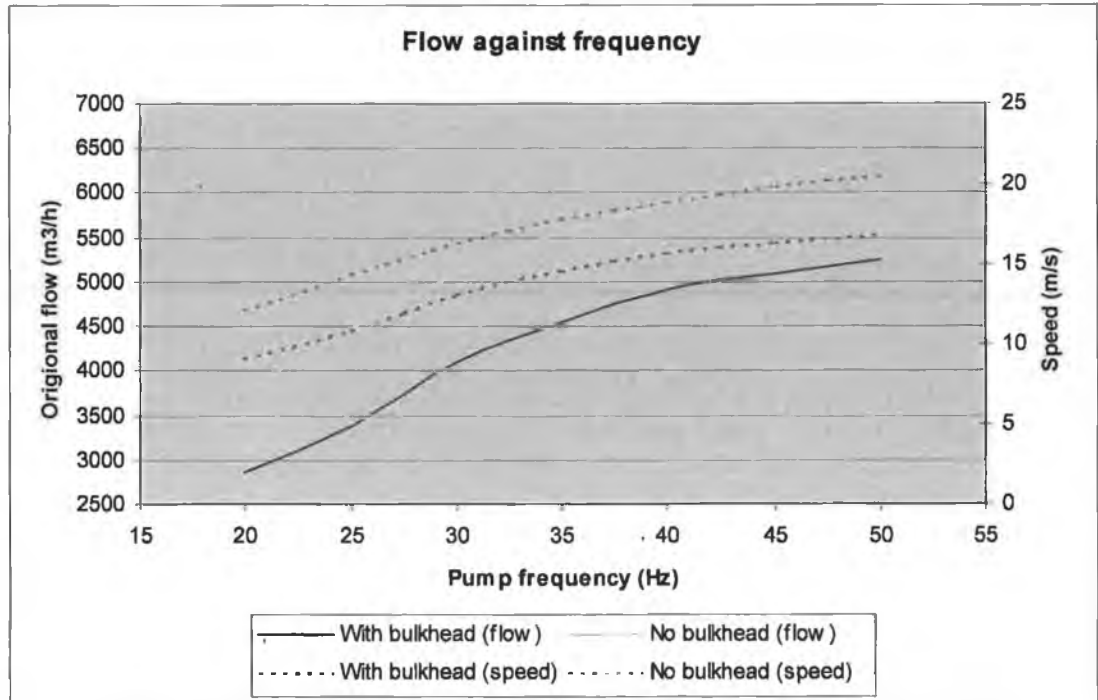


Figure 3-22: Measured performance curve of the pump

3.5 Scaling the cargo

The height of the cargo will be 2300 mm (scaled 460mm) at maximum to leave the 300 mm above the cargo where there is no load allowed. This 300 mm line is a little under the outlet of the refrigeration unit, so the full flow will initially go over the cargo.

The material to be used for the cargo simulation has to be easy to form, and needs to have a smooth surface. According to similarity rules, the surface finish of the simulated cargo should have a surface roughness of one fifth of the original cargo.

A soft material will be preferable since the form can easily be changed if needed, and the material should ideally have a high density so it won't float. This might however be of minor importance since the cargo has to be restrained anyway, but will ease the pressure at the bottom.

Possible candidates for simulation the cargo are shown in the table below and their advantages and disadvantages identified. The materials are given rated from 1-4 indicating their suitability relative to each other:

Table 3-10: Cargo simulation selection

	Roughness	Ability to form	Change shape later	Density	Total
(Sheet) metal:	4	2	1	3	10
(Polyurethane) foam:	2	4	4	1	11
Wood:	3	3	3	2	11
Bricks:	1	1	2	4	7

Looking to the table above, polyurethane foam is the best possible cargo simulator discussed, mainly because of its flexibility. The ease of forming and changing shape if needed for additional tests makes it very suitable for our simulation of different cargo types. When using metal or wood, shaping afterwards is difficult or even impossible in the case of metal where you have to make a new design, punch the parts out, bend them, weld them and paint them.

Low density is not a major issue since the cargo has to be connected to the bottom of the simulation tank anyway to make sure it is not blown away by the high water pressure. This connection will be accomplished with the use of the stainless steel matrix mentioned in paragraph 3.2.4, mounted to the bottom of the tank.

Initially, the polyurethane will be made into the shape of a square cargo block, including the shape of the pallet at the bottom. For further testing, these blocks can be cut in lower pieces to simulate cargo in different heights. These can be joined or glued together at a later stage again if required.

The problems with the roughness can be overcome by applying glass fiber sheets to the outer side. This will make a smooth surface, which may be desired for an accurate simulation, but will be omitted initially.

Chapter 4

Development of measurement equipment

4.1 General

Part of this project will be the development of a measurement system which analyses fluid flow in a simulation of a refrigerated trailer. This simulation system will contain a visual aid such as a dye or particles seeded in the fluid flow. Seeded particles in the water being analysed will be illuminated by a light sheet and captured using a CCD/CMOS camera. These acquired images will be analysed using a personal computer. The velocity and position of the seeding will be recorded and exported for further use and analysis.

Particle Tracking Velocimetry (PTV) and Particle Image Velocimetry (PIV) systems are widely used in practical fluid dynamics in different fields of operation. These systems can analyse fluid flow from two-dimensional to a full three dimensional spectrum. A lot of research has been completed in recent years and the PIV and PTV systems have been significantly improved in accuracy and ability with the availability of cheap mathematical calculation resources in the form of the personal computer.

Existing PTV and PIV systems however are far above the budget of this project, so the decision was made to create a system especially adapted for the purposes of the project.

The most expensive part of the system is the laser which will generate a light sheet on a chosen frequency. An important and extensive part of the task will be to find an affordable way of generating this sheet of intensive light.

This measurement system will roughly be divided into three sections:

- The flow visualisation
- The visual acquisition of the flow
- The analysis of the acquired digital images

The flow visualisation will take a deeper look into methods of seeding the flow with a dye or with seeding particles. Methods to illuminate the area of interest and the obtaining of a sufficient view of the flow will also need to be realised.

A digital camera will be used to acquire the images of the flow which are processed with the use of a personal computer. The data captured will then be stored for further analysis.

The software to analyse the acquired images takes the data from the digital high-speed camera and runs motion detection algorithms to calculate the flow velocity. The result of the analysis will provide data on the velocity, position and direction of the flow along with the possibility of generating a vector plot of this data.

4.2 Visual acquisition of the flow

4.2.1 High speed Camera and interface hardware

A high-speed camera is used to capture visual data from the simulation model. In general cameras have a sufficient density resolution to perform the analysis with a typical specification of 768 x 480 pixels.

Cameras are made with two different photonic chips, a CCD and the more recent CMOS.

All digital cameras consist of an array of *Charge Coupled Devices*, CCD's, each of which converts photons into electrical signals via the photoelectric effect. Essentially, a CCD consists of semi-conducting material bordered by a conductor. A small voltage is applied across the semiconductor. A potential well is thereby created within it. When a photon of the appropriate frequency enters the semiconductor, an electron-hole pair is formed. The hole is absorbed in the p-layer of the semiconductor, while the electron moves towards the potential well, where it is stored. Electrons accumulate within the well throughout the duration of the exposure. The amount of charge is proportional to the total light received. This CCD is also

called a *pixel*; digital cameras generally consist of an array of thousands or millions of these pixels.

In order to generate an image, the charge built up in each pixel must be measured; this is the main distinction between the different types of digital camera. Each photosensitive area is coupled to a Charge Transfer Device, or CTD, which is responsible for shifting the charge accumulated in each CCD to a common output without interference between the individual charge packets. These charge packets are then passed through a charge-to-voltage converter, which outputs a voltage proportional to the charge and thus the amount of incident light arriving at the CCD.

The difference between the CMOS and CCD models is to be found in the performance. The more recently developed CMOS chips are capable of higher resolutions at a higher capture speed.

Recent improvements in CCD cameras enable them to be much more sensitive to light, especially in the near infra-red light end of the spectrum. CMOS cameras are as sensitive to light as the traditional CCD chip as pointed out in Figure 4-1. This graph is sourced from the manufacturer of the camera.

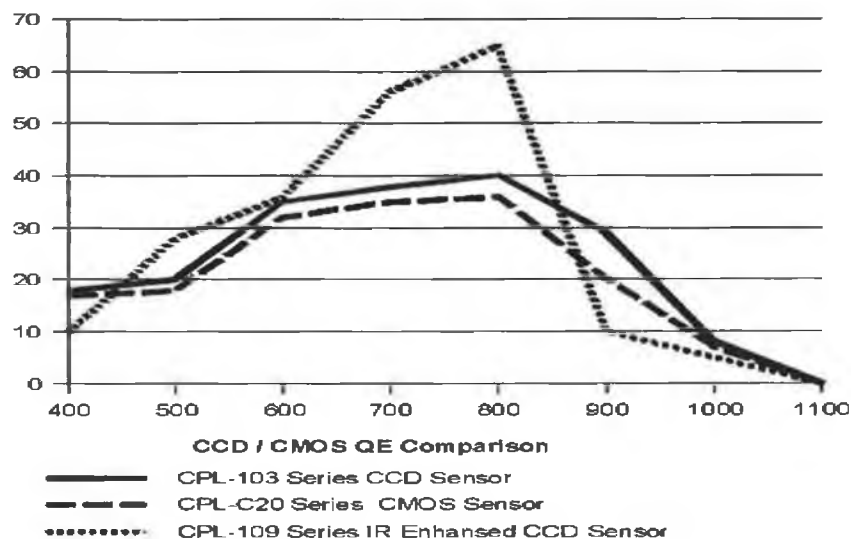


Figure 4-1: Comparison of sensitivity of CMOS and CCD photonic sensors

4.2.2 Capturing illuminated particles

The main difficulties in capturing illuminated particles can be summed up in:

- The exposure time
- The effective area
- The trigger of the camera

The exposure time is the time in which the CCD sensors accumulate the photons. A very quick shutter speed is needed to get a sharp capture of the particles on high speed. A quick shutter speed requires the image to be very brightly illuminated so as to capture it. This created the need for a very powerful light source as the CCD sensors need a certain time to accumulate the photons. A higher frame rate is needed when capturing a smaller area of flow since the flow will move relatively faster if looked at from close range. A brighter image is needed since the shutter speed needs to be faster to obtain a sharp image. The light, however, can be focused on a smaller area if indeed a smaller area is investigated.

The area that can be captured depends mainly on the size of the particles. The flow pattern will be less disturbed when the particles are small. If the area of capture is small however, a flow pattern will not be created due to the fact that the turbulence waves will then be bigger than the whole area of capture. If bigger particles are used, the flow will be disturbed by these particles. The problem of an incorrect reflection of the reality may occur although there will be a better overview of the entire pattern.

The camera operates within a typical high-speed PIV system synchronised with the trigger of the light sheet. Originally two pulses of the light sheet were captured in one frame. In the case of a PIV system the 'double exposed' frames were cross-correlated to get the flow pattern. This leads however, to a directional ambiguity arising because it is not known which pixels are from the first and which are from the second exposure.

Another option is to synchronise the camera to get two exposures in two different frames. This can be seen in Figure 4-2, which is usually called 'frame-straddling'.

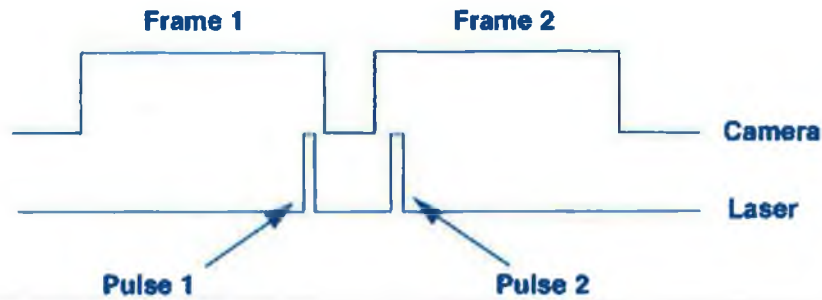


Figure 4-2: Synchronisation between the camera and two laser pulses

However, the problem is that the time between two exposures is dictated by the time the camera needs to read out the data from the first exposure and is ready for the next exposure. Specific modern cameras however, have ‘progressive scan’ methods, whereby the data is read out of the memory while the camera captures the image. This reduces the readout time gap between two images to milliseconds. This is very suitable for ultra high-speed capturing of images.

An optimum distance has to be found between the area that is being captured and the speed of the camera keeping in mind the limits in capture speed. The following example is extracted from the paper “visualization and PIV measurements of high-speed flows and other phenomena with novel ultra-high-speed CCD camera” [82].

If an area of 10 cm x 10 cm is reviewed and a resolution of 1000 x 1000 pixels is used, a particle travelling at 10 m/s (which happens in the case considered here) will travel 10 frames with 100 μ s between two exposures. The maximum exposure time has to be less than 10% of the time between two sub sequential frames to prevent blurring. The camera used for the experiment can only handle a fraction of the speed given above, as the camera cannot read out the acquired images quickly enough. The initial aim will be ‘double exposure’ capturing where two pulses will be captured in a single frame or alternatively achieved though looking at a bigger area in order to lower the speed that is required. An important factor will be the restriction dictated by the minimum exposure required to be able to register the particles as such by the high-speed camera. It also has to be reviewed whether high speed flow needs to be captured or whether the relative slow flow gives enough data as it leaves the main stream.

4.2.3 Camera calibration

4.2.3.1 Camera timing

To calculate the quantity of errors that occur in the time between different pulses the camera timing must be calibrated. This can have a big impact on the results from the software.

Calibration is achieved by connecting a scope to the output of the camera. This output gives the signal in which the camera captures the frames. This signal is a low output when capturing and a high output when idle. The metre used was a Fluke 105B Scope metre series II, which can analyse the signal and give accurate information on the duration of frequency of the pulses. The metre was recently calibrated.

The result of the analysis is that the requested frequency at the range to be used is approached to within one percent of its actual value and within half a percent of the value given by the software (due to a round off). The same error is found in the higher frequencies (tested up to $15 \cdot 10^3$ FPS). The value reached at those speeds is usually within 5% of the requested value.

The exposure shutter time is calibrated in order to determine the speed of particles by measuring the displacement during a frame, and results in an accuracy within half a percent at medium resolutions and within 2% at the highest resolution (1280 x 1023).

4.2.3.2 Image calibration

The image taken by the camera has to be reviewed. The camera has a lens that deforms the image, and the exact length of the path that a particle travels needs to be known in different planes (cross section on a certain distance from the lens) of the tank.

A schematic representation of a camera with lens is shown in Figure 4-3.

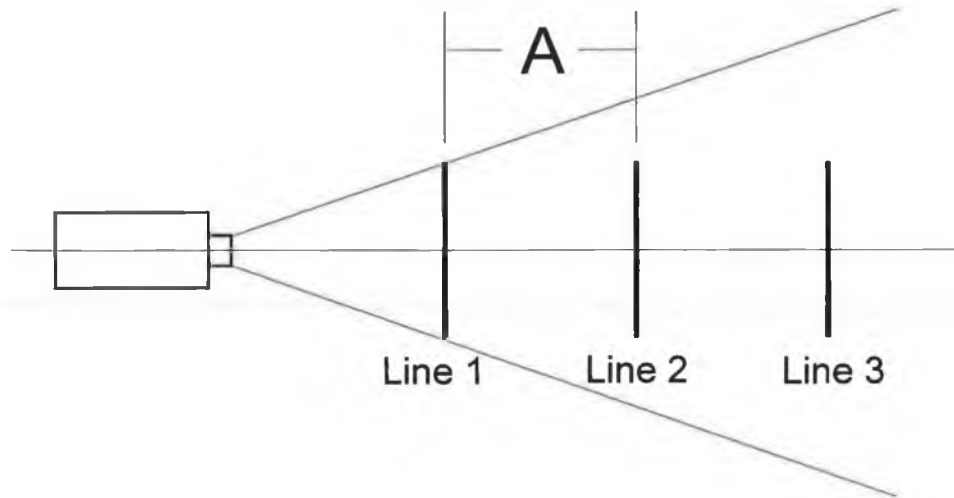


Figure 4-3: Schematic representation of a camera

The length of the lines 1,2 and 3 are the same, but the last line appears to be smaller than the first on the screen. Assume line 1 and line 3 are the outside glass planes of the tank, and line 2 represents the light sheet. The scaling has to be calculated since it is not possible to measure a distance in the tank, only outside the tank. This will be achieved by making a formula dependent of length A from the front, where we can measure the length of line 1 (represented by for example a ruler stuck to the glass) and so calculate the length of line 2 as recorded by the camera.

Figure 4-4 shows the geometry of the calculation involved. The formula to calculate the length of line 2 in pixels can be seen in equation 4-1 and is illustrated in the picture below.

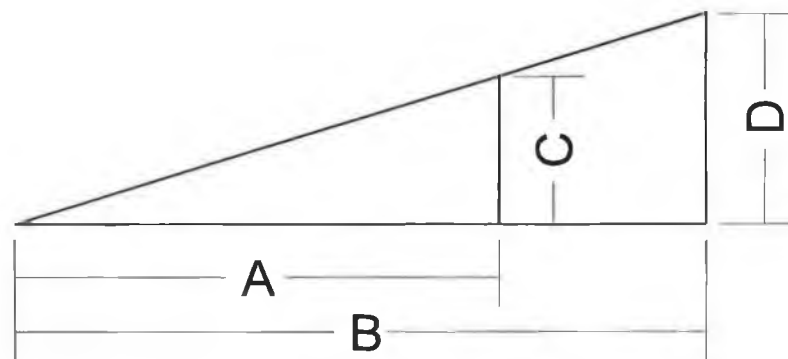


Figure 4-4: Geometry of the deformation of the image on the camera

$$Pix_D = \frac{Pix_C}{\frac{l_B}{l_A} \cdot l_C} \cdot l_C = \frac{Pix_C \cdot l_A}{l_B} \quad (4-1)$$

In which:

Pix_C = the amount of pixels on the image representing line C

Pix_D = the amount of pixels on the image representing line D

l_A = the length of line A

l_B = the length of line B

l_C = the length of line C

The above formula can be used to calculate the movement per pixel of the particles captured with the camera at all positions of the light sheet. The speed per pixel of the particles can be calculated when the time between two frames is added in the formula. This is illustrated in equation 4-2, where Δt is the time between two frames and V_p the velocity of the particle.

$$V_p = \frac{Pix_C \cdot l_A}{l_B \cdot \Delta t} \quad (4-2)$$

This velocity can then be used as a parameter in the program to get the actual velocities in m/s in the vector plot.

The above method was tested and approved by capturing a ruler in the positions one, two and three and comparing them with the calculated length of the ruler with the image one as base. The method is accurate according to the results.

4.2.4 Ideal distance to capture the flow

Some thought has to go into the ideal distance from the tank to capture the flow. The capture speed and the light intensity can be lower and the particles bigger when the camera is far from the tank. The light sheet however has to cover a bigger area.

If a flow of 1 m/s is to be captured with a camera resolution of 1000 x 700 pixels. Initially this will be at a distance so the image will represent 500 mm x 350 mm and the max desired displacement of a particle in a frame is 10 pixels. This means that the particle can only travel 5 mm in a frame, resulting in a needed capture speed of 200 fps.

The same situation could be taken again with the camera closer to the object where it represents 250 mm x 175 mm. This means that 10 pixels represent 2.5 mm. Hence, 400 fps will be needed in this experiment.

The light sheet only needs to cover 250 mm but at 400 fps, resulting in 250 mm times 400 fps, which will give the same result as the previous example suggesting that the same amount of light is needed.

The conclusion from the above short example is that the intensity of the light out of the light sheet will be approximately the same for every position of the camera. The speed on which we have to capture the flow however increases when we move closer. This means that it is easier to capture at a greater distance since the capture speed can be lower and the area covered by one shot is larger making the analysis of the whole tank quicker and easier. It means however that the seeding particles have to be sufficiently large to be identified by the software.

4.3 Flow visualisation

This chapter will deal with the visualisation of the flow inside the simulation tank. This involves the seeding of the flow with the use of a dye or with seeding particles and the generation of an intensive light sheet to highlight the zone of analysis in the flow.

4.3.1 Dye injection flow visualisation

The first idea was to inject a dye in the fluid flow. A dye is a coloured fluid injected in the flow to visualise flow patterns. There are different types of dyes as discussed in the literature review, and a dye suitable for our application is one that will be illuminated by a certain wavelength of light as we only want to see a cross-section of the flow pattern in the tank. The dye should not be visible or nearly invisible under normal circumstances.

This means that we need a dye that reacts to a wavelength that is not so much present in normal light, thus keeping the dye invisible, so normal light can be present in the laboratory. A special light may then be used to illuminate the dye as desired.

The disadvantage of a dye however, is that it cannot be circulated, as could particles seeded in the flow. There is only one shot after the dye is injected into the flow, where the pattern of the dye flowing through the water has to be captured instantly in order to analyse the flow and the flow pattern. The dye will, because of the high turbulent state of the flow, mingle very quickly – possibly resulting in an unclear picture of the flow development. Another problem is that the dye will saturate the water inside the tank relatively quickly as smoke does in a trailer. This is probably the biggest issue since this will mean that the dye either has to resolve in a short time or that the water has to be replaced. Replacement of the water after every test is not feasible since the tank holds more than 800 litres of water, so the only option is to get the dye out of the water or let it gradually dissolve .

The overall conclusion about using a dye is that it might be a suitable option for demonstrations but is not a feasible option for the flow analysis at this stage of the project.

4.3.2 Gas bubbles visualisation

Another possible visualisation tool is the use of a gas. It is possible to inject a gas like air into the water, which will give a flow pattern in the water, but will be slightly inaccurate because of the difference in density between air as a gas and water as a liquid.

Heating up the water is a method where bubbles will appear which can be used for tracking the flow as well, but the disadvantage of this method is that the bubbles will dissolve quickly and acquisition of the flow must occur close to the generation of the bubbles. Moreover generation of the bubbles in a high-speed flow might not be feasible at all due to the amount of heat that is needed to create them.

Another possibility will be the use of air injected into the water before being mixed in the pump. Cavitation in the water stream may result as well in bubbles in the water, and for example the obstruction caused by a globe valve will help to generate them. The problem when adding air to the system is that the air will disturb the flow since the air bubbles are very bright and big and will therefore be seen by the camera - even outside the light sheet. Big air bubbles make motion detection almost impossible.

The use of a gas as visualisation is therefore not the most preferable way and although it is clean and easy to create, visual analysis will be almost impossible. This renders the idea less preferable above the next method - seeding with particles.

4.3.3 Visualisation with seeding particles

Particles for flow visualisation and PIV/PTV systems are available on the professional market, and have a wide variety of characteristics. Particles for these simulations have a number of properties that are important:

- Size
- Density
- Colour

The size of the particles is one of the important properties. Professional fluorescing particles are available from a few μm to 300 μm , but this is not big enough for our

purpose of tracking particles with the use of a high speed CCD camera. The particles have to be between 500 μm -1000 μm for our purposes. The problem with those particles is that they don't adapt as well in the flow as smaller particles. It has to be verified that the particles fully integrate in the flow in velocity as well as direction.

Particles should have a density close to that of the fluid which is used for the simulation to prevent gravitational effects in the movement of the particle in respect of the fluid. This is a property which becomes less important when the simulation speed has a high velocity.

The particles should reflect enough so it is possible to apply a sheet of light to highlight a certain region of the tank. Transparent particles will be the best since they will not inordinately disturb the image before the light sheet and will scatter the light when passing through the light sheet.

Three types of particles have been acquired where the paper published by ZARM [83] has been the basis for the selection. The particles were:

- Vestisint 2157 nc from Kunststoff Vertreib GmbH, Germany
 - Density 1.016 g/cm³
 - Size 57 μm
 - Colour transparent
- Omya Q-cel 6019
 - Density 0.20 g/cm³
 - Size 75 μm (mean, between 5 - 160)
 - Colour transparent
- Nova Chemicals Polystyrene
 - Density 1.06 g/cm³
 - Size 100 μm
 - Colour transparent

The polystyrene and the vestisint were tested in the water tank; the Q-cell was not since it is hazardous for health and environment. The vestisint gives the best result as it has a density that is almost the same as water and mixes well with the fluid, in our case water. The particles are very small giving a very good representation of the flow. The reflection of the light is near perfect so the vestisint is a well recommended

seeding powder. The size of the particles is, however, so small that it requires the camera to be very close to the tank and zoom in on a small area as discussed in paragraph 4.2.4.

The polystyrene particles are less suitable than the vestisint as they are slightly heavier than the water, not as good in reflecting the light and are not as uniform in size and shape. They are however on average twice the size of the vestisint particles. This in combination with the weak light source makes tracking the particles much more feasible considering the distance from which the flow will be captured using the high-speed camera. The particles follow the flow well and will be the main utilised seeding material used in the experiments. Vestisint however should be kept in mind if at any stage in the project detailed flow details are to be captured in a small cross section of the flow.

4.3.4 Light sheet

4.3.4.1 Developing the light sheet

A clearer understanding of the light intensity needed for PIV/PTV applications was acquired after the first tests. Halogen and metal-halide lights were initially utilised. The halogen light had a power of 250 Watts and was not powerful enough and, therefore, the light was not intense enough. Tungsten lamps (such as the halogen light) have only an efficiency of 10% resulting in only 25W of light power, the same amount of light an 83 W metal-halide lamp will give.

The metal-halide lamp gave an excellent white bright light after the warming up period but the light intensity was not, to being with, enough for optical acquisition with the camera. The light was working on the frequency of the power mains as well, which is 50 Hz. This means that the light goes on and off 100 times a second as represented by the harmonic curve in Figure 4-5 where the net frequency is 50 Hz. The camera speed has to be at 100 Hz, meaning that we need to acquire the images at a longer distance from the tank as illustrated in paragraph 4.2.4 because of the low frequency.

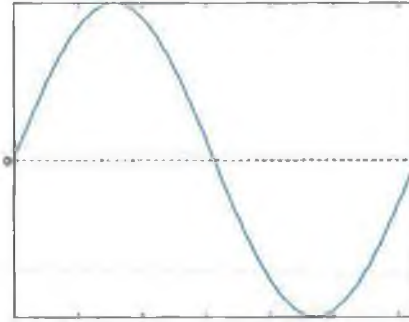


Figure 4-5: The sinus curve of the power supply on 50 Hz

The resulting light sheet looks as seen in Figure 4-6, which is well suitable for visualisation purposes and the primary image acquisition.



Figure 4-6: Flow visualisation with a Metal-Halide lamp



Figure 4-7: Metal-Halide lamp illuminating the particles in the tank

There is however the possibility of using 3 lamps and putting them all on a different phase of the main power supplies. This might eliminate the flickering sufficiently so as to make it suitable for the high-speed camera and it would also give more light. A 400 W Metal-Halide light became available later which was used for the next test, which gave a better result than the 250 W, but was not intensive nor even enough for accurate measurement throughout the whole field of view.

A histogram of the intensity measured over a very good frame was captured with the high-speed camera as seen in Figure 4-8. This indicated that the main intensity is between 50 and 100 of the complete 255 light intensity range. The conclusion can be made that there is not much of a contrast in the image where the distribution is limited to a small range. Stretching this over the whole spectrum range can sharpen

the image, but it means that the contrast between the particles and surroundings is very small. This illustrated the need for a very bright light source or at least a very good reflection to get more of a contrast between the particles and the surrounding areas.

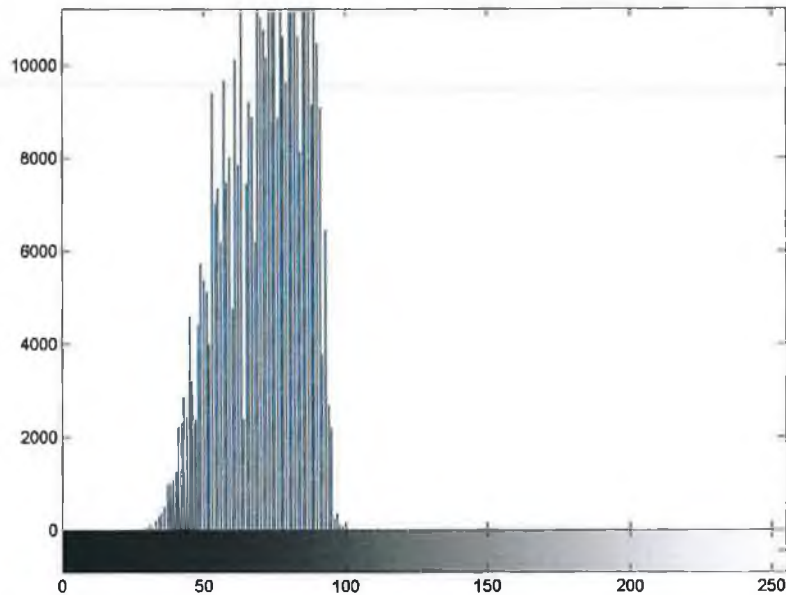


Figure 4-8: Histogram of intensity over an image

The first test with a laser used a Helium-Neon laser, which has a continuous beam with an approximate output of 2 mW. Particles are clearly visible while using the beam with its original diameter of approx 0.8 mm. The result gives an idea of the power of the laser, but this particular laser is not powerful enough to generate a light sheet suitable for this project.



Figure 4-9: Tank set-up with the high-speed camera and optics



Figure 4-10: The 2mW laser used for initial laser tests

These findings indicate that a higher amount of power was needed and contact was made with the National University of Ireland, Galway (NUI, Galway) to use their PIV system to test the intensity of a laser diode and compare it to their Nd:YAG laser.

The laser diode used has a measured output power of 17.1 mW. The frame as seen in Figure 4-11 is made with an illumination time of seventeen microseconds, which is unacceptable for the application where the exposure time should not exceed one microsecond to prevent blurring. The exposure of seventeen microseconds, however, gives the equivalent of 0.29 mJ over the pulse length over a width of 50 mm, generating the need of a power of at least 1 mJ per pulse. This estimation is based on the width of the light sheet and the width for the application as well as the concentration on the edges of the line. All these factors render this laser unsuitable for use.

The frame made with the Nd:YAG laser is seen in Figure 4-12. The estimated power of the laser pulse is 10 mJ and that is more than sufficient. It is however over only 100 mm meaning that we need 4.5 –5 times as much power to get the same result with our set-up. A difference with the system as developed in this project will be the particle size and type. The particles used at this experiment have a mean diameter of 5 μm instead of a mean diameter of 100 μm , and the material is Polyamide 12 instead of polystyrene. The effect of the different particle size is not tested.



Figure 4-11: Laser diode



Figure 4-12: Nd:YAG laser

4.4 Analysis of the acquired digital images

4.4.1 Software package

Matlab, from the Mathworks and Fortran, was chosen. Matlab has the option of using the conventional way of programming and the schematic method. However, Matlab is slow if it comes to image processing. Another option is to use the C++ compiler and compile the Matlab program before use which can result in a speed increase of up to 40%.

Fortran is the mathematical programming language commonly used when performance is needed, and will be used to compile programs for the heavy calculation work.

4.4.2 Methods of analysing the motion

There are essentially two classes of particle image velocimetry (PIV) systems: algorithms that use grey-levels to operate (e.g. standard cross correlation) and methods that operate using particle coordinates.

The first group performs well in high particle density flows, but is limited by spatial resolution and the noise volume. Correlation based methods perform well if the window size is small compared to the local change in velocity but does not perform if the local change of the particle displacement exceeds the diameter of the particles itself. This can happen in places where vortices happen, or where heavy turbulence is encountered.

Conventional PTV methods perform well in low seeded fluid flows where the displacement between two recorded frames is small compared to the distance to the next neighbouring particle. PTV methods however are strongly affected by out-of-plane noise.

A method to increase the performance of PIV is to combine it with PTV, giving a spatial resolution, which is close to the theoretical limit and allows a reasonable particle density.

The use of light intensity offers a different method of analysis. This method is not previously used as far the literature review is concerned. The light intensity analysis (LIA) works on the principle of the CMOS chip of the camera. The chip counts over

the exposure time the amount of energy that is submitted to it. This information can be used for the analysis. Rather than pioneering this method, results were initially sought using more conventional methodology.

4.4.2.1 PIV and light sheet distribution

It is especially important for PIV that the distribution of light over the exposed image is uniform. The two images below illustrate this:

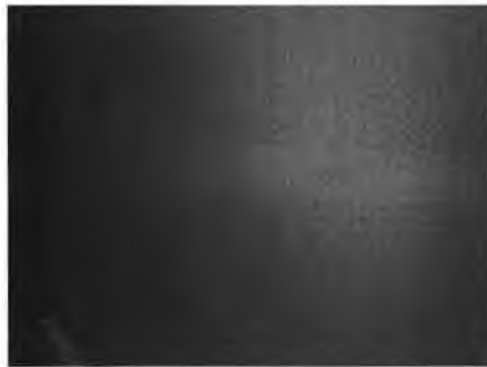


Figure 4-13: Original image

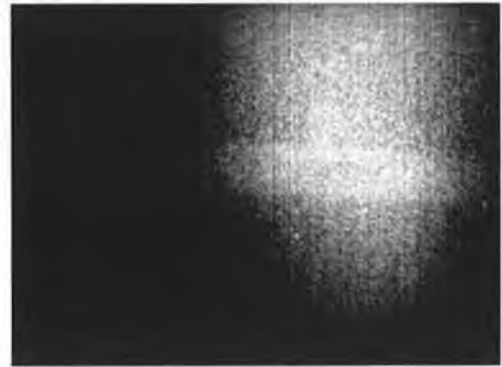


Figure 4-14: Image enhanced by software

Although the original image seems very usable, enhancing it to a higher quality of usability with image analysis software points out that the intensity distribution over the whole of the image is not equally spread out. The result is that only a small part of the frame can be used for analysis.

A way around this is to enhance the image by taking small parts of the image and enhance them individually and then combine them again in an overall image. This however will be a very complicated procedure as there cannot be any sudden changes in the intensity of the image since this will disrupt the recognition process. PTV is a little less sensitive to intensity changes since it mainly has to recognise individual particles and does not cross correlate. This will be discussed further in the next chapter in which the creation of recognition software will be outlined.

4.4.2.2 Preliminary PIV tests

Sample PIV code written in Matlab was found after doing some background study. Three different codes were investigated:

- MatPIV J.K.Sveen, Department of Mathematics, Mechanics Division, University of Oslo, Norway
- Mpiv Nobuhito Mori, Department of Fluid Mechanics, Central Research Institute of Electric Power Industry (CRIEPI), Abiko, Chiba 270-1194, Japan
- UraPIV Alex Liberzon and Roi Gurka

MatPIV gave the best results of all three and was the most complete package and almost the fastest code. Above codes were, however, successful in only one simulation run at ideal circumstances with a very low speed and a small area to review. This result is shown in Figure 4-15.

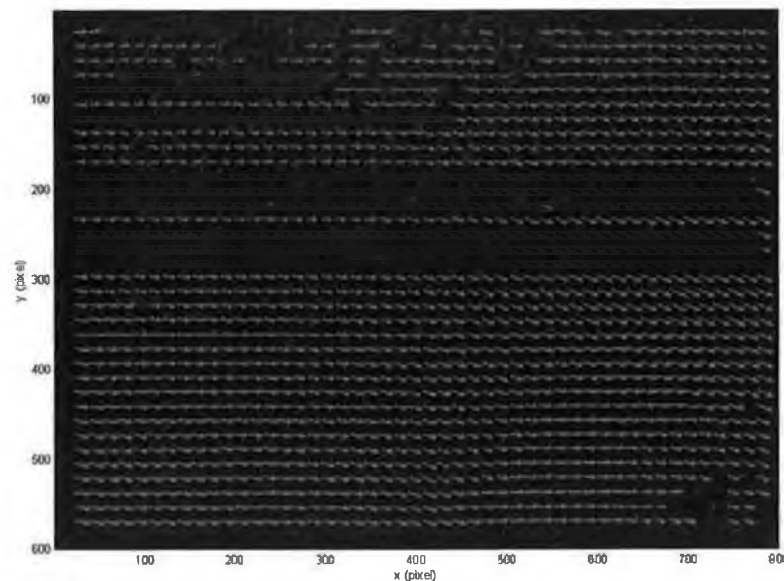


Figure 4-15: Some of the first successful PIV results in ideal circumstances

It proved, after additional testing, however, to be very difficult to get consistent results even in the same ideal circumstances at an almost still standing flow. The idea of using PIV seems not to be viable at this point due to the low light intensity available. PIV results are usually taken from an image pair with a very high contrast which can possible with to a very powerful laser over a very small area. However, such a laser was not available for the above tests.

4.5 Creating the program

4.5.1 Extracting the particles from the image

As mentioned before, the quality of the image coming from the camera is very low compared to what existing PIV and PTV software usually work with. PIV and PTV work with different methods, where noise is a smaller problem with PIV as long as there is a good contrast in the image, and can cross correlate a certain area of the image between two frames. PTV however needs to identify every particle, and needs an enhanced image, but needs less contrast compared to PIV.

It is desirable basically to separate the background from the image resulting in only the particles being displayed. The normal way to separate the particles from the background, and in this way identify them, will be by using a threshold value to represent the background intensity, where all pixels with a lower greyscale value will be ignored and all above it identified as a particle. This however requires a very uniform intensity level over the image, which we do not have with the current equipment. More information on those processes can be found in the appendix: PIV/PTV systems.

4.5.2 Speed comparison Matlab, Fortran

An early stage benchmark is performed to decide if an additional programming language is needed beside Matlab to do the bulk of the mathematical calculations. The speed benchmark was between Matlab and the mathematical programming language Fortran since it is the fastest mathematical programming language available.

The program at that stage took 64.11 sec in Matlab to complete where an 11.28 sec was enough for the compiled Fortran program. This is a big improvement, where most of the time is taken up to write the data to a file from Matlab, read it in Fortran and then vice-versa. The Fortran code itself takes approximately 2.68 seconds to complete including reading and writing to the disk, where the bulk of the 64 sec Fortran does the same as Matlab in less than 2 sec.

The results of the two methods are exactly the same, so Fortran is used in addition to Matlab for the heavy calculation.

4.5.2.1 Pixel identification

The decision was made to investigate the possibility of creating our own software to extract the particles and possibly trace them afterwards. A PTV system will work better for our application since the quality of our initial light sheet produces frames with not enough contrast for PIV systems.

The first idea was to make a variation to the threshold function where a cut-off value is chosen to decide if a pixel is related to a particle or not. The image is divided in multiple sub-sections because of the non-uniform light distribution over the whole image (as seen in Figure 4-16, where the intensity of light is highest at middle-top).



Figure 4-16: Frame of movie fragment used for developing the program

The average intensity of each subsection is calculated as the background noise and as well the maximum value in the subsection that represents the brightest pixel. Then a decision if a pixel is part of a particle is made according to the next two rules:

1. The value of the pixel has to be higher than a 'cut-off' value above the average to cut out noise. (Equation 4-3).
2. A relative value calculated between the maximum value of the subsection and the average, and has to be above a 'trigger' value. (Equation 4-4).

$$image(x, y) - avg > cut - off \quad (4-3)$$

$$\frac{\text{image}(x, y) - \text{avg}}{\text{max} - \text{avg}} > \text{trigger} \quad (4-4)$$

The result of the algorithm is seen in Figure 4-17, where a low cut-off value is used to underline the weaknesses. Analysing the image brings forth two major problems:

1. Lines seem to be detected as a result in intensity fluctuations within the image, which will be dealt with in paragraph 4.5.2.2.
2. The detection does not work well enough within the different subsections where a shift of detected pixels occurs over the box as the pixel values change too much within one subsection. This is caused by an uneven background noise value over the subsection. Smaller boxes will improve this slightly but do not have much effect since the decision is made relative to the values in the box. A new code proposal can be found in paragraph 4.5.2.3.

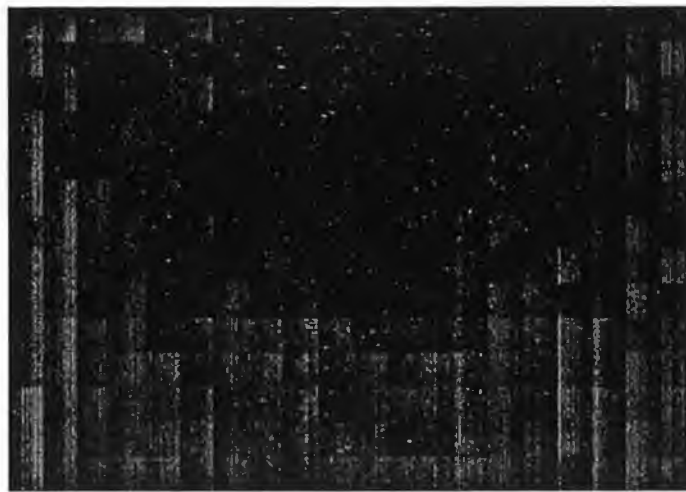


Figure 4-17: Result of the first calculation algorithm

4.5.2.2 Intensity fluctuation in the image: levelling algorithm

The first algorithms result in a very good initial result after tuning the parameters.

However, a shifting in intensity every second line in the image (Figure 4-18) appears due to the fact that the camera reads out every second line in one round after which it takes the remaining lines. This was created by the calculation algorithm due to the low contrast in the image.



Figure 4-18: Different intensities on every second line causing stripes

This issue had to be addressed first with a calculation algorithm to level out the difference. The algorithm calculates the difference between every two pixels on a line, and takes the average of all those values. Every second pixel was corrected with this value to reduce the contrast between the lines.

This resulted in an image where the fluctuation between two frames was typically not more than 1 grey value as seen in Figure 4-19, which is the same as seen in Figure 4-17 with added levelling algorithm.



Figure 4-19: Frame after introduction of levelling algorithm

The problem of the lines is now solved although there is still the problem of an uneven distribution throughout the different subsections and that will now be dealt with.

4.5.2.3 Background analysis algorithm

After the image is levelled out and the intensity problem solved, a new way of determining the background value on pixel level has to be developed.

The problem with the averaging of a box is that it only gives an accurate value for a small region within the box. This means that a calculation algorithm has to be developed to make a dynamic representation of the background intensity.

A one-dimensional variable background value can be created if the background values on different points on a line are known and the rest can be interpolated. So, if from different subsections the average values are known and those are used to interpolate over the whole length of the line then an accurate representation of the background value on pixel level should be achieved.

Thus a formula was created that calculates the relative value of every pixel between two points proportional to the position between those points and then multiplies it with the values of those points. It can be seen in equation 4-5.

$$f(x) = \frac{x_2 - x}{l_x} V_1 + \frac{x - x_1}{l_x} V_2 \quad (4-5)$$

Equation 4-5 follows out of equation 4-6 and equation 4-7 with the value V_1 and V_2 , which respectively represent the values as x_1 and x_2 , where Figure 4-20 and Figure 4-21 explain those formulas. The length l_x is the calculated difference between x_1 and x_2 .

$$N1(x) = \frac{x_2 - x}{l_x} \quad (4-6)$$

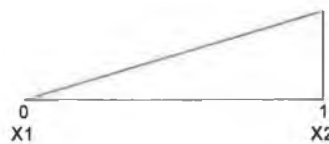


Figure 4-20: Schematic representation of equation 4-6

$$N2(x) = \frac{x - x_1}{l_x} \quad (4-7)$$

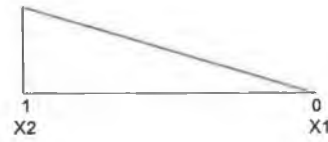


Figure 4-21: Schematic representation of equation 4-7

If we now apply this theory to a two-dimensional block then we could create a formula giving an interpolated background value for every pixel in the subsection and do the whole image sub sequentially.

The coordinate system and the values in the following formulas are seen in Figure 4-22, and the formula for the two-dimensional situation is given in equation 4-8.

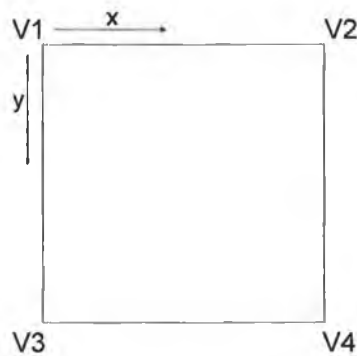


Figure 4-22: Explanation of the coordinate system and values V1 to V4

$$M_1(x, y) = \frac{x_2 - x}{l_x} \cdot \frac{y_2 - y}{l_y} \quad (4-8)$$

$$M_2(x, y) = \frac{x - x_1}{l_x} \cdot \frac{y_2 - y}{l_y} \quad (4-9)$$

$$M_3(x, y) = \frac{x_2 - x}{l_x} \cdot \frac{y - y_1}{l_y} \quad (4-10)$$

$$M_4(x, y) = \frac{x - x_1}{l_x} \cdot \frac{y - y_1}{l_y} \quad (4-11)$$

The values of V₁, V₂, V₃ and V₄ are calculated from the averages of the different subsections as can be seen in Figure 4-23:

- Point 1, and all the corner points will be the same as the average of that subsection.
- Point 2, and all points along the edge are an average of the average of the two aligning subsections.
- Point 3, and all internal points are an average of the four subsections around.

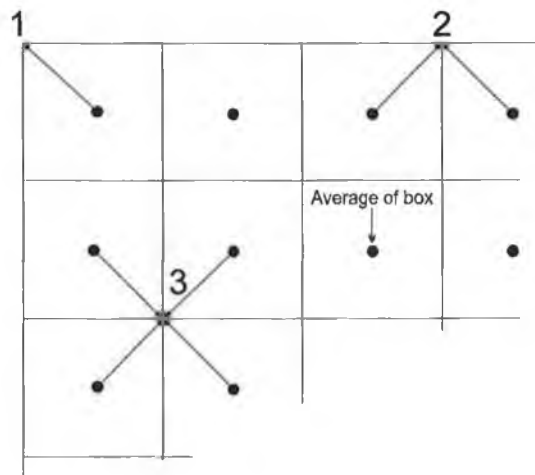


Figure 4-23: Averaging rules used to calculate corner values.

This will give a representation of the background if the subsections are kept small enough relative to the complete image (not bigger than 10%-15% of the total).

To test the algorithm, a gradient image is created and run through the algorithm. The recreated image of the algorithm should give a good representation of the original picture, especially if there is no disturbance or background noise within this example.



Figure 4-24: Original image



Figure 4-25: Re-created image

The resulting image is an almost identical image except that it is a bit lighter in the left top corner, and darker at the right lower corner due to the use of the average value of the subsection on the sides instead of an average of multiple subsections in the middle.

An analysis of the movie frame as used before gives the result as seen in the figures below, where a 3D plot of the actual grey values of the image is presented. The spikes in Figure 4-28 represent particles and background noise, which are eliminated in Figure 4-29. The overall curve on both the images is the same, which confirms that the calculated image is a good representation of the background of the original image.



Figure 4-26: Original frame



Figure 4-27: Calculated background

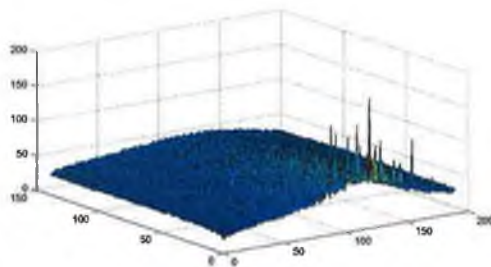


Figure 4-28: 3D grey value plot original

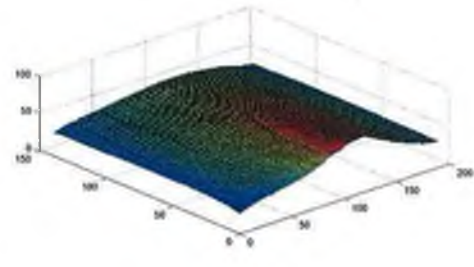


Figure 4-29: 3D grey value plot calculated

The conclusion so far is that this method of regenerating and identifying particles has a good chance of achieving positive results in combination with PTV calculation algorithms. Particle Image Velocimetry (PIV) will probably not work with those images since the density and equality of the image is not suitable.

4.5.2.4 Eliminating neighbour points

A routine is added to eliminate neighbour pixels preventing the tracking algorithm from detecting a zero velocity with detected pixels just beside the pixel under investigation. This is needed since some particles are spanning 2 or three connected pixels. Since this represents only one particle, only one pixel should be highlighted in order for the tracking algorithm to handle it as such.

This routine is currently very simple and works on the principle given below. It can be improved by developing a more 'clever' selecting algorithm in which the middle of a series of points connected to each other is calculated and replaced by a single point. The current algorithm looks only at a maximum of 6 positions around the point under investigation.

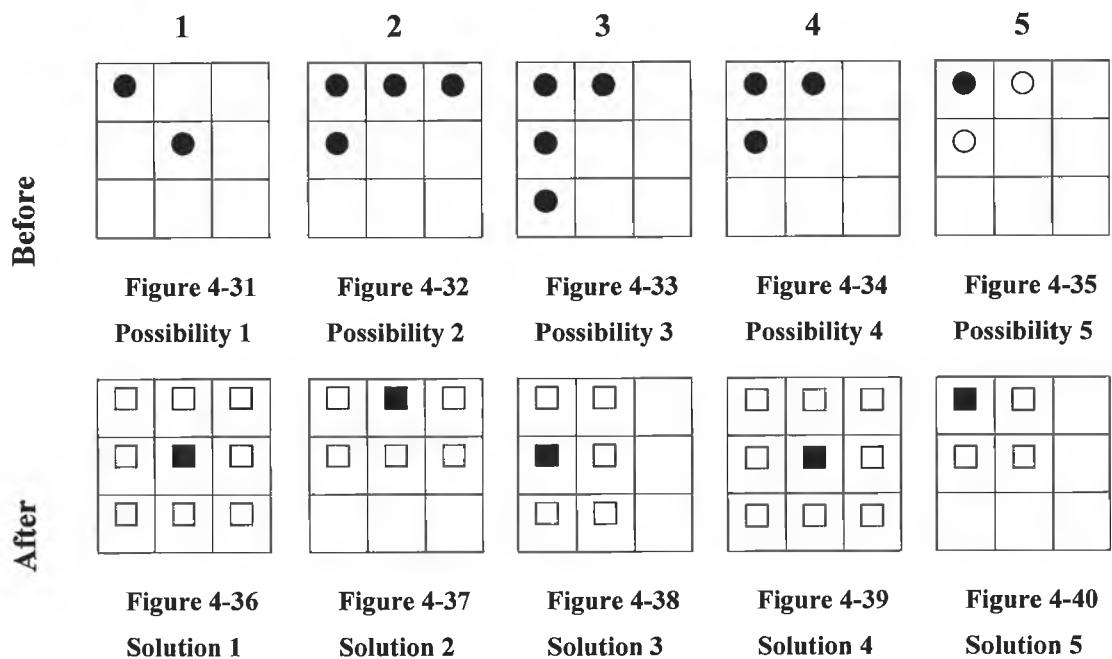
Figure 4-30: Matrix used to identify the six positions

1	2	3
4	5	6
7	8	9

The numbers referenced below are represented in Figure 4-30. The routine uses the following rules in the following order (high is used to represent a pixel/particle):

1. If cell 5 is high then clear cell 1 to 9 and make cell 5 high
2. If cell 2, 3 and 4 are high then clear cell 1 to 6 and 7 and make cell 2 high
3. If cell 2, 4 and 7 are high then clear cell 1 to 3, 4, 5, 7, 8 and make cell 4 high
4. If cell 2 and 4 are high then clear cell 1 to 9 and make cell 5 high
5. Else clear the points on cell 1,2,4 and 5 and make position 1 a high.

The figures below give some examples.



This system will clean out most of the neighbouring pairs occurring but does not cover large errors in the image as, for example, when a reflection on the window results in a bright white spot in which the current algorithm fails to provide a good detection.

It has to be reviewed how well this cleaning algorithm has to be. This is because the calculation algorithm can take part of the responsibility if it calculates vectors based on the common quasi-rigidity condition as described in the next paragraph.

4.5.2.5 Particle tracking

The particles as identified after subtracting the background and using the algorithm as explained in paragraph 4.5.2.1 have to be tracked down during sub sequential frames. A hybrid method where a combination of PIV and PTV is used does not seem to be an easy option since the particle density is not high enough for PIV analysis and preliminary testing with PIV software has failed.

The first attempts will be to start off with an algorithm with a simplified reasoning as described by S.J. Baek and S. J. Lee [84]. This method analyses two frames and decides on particle pairs using the following rules:

5. *Maximum velocity.* The maximum velocity a particle can have is known. If this velocity (U_m) is taken over a frame interval Δt , a distance $U_m \Delta t$ between the two images can be travelled. This means that a particular particle can not travel beyond a present threshold T_m .
6. *Small velocity change.* The velocity of a particle will not change much in the small time interval Δt , since the particle has a finite mass.
7. *Common motion.* Multiple particles will move in one direction forming a region of common motion ($=T_n$). This is a group of particles in a small region showing a pattern of similar movement.
8. *Consistent match.* Two points from one image generally do not match a single point from another image.

The small velocity change and the common motion heuristics can be combined into the quasi-rigidity condition ($=T_q$). The match probability algorithm is mainly based on maximum velocity and the quasi-rigidity condition.

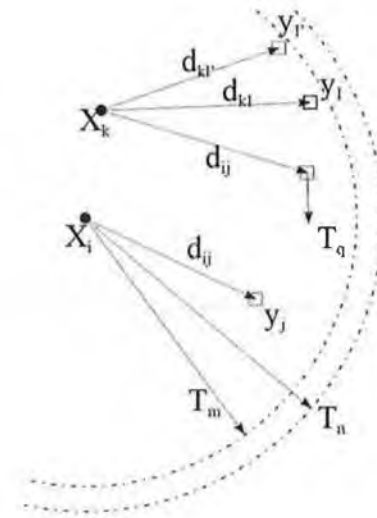


Figure 4-41: Illustration of the method presented by S.J. Baek *et al.*

Initially the points 1 and 2 are to be used to create the PTV software, which will give sufficient logic to create a basic PTV system where the third frame will be analysed to verify the result. The other points can possibly be added in an enhancement of the software.

It can be noted at this stage that a multi-exposed method not only has the crucial advantage of knowing the direction of the flow, but also the potential to verify the motion calculated with a following frame or frames after detection.

The algorithm will use two parameters as input from the user:

1. The maximum distance a particle is likely to travel to limit the search window of the algorithm in finding matching particles
2. A tolerance parameter, which contains the maximal distance in pixels, dictates how much the particle is allowed to be off the calculated position in the third frame.

The algorithm currently neglects the 10 pixels on the outside of the frame since we the initial work will be with frames where the maximum displacement will be taken at 10 pixels. The reason for this is that the software will search around the pixel under investigation and will give a fatal error when searching outside the matrix. This simple method was chosen to avoid the necessity of developing a more complicated algorithm for this initial test since it was not clear if the system would even work at all. This is one of the important issues, which needs to be reviewed

since a maximum displacement with a faster flow of more than 10 pixels will give a potential error as well. .

The software will now search through the matrix of the first frame until it finds a detected pixel. It then starts to search with an offset of the value in the parameter radius in the second frame. With every detected pixel it finds it checks the position in the third frame by calculating the position according to the newly found vector and looks within the offset given by the tolerance parameter. If a match is found the position in the first frame with the displacement vector is put into a matrix containing the results. A more detailed investigation is needed to identify whether the analysis of a fourth frame is useful to eliminate more erroneous vectors. This investigation would also determine whether it would be more useful to improve this algorithm so as to get a denser and more accurate representation of the flow.

The above represents a short description of the algorithm currently used to detect the vectors. A listing of the program code can be found in the appendix, which gives an idea of the complexity of this relatively simple detection method. The algorithm seems to provide a good result despite many errors being detected-especially on the edges of the flow and near places where reflection can occur. An example of this is the frame of the tank. This is due to the low contrast in the picture and will improve with a better light sheet, a cleverer cleaning method and enhanced detection algorithm.

4.5.2.6 Preliminary motion detection

The results of the first test with the software described above can be seen in Figure 4-42 where a simple vector plot is made with the program Matlab. This plot results from the analysis of one set of three frames by the software written in Fortran.

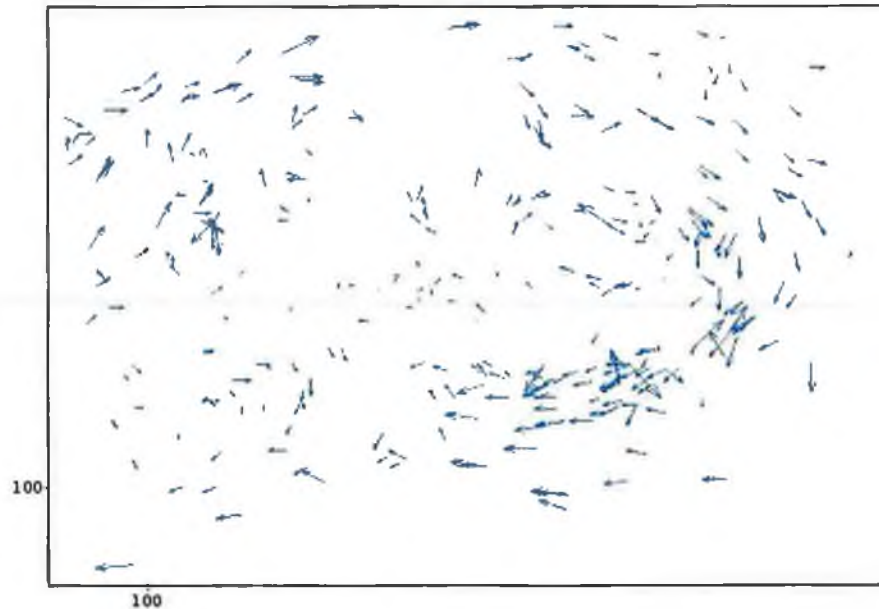


Figure 4-42: Preliminary Vector plot

This vector plot gives a good idea of how the software works. Analysing the plot shows that although most of the vectors seem to follow a common motion some errors are generated where conflicting velocities within a small region are found. It is obvious that this is due to the simple detection algorithm and will improve if ideas like the quasi-rigidity are introduced. The plot is created with Matlab, which has a built-in function for creating such plots.

4.5.3 Methods to present the results

There are numerous methods to present the flow results. The paper “Dedicated analysis and visualisation technology for large discrete data sets” [85] explains the current need for new visualisation methods to visualise large amounts of data especially in 3D flow problems. For preliminary results, however, the two most common methods, namely the vector plot and the contour plot will be sufficient for our 2D analysis.

The vector plot is basically a two dimensional graphical representation of the flow velocity; the magnitude of the flow and its direction are expressed by an arrow. The contour plot identifies an area of vector arrows of equal velocity with a colour, thereby identifying the average velocity in an area.

4.5.3.1 Velocity calculation

The first step for velocity calculation is the defining of the World Coordinate System (WOCO). It is needed to put multiple analyses in one flow picture where all the data will be displayed in the correct position in relation to each other. The world coordinate system is the link between the visual data without any information on place and size, and the real position and location in the simulation tank. It basically establishes the relation between the pixels of the image and the distance it represents.

The world coordinate system can be created with the use of calibration images. These will be analysed and the relation between a pixel and the length of a known object will be calculated.

A calibration grid can be placed at the front and at the back of the tank producing the coordinates of the same point on the grids. The knowledge of the distance between the two calibration grids and the distance to the target plane will allow the interpolation of coordinates on the target plane. The knowledge gained by analysing the disturbance can now be used in the case of an obstructed view, when the tank is loaded with blocks, for example of this grid can be seen in the picture below.



Figure 4-43: The calibration grid as captured by the camera

It is also possible to calculate the relation between the distances at the front of the tank in relation to pixels captured on the light sheet as a function of this distance, i.e. the distance to the light sheet as explained in paragraph 4.2.3.2. Comparing the results of the grid on multiple positions in the tank resulted in the conclusion that the

calculation method is accurate enough and that the lens in combination with the camera does not badly deform the image.

The velocity can now be calculated and given as a parameter in the function. The calculation is explained in paragraph 4.2.3.2. The parameters given are the displacement per pixel in mm and the number of frames per seconds recorded. This value will be the displacement per pixel in the time between two frames.

The velocity of the particles can be plotted in the vector plot with the velocity known. The result after adding labels to some of the vectors gives an idea of the magnitude and is shown in Figure 4-44.

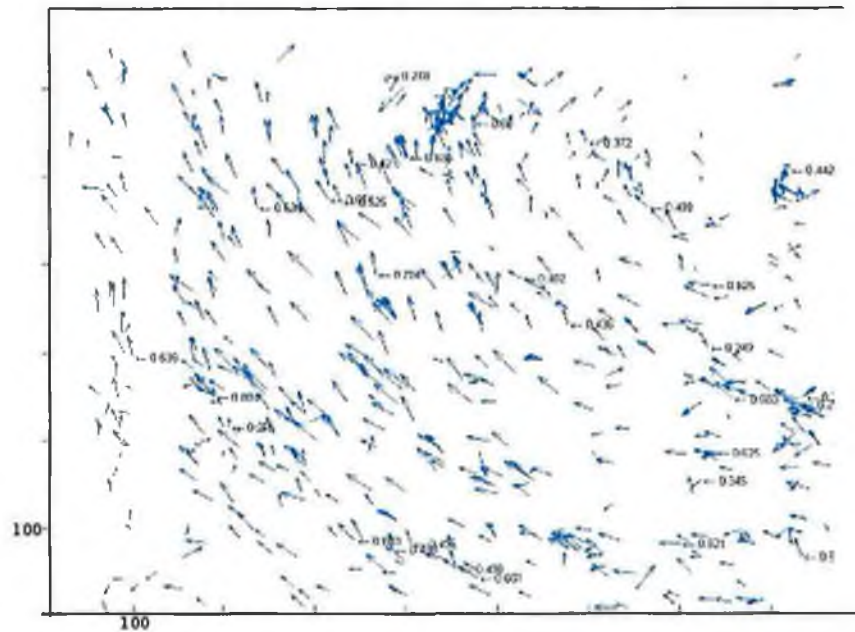


Figure 4-44: Vector plot made over multiple frames

This plot represents multiple iterations to get a higher vector density. The image above gives a good idea of the magnitude and direction of the flow.

Analysing multiple pictures and putting the results beside each other in the right position in reference to the simulation tank can accomplish a vector plot of a whole trailer. An example can be seen in Figure 4-45.

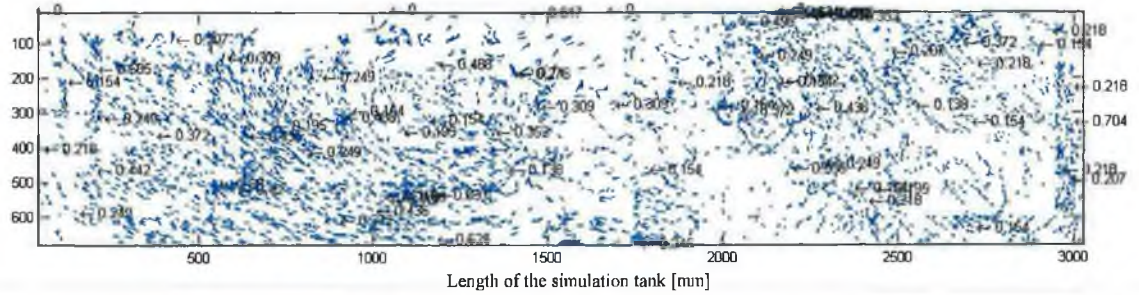


Figure 4-45: Vector plot of the whole trailer made over multiple frames (vectors in m/s)

4.5.3.2 Improving presentation of the results

A further possible enhancement of a full size vector plot would involve limiting the number of vectors plotted and to instead take an average velocity in small blocks. This will result in a structured vector plot. This vector plot will not give as much detail of the flow as the full vector plot but is easier to understand and interpret. This principle in an early stage is seen in Figure 4-46.

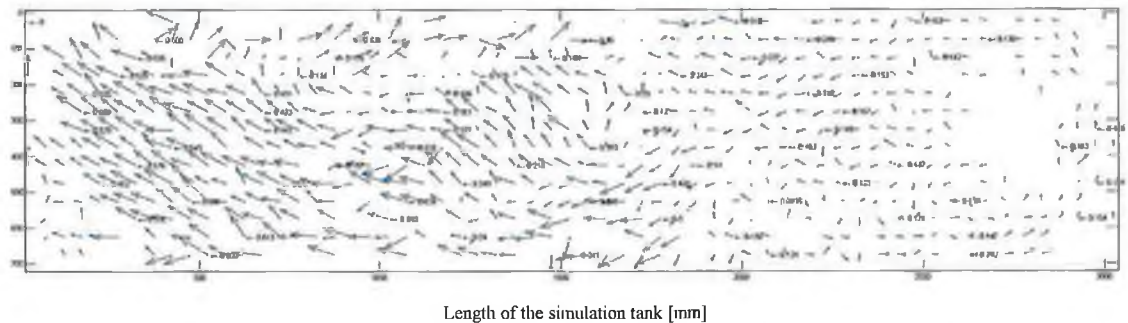


Figure 4-46: Example of vector plot (vectors in m/s)

It must be kept in mind at this stage that the results of the program are not yet perfect, especially given the lack of a good light sheet. The un-enhanced plot produces a denser result and retains the option to fully analyse the flow whereas the 'cleaned' plot presents only the averages. The disadvantage of using the averaging system in an area with conflicting vector directions is that the results might cancel each other out. It is possible to improve on this by cutting out extreme values when averaging but it is better to pre-emptively improve the analysis algorithm so as to prevent erroneous vectors from appearing.

A further improvement would be to use different colours for the different velocities: a high velocity is identified by a red colour, a low velocity by a blue—the same principle as seen in a contour plot.

A contour plot will be another way to enhance the present visibility of the data. A contour plot sacrifices some detail but enhances the visual presentation for general purposes. This will, however, be beyond the scope and time frame of this preliminary program since the values have to be averaged to produce a gradient velocity field. An example representation of such a plot can be seen in Figure 4-47 and Figure 4-48.

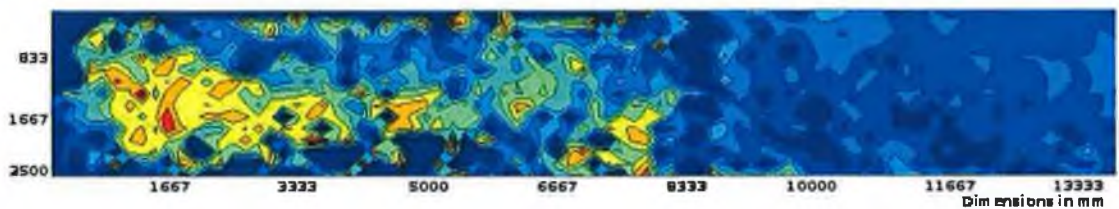


Figure 4-47: Velocity magnitude contour plot of a refrigerated trailer



Figure 4-48: Velocity magnitude contour plot of a refrigeration unit

4.6 Results of the program

The program, or more accurately set of programs, currently produces a reasonable result by looking at the quality of the images captured by the camera of the flow in the tank. An improved light sheet will significantly improve the results of the program; this provides an opportunity to enhance the program code as soon as the problems are identified.

The program can currently analyse one set of frames (a set is 3 sub-sequential frames), multiple sets in a single capture or multiple recordings to investigate the whole tank. The results can be presented in a normal vector plot where all the vectors are plotted or a structured vector plot where a limited amount of vectors represent the average of a region. Initial trials in developing a contour plot have been performed but further work is required and quite probably a rewritten algorithm.

Improvements are needed on the image cleaning process in which regions of pixels are identified and replaced by one pixel at the centre of the group. The particle-tracing algorithm has to be reviewed and, according to the information published in various papers, enhanced so as not to produce erroneous vectors. A dynamic code might be created to work with the common motion of fluid flow and to detect the maximum change of motion of two frames: the flow velocity and the common direction of the flow.

The overall quality of the program is sufficient to produce results and to perform tests which identify how close the simulation in the tank compares to the airflow in a real trailer. The first results can be expected to give an idea of the flow inside a trailer and the first subsequent recommendations for flow improvements can therefore be formulated from these results. The results of the program will be of greater value, however, if an intense and uniform light sheet is available hence enabling the program algorithm to be enhanced.

4.7 Recommendations on the software

4.7.1 Neighbouring parts algorithm

Creating a more interactive function to clean out the image can enhance the cleaning algorithms. Multiple pixels representing one particle have to be reduced to a single one where the centre of the group of particles has to be calculated so as to represent the whole picture. This means, however, that the algorithm must investigate and follow all points that are connected to each other and analyse where the middle of the group of pixels is most likely to lie.

The software requires the further development of tracking algorithms to improve accuracy and reduce erroneous vectors.

An enhancement that will have a positive effect on the calculation algorithm tracking the particles is the introduction of the points 3 and 4 as mentioned in paragraph 4.5.2.5. This will mean the introduction of *common motion* where multiple particles will move in one direction forming a region of points sharing a common motion ($=Tn$) and *consistent match*, where two points from one image generally do not match a single point from another image.

This will drastically reduce the amount of erroneous vectors and improve the overall quality of the vector plot, especially where averages of a region are used.

4.7.2 Further evaluation of the results

The results so far have been examined by verifying the detection and tracking of the particles. These results seem to be accurate. This initial verification was done by allowing the program to overlay the detected particles on the original frames and by verifying the correct positions of these particles. The program can plot the vectors in the picture and animate the sub-sequential frames. Manual tracking of the particles will allow verification of these vectors.

A test program can be developed creating particles, or groups of particles, with random velocities to test the program and to ensure the program gives the right velocity and positions.

4.7.3 Creation of an interface

Finally, a user-friendly user interface should be developed making the operation of the program easier and more straightforward. Currently Matlab and Fortran executables are used in the program in which a lot of parameters have to be given in the call of a function or program. This should all be integrated in to one easy-to-use interface where only one program will be used. This will reduce the processing time by cutting out the time needed for the transfer of data between Matlab and the Fortran executable.

Chapter 5

Results of experimental and numerical analysis

5.1 *General*

This chapter will give a short review of the results of the experiments performed to evaluate the airflow in the trailer and measurements taken in a real size trailer. Additional results were gained by using computational fluid dynamics (CFD).

The accuracy of the simulation method when water is used in a scale model instead of air is determined by comparing the results with measurements from a real size trailer and the predicted results of the CFD.

It will be hard to know if the Reynolds number in the simulation tank is comparable with the original trailer as it is in the turbulence area. Problems may arise when determining what the required simulation velocity is compared to the real size trailer. This is due to the fact that we will be trying to get an equal Reynolds number in both simulation and the real size trailer in order to maintain dynamic similarity. The shape of the flow has to be compared to see if the flow pattern produced by the pump is comparable with the flow of the current refrigeration unit.

5.2 *Visual flow analysis of the simulation tank*

The first analysis on the flow was completed visually on the simulation tank. The flow in the tank was examined and discussed with a senior engineer who has been working on the airflow delivery system of the current Thermo King units. His comments will give an idea on the flow of the model compared with the real trailer. Smoke was used to visualise the flow inside the real trailer.

5.2.1 *General flow*

As seen in Figure 5-1, the fluid on entering the tank at a pump frequency of 25 Hz (average outlet velocity ≈ 5.7 m/s) sticks to the top of the tank and does not start to

descend until about 1.5-1.6 metres into the tank. At 45 Hz (average outlet velocity ≈ 7.9 m/s) the flow travelled 1.7-1.8 metres. It then quickly moves down and some of it starts to return and partly re-circulate at the back (as seen in Figure 5-1).



Figure 5-1: Flow inside the tank (visual)

Where the fluid circulates at the back of the tank a few small vortices appear but the main flow continues to circulate back to the front of the tank. A less obvious quantity goes back into the pump while most of the returning flow seems to be drawn back into the entering flow and re-circulates. Most of the flow going back into the pump must be coming from the bottom and the sides, as the flow in the middle is mainly sucked back into the entering flow. The flow in the horizontal plane divides after entering the tank and the overall flow picture is more or less symmetrically mirrored around the outlet plane.

The flow in the trailer has the same general pattern but seems to be much more turbulent. The experiment is carried out without the airflow deflector bending it to the back corner and aimed straight back to reflect the simulation in the water tank. The flow seems to drop faster than in the tank and returns a bit earlier. This is possibly because of the faster divergence and more turbulent flow pattern (Figure 5-4).



Figure 5-2: Flow inside trailer, straight to the back (visual)

Good visual analysis however is almost impossible as the smoke used to visualise the flow saturates the air quickly and observation has to be carried out from within the trailer.

A slightly different effect is seen when the flow is aimed at the side/back corner with the deflector in place. The flow now goes along the inner walls of trailer, in which there is a plane in the middle of the trailer towards the back where there is no flow (Figure 5-3). The flow starts off over the centre of the trailer and flows to the lower back corner before it goes around and rises flowing back where most of the flow travels half the height of the trailer.

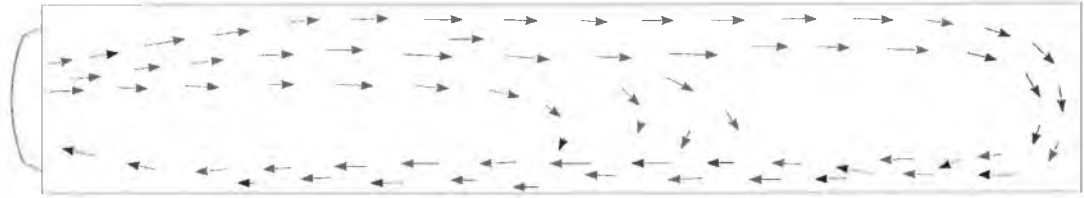


Figure 5-3: Flow in a trailer with a refrigeration unit (top view)

The main difference between the flow as seen in the tank and in the trailer is the amount of turbulence. The flow in the water tank does not seem to be as turbulent as the flow in the trailer. An explanation is that the centrifugal fan driving the flow in the Thermo King refrigeration unit creates two very strong vortices that break up the flow. This vortex expands when it travels further in the trailer causing the flow to separate from the ceiling and descend earlier.

5.2.2 Effectiveness of the flow to the rear of the trailer

The velocity at which the flow is entering the trailer does not significantly influence the distance of the flow in the trailer. This conclusion can be made after analysing the flow in the real size trailer as well as in the simulation tank. The difference between a high-velocity flow and a low velocity flow (14.4 m/s versus 19.8 m/s in a real size trailer) would be the equivalent of 1 metre in a 13.6-metre refrigerated trailer. It can be said that it is not worthwhile putting a lot of effort into speeding up the flow to reach the back, as this does not seem to work. Furthermore it puts more energy into the trailer thus reducing the refrigeration efficiency.

The flow in the trailer reaches the back of the trailer when the flow is directed to the side and back and there is enough speed for good circulation. The main flow does not go into the back if directed straight back except a small quantity, which will circulate

there. This illustrates that the Coanda effect is an excellent method of getting the airflow to the back of an empty trailer. The effect of directing the flow to the side of a loaded trailer is not yet known. The simulation tank is currently incapable of simulating the Coanda effect in the manner in which it occurs in the current refrigerated trailers equipped with the Thermo King refrigeration unit. Loading tests have not yet been performed but future testing will bring more of this to light.

Methods to improve the flow to the back of the refrigerated trailer have to be examined in order to see their effect is on an empty trailer as well as a (partly) loaded trailer. It is possible that directing the flow to the side has a positive effect on the flow in an empty condition but does not improve the performance under loading conditions. It has to be reviewed also how often and in which situations the flow to the back in the empty trailer is needed. The reality is that most of the refrigerated trailers have a chute or duct fitted to guide the airflow to the back rendering special adjustments to get the flow to the back useless and unnecessary.

5.3 Flow measurements

The measuring of the flow is performed with the newly created measuring system in the simulation tank, and with a wind vane anemometer in the real size trailer. Comparing these results later in this chapter will hopefully give a degree of confidence in the simulation tank results and give a good preliminary idea on what goes on in the tank. Furthermore, comparison of the results will highlight the important points in the management of an airflow system.

5.3.1 Full trailer vector plot

A full measurement of the simulation tank is performed with a simulation speed of 25 Hz, which is the equivalent of 14.4 m/s (4479 m³/h) in the real size trailer. The frames were captured with 99 fps to match the frequency of the Metal-Halide lamp used for the illumination. The movement per pixel was calculated with the use of calibration images as shown in equation 5-1.

$$Pix_{middle} = \frac{Pix_{front} \cdot l_A}{l_B} = \frac{531.5 \cdot 1200}{1450} = 439.9 \text{ pixels} \quad (5-1)$$

This means 300 mm / 439.9 pixels = 0.682 mm/pixel. The resulting velocity can now be calculated and put into the analysis program. The program will also convert measured velocities and dimensions in the tank to dimensions and speeds compatible with life-size trailer allowing comparisons. The flow representation in a life size trailer is presented in Figure 5-4 and Figure 5-5, where the velocity is given in m/s and the dimensions in mm.

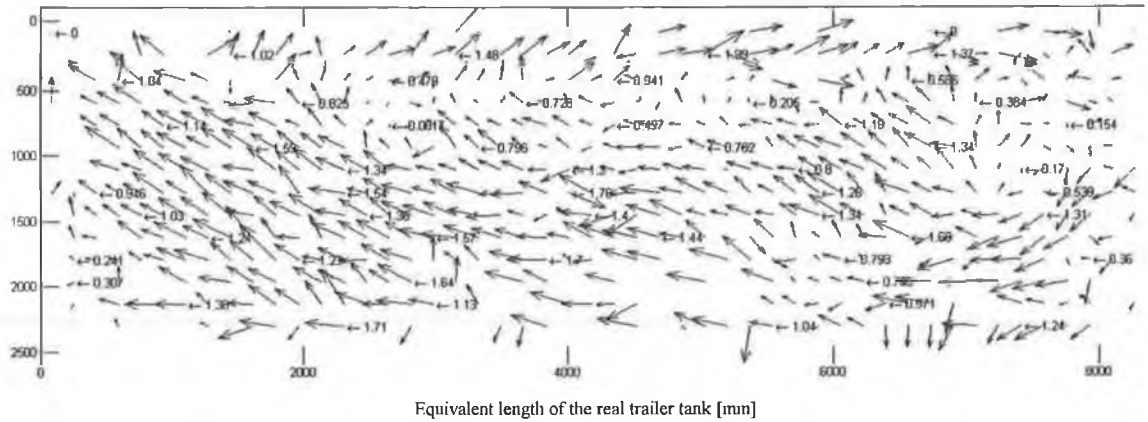


Figure 5-4: Vector plot of the front part of the trailer (vectors in m/s)

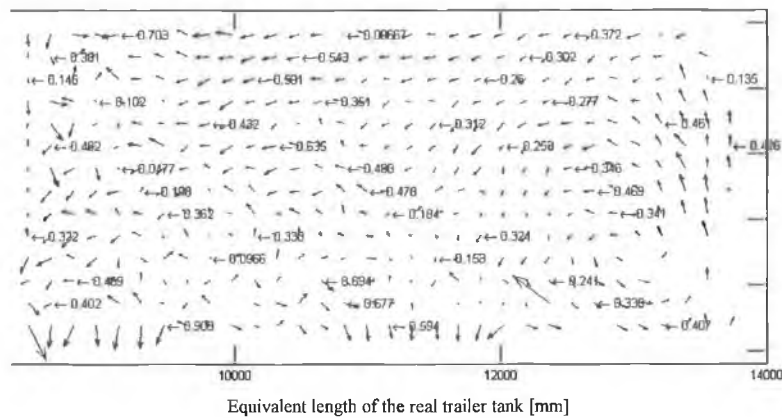


Figure 5-5: Vector plot of the back part of the trailer (vectors in m/s)

The blue arrows are the vectors visually indicating the speed. The numbers indicate the speed, where the black arrow points to which vector this speed is relevant to.

The vector plot currently does not identify the high-velocity flow at the top of the trailer because the current measuring system is not advanced enough to detect the high velocity flow. This is due to the lack of light intensity and the limitation to 100 Hz dictated by the metal-halide light. However, the data that is available gives a good indication of the remaining flow.

It can be seen that the flow progresses about eight metres into the trailer, after which it starts to break up and returns to the front of the trailer. This effect is discussed in paragraph 5.2.1 where most of the flow turns back and re-circulates into the flow stream entering the trailer. Only a small amount of air circulates at the back of the trailer.

5.3.2 Influences of velocity on the flow

Different simulations are carried out to establish the effect of a larger flow and especially a higher velocity flow. Circulating more air through the trailer means that there is more energy needed to accelerate the air. This energy ends up as heat in the refrigerated compartment and thus decreases the efficiency. It is therefore important to establish the required rate and velocity of flow and to determine the point at which increasing the flow rate does not gain much advantage in refrigerating the load.

The distance the flow travels into the trailer before it turns back increases if the flow velocity is increased as can be seen in Figure 5-6 to Figure 5-9 (m/s are approximate equivalents in a whole trailer).

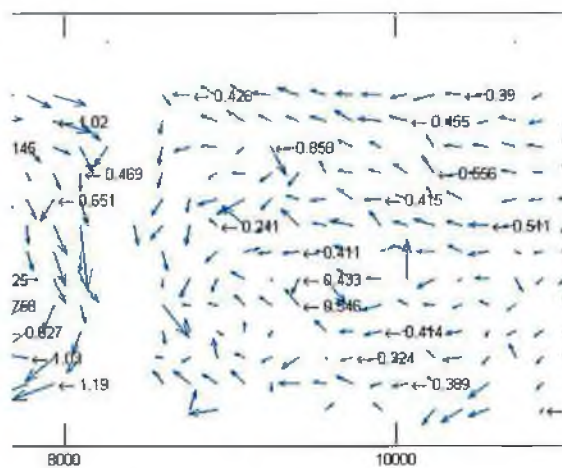


Figure 5-6: 12.17 m/s

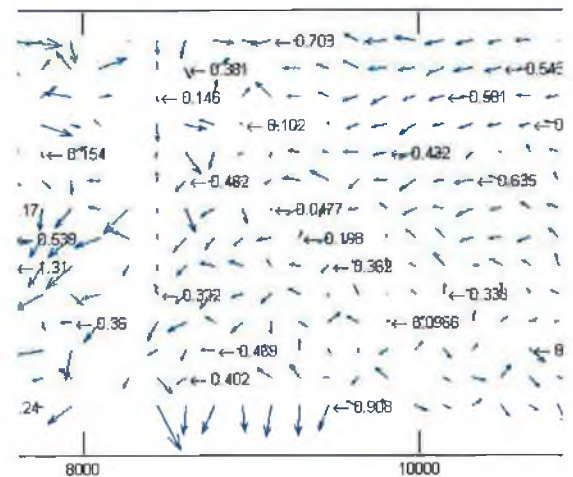


Figure 5-7: 14.4 m/s

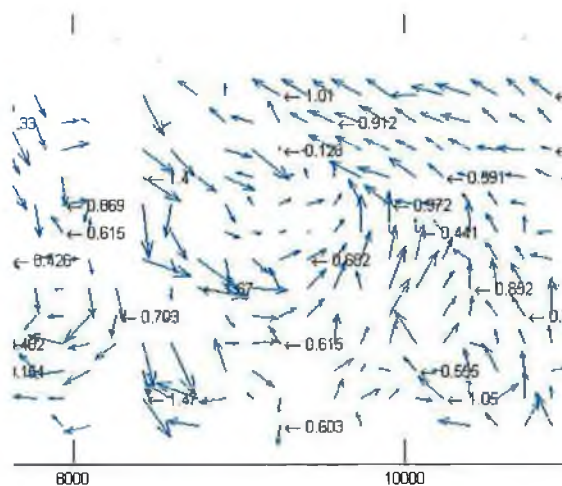


Figure 5-8: 17.88 m/s

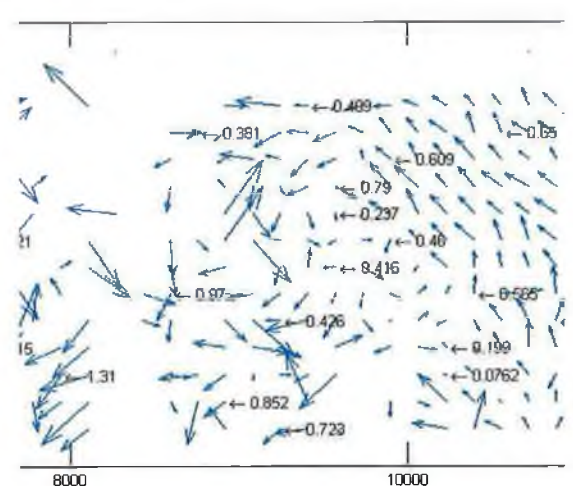


Figure 5-9: 19.86 m/s

However, it can be seen that the cut-off point in Figure 5-6 is approx. 7.8 m, where Figure 5-7 gives 8.1 m, Figure 5-8 approximately 8.5 metres and Figure 5-9 approximately 9.0 metres.

Figure 5-10 shows a graphical representation of this information. The light blue line represents the data from the experiments, where the dark blue line is an estimated function representing this data. Although this estimated function does not have enough data points to be considered accurate, it does represent the expected trend. .

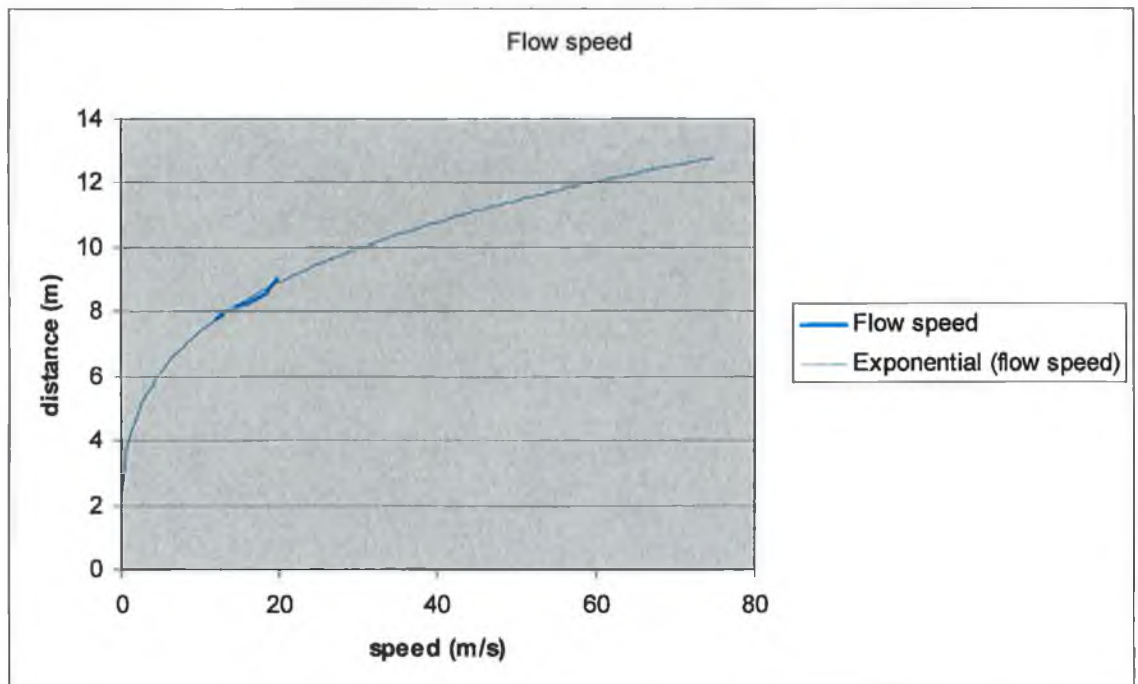


Figure 5-10: The estimated effect of air velocity

The graph gives a reasonable representation of the air velocity entering the trailer against the distance it can still be measured. The conclusion can be made that a high increase in velocity is needed to get the flow to go to the end of a 13.6 metre long trailer (at least three times as much a velocity is needed to get the flow the whole way to the back of the trailer). The generation of such a velocity will cost a significant amount of energy, significantly reducing the efficiency and limiting the capacity of the refrigeration unit. The question is how important a perfect flow is in an empty trailer as a uniform airflow is only required in a loaded condition, and what amount of airflow allows for sufficient circulation while maintaining efficiency.

5.3.3 Comparison with real trailer

A Thermo King refrigeration unit was modified to throw the air straight back into the trailer. The trailer used however is only 12.6 metres long and not 13.6 metres as the simulation represents which might give a small difference in results because of the length the flow travels along the trailer. The unit is run at high speed (5500 m³/h) and at low speed (3400 m³/h).

The measurements are taken with a wind vane anemometer, which only gives a one-dimensional estimation of the flow velocity with accuracy, which could be as low as 20%. These values can only be used as an indication of the flow velocity. The low velocity measurement will be almost equivalent with the simulation on 20hz. The units on the axis are equivalent to a real size trailer in mm, and the vectors in m/s.

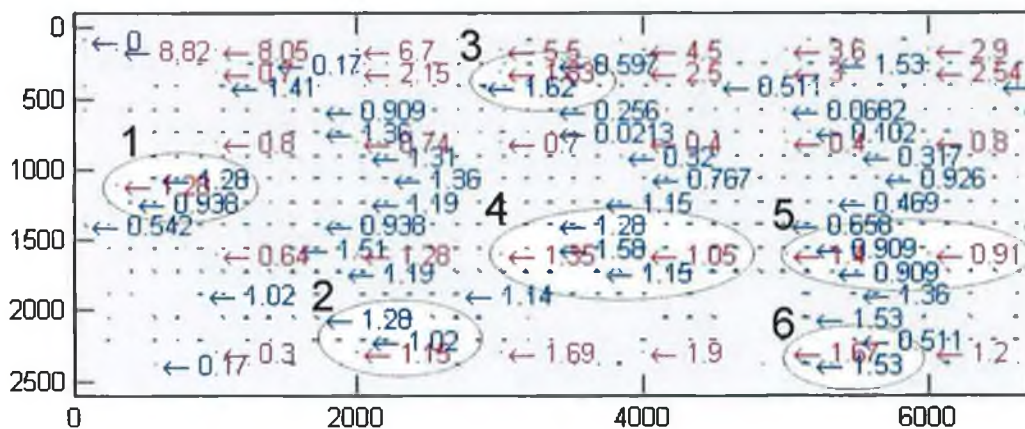


Figure 5-11: Measured values (red) versus simulation results (blue)(m/s)(front)

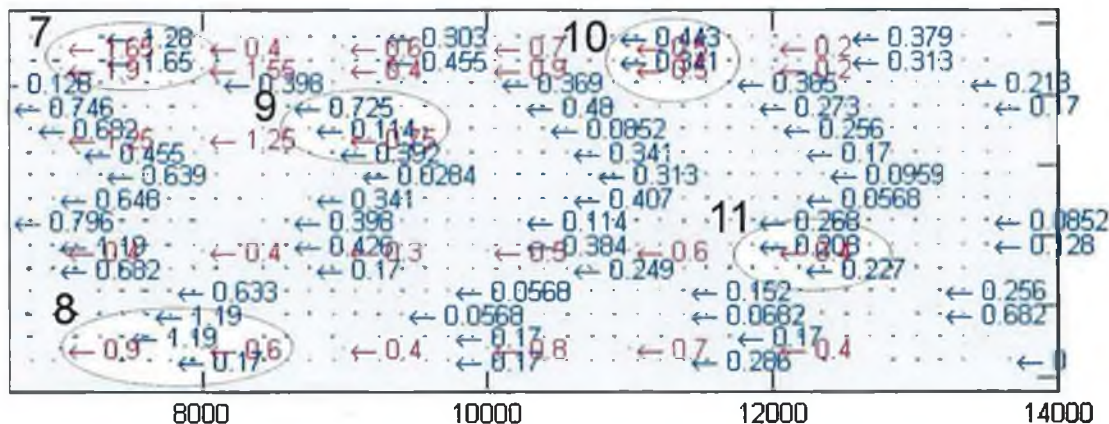


Figure 5-12: Measured values (red) versus simulation results (blue) (m/s)(back)

Some points are highlighted in Figure 5-11 and Figure 5-12, which are summed up in Table 5-1. The values given for the water simulation are calculated to be comparable with the values measured in the trailer.

Table 5-1: Comparison between the measured air velocity in the trailer and the simulation

Point	Measured in the trailer	Measured in simulation	Percentage error
1	1.28 m/s	1.28 m/s	100.0 %
2	1.15 m/s	1.02 m/s	88.7 %
3	1.83 m/s	1.62 m/s	65.6 %
4	1.35 m/s	1.58 m/s	117.0 %
	1.06 m/s	1.15 m/s	108.5 %
5	0.91 m/s	0.91 m/s	100.0 %
6	1.67 m/s	1.53 m/s	91.6 %
7	1.65 m/s	1.65 m/s	100.0 %
8	0.90 m/s	1.19 m/s	132 %
9	0.73 m/s	0.75 m/s	102.7 %
10	0.50 m/s	0.43 m/s	86.0 %
11	0.40 m/s	0.21 m/s	52.5 %

The difference at the lower velocities can be explained by the fact that the wind vane anemometer is not capable of recording a flow lower than 0.4 m/s and is especially inaccurate at low velocities. The measurement software can measure velocities much lower than that as long as there is a difference between two frames of more than a few pixels.

There is a small error where the flow in the trailer seems to leave the ceiling and flow down more than the flow in the tank does, which probably means that the flow pattern of the fan in the unit does not exactly match the flow out of the pump.

The overall picture is that the measurements in the trailer are very close to the measurements in the simulation tank in terms of the magnitude and the overall spread through the trailer. This proves that the concept of using a scaled water model to simulate the airflow in a refrigerated trailer and the created software to analyse this flow can be used to acquire trustworthy flow field information.

5.4 Effect of loading/unloading

A start was made in the simulation of loaded refrigerated trailers. However, accurate tests on a loaded trailer failed due to a wrong decision made on the material

to be used in the simulation of the cargo. Polyurethane foam was used to represent the cargo in the refrigerated trailer. The blocks were cut in the shape of the cargo combined with a pallet and were restrained to a mesh of stainless steel strips and bars (Figure 5-13). These strips are designed to keep the blocks strapped against the floor. Polyurethane has a relatively low density compared to water. The strips were connected to the bottom of the tank with the use of 16 bolts.

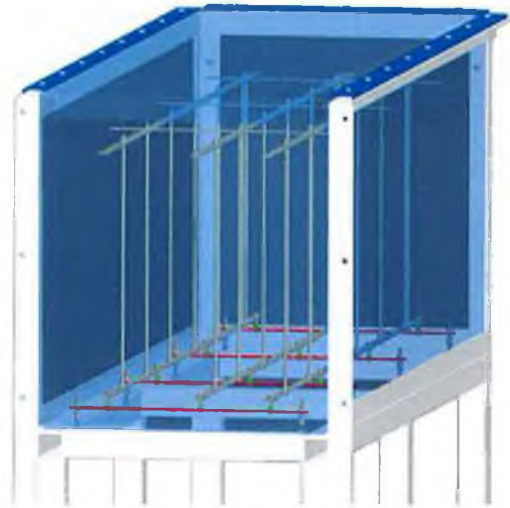


Figure 5-13: Cross-section of the simulation tank with the cargo restraints

The force generated by the polyurethane block was much higher however than was foreseen. This resulted in the strips being bent while the tank was filling up so that the force on the bottom of the tank caused it to leak. The filling of the tank was stopped when it was half full to prevent any permanent damage being done to the tank.

A temporary solution was to put pins between the strips and the top of the tank to prevent the block from floating. This method was partly successful and allowed the opportunity to do some preliminary tests. The blocks did float up slightly and the top cover was slightly deformed under this pressure. This combined with the extra obstruction the pins caused resulted in a less accurate representation of the flow.

5.4.1 A trailer loaded with pallets

The cargo arrangement is designed to be able to be used in a 32 and a 33-pallet arrangement. Tests described in this thesis only look at the 33-pallet arrangement due to the problems experienced with the block of foam used to simulate the cargo. The results of the analysis done on the loaded situation had only limited success. The analysis software was not able to accurately detect the contrast between the particles and the foam blocks due to the limited performance of the light sheet. The blocks are painted black to act as a contrast but it is very hard to distinguish the particles from the blocks as can be seen in Figure 5-14. There is a lot of air in the simulation due to the block pushing against the top, which confuses the mathematical algorithms.



Figure 5-14: shot of the flow beside the cargo with the velocity vectors plotted in.

The software was however able to detect some of the flow as can be seen in the above image, giving a general idea of the flow direction at the front of the trailer. The data collected however is not dense enough to create vector plots as was done for the empty trailers.

The flow as seen in the simulation environment can be summarized as presented in Figure 5-15 and Figure 5-16.



Figure 5-15: Side view from the flow along the cross section of the trailer

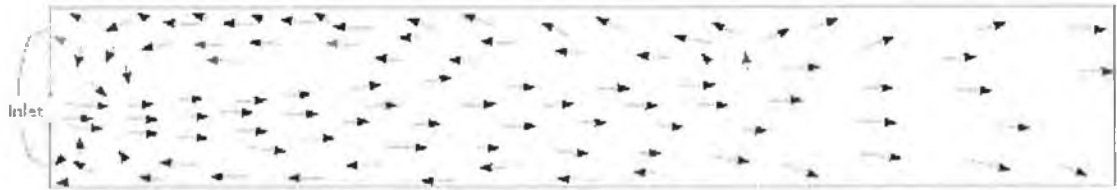


Figure 5-16: Flow pattern as seen from the top of the trailer

The main part of the flow follows the same profile as the flow in the empty trailer with the exception that there is no re-circulation at the back. The air continues to flow to the back instead of returning to the refrigeration unit in the front. It also circulates at the back of the trailer. There also seems to be liquid movement all around the cargo. It is however hard to estimate the quantity and velocity of the flow as the result of the measurement system does not work as aforementioned.

5.4.2 Bulkhead effect on the airflow

A few preliminary tests were conducted to determine the effect of a bulkhead on the airflow through the refrigerated trailer. All the tests performed with blocks in the trailer had a bulkhead installed. A bulkhead is required in all loading conditions to allow the airflow to return to the refrigeration unit. The bulkhead used, however, is a copy of an American design, whereas European bulkhead designs are forced to be much slimmer because of dimensional restrictions as pointed out in previous chapters.

The bulkhead has a standard layout where most of the air has to return through the bottom of the bulkhead. The sides are closed and only a small amount of air is permitted to flow over the top. The inside of the bulkhead consists of specially formed and positioned stiffeners which give structural integrity and mix the airflow to get a more uniform temperature mixture going into the evaporator. A European

design would be much slimmer and might need more air entrance at the sides to reduce the static pressure loss.

The use of the American design in the following tests will result in a distorted picture of the performance of the trailer in a loaded condition, but will give a general idea of the two tested configurations.

The first test performed was with an open area on the top of the bulkhead giving the air the possibility of returning mainly through the bottom, but partly through the top as well. The pictures below give an indication of the effect of a bulkhead on the overall airflow.

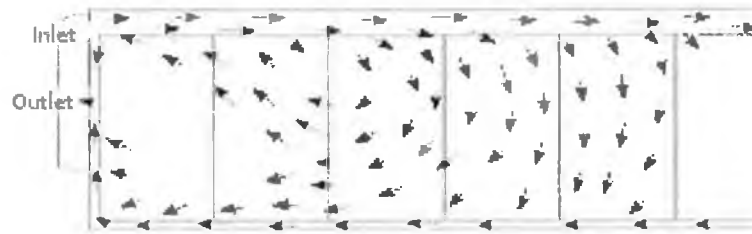


Figure 5-17: Flow pattern with a bulkhead open on the top

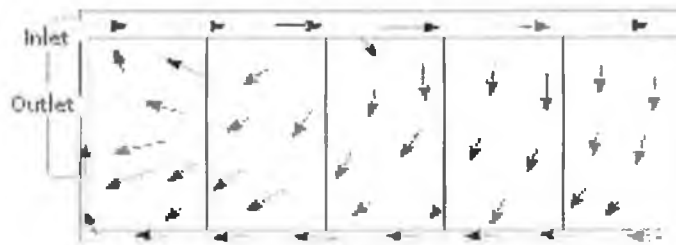


Figure 5-18: Flow pattern with a bulkhead closed on the top

5.5 Computational Fluid Dynamics

A preliminary test was conducted with Computational Fluid Dynamics as a tool for more detailed flow analysis. Results obtained from CFD give more detail than the current measurements since it produces a three-dimensional flow model instead of a two-dimensional flow model. The preliminary test that was run on an empty trailer was carried out to determine the complexity and suitability of the model and to get an indication as to how well the numerical results reflect the experimentally measured data. A three dimensional approach was taken as a two dimensional approach would not be comparable with the measurement taken in experiments, even though the measurements are taken in two dimensions. A two dimensional slice of the three dimensional data can then be taken to compare with the experimental results.

5.5.1 General CFD

Computational Fluid Dynamics (CFD) is a method used to predict internal as well as external flows and its use has dramatically increased in the past decade. Where CFD was a niche in the 1980s for the academic, postdoctoral or postgraduate researcher the wide availability of powerful computers and workstations and the development of commercial CFD codes has opened the way for the code to be used in industry.

The pressure on the engineers in the industry however does not allow for the long learning curve needed to gain experience in the capabilities and more importantly the limitations of CFD. This experience is crucial to ensure trustworthy results and an extensive training, test and validation period is required before sensible results can be created out of complex flow situations.

The unique advantages of the method can be exploited however when appropriate simulations are performed with CFD:

- Substantial reduction of lead times and costs of new designs
- Ability to study systems where controlled experiments are difficult or impossible to perform
- Ability to study systems under hazardous conditions at and beyond their normal performance limits
- Practically unlimited level of detail of result

The cost of an experiment in terms of facility and labour is proportional to the number of data points and configurations tested. CFD codes on the other hand can produce large volumes of data at a minimum additional cost after the CFD code is created.

5.5.2 Results of CFD

A few results of the CFD will be discussed and reviewed to give an idea of the potential of this fluid flow analysis tool. All simulations so far were carried out with empty trailers. CFD results have to be closely examined and verified with test data to ensure that they are correct. Computational Fluid Dynamics is a specialised skill and a lot of experience is needed to guarantee a trustworthy result. This is why a close comparison between experimental results and the results produced by the CFD is mandatory at the start.

The preliminary models fashioned under this project started off with the creation of a straight square box, with an inlet fan boundary condition [86] on one end, and a free boundary at the other end. There was a radiator halfway down the tube creating pressure loss and a fan curve from a Thermo King refrigeration unit was used on the inlet fan boundary condition. There was a bit of recalculation needed to tune the CFD results to the manually calculated pressure losses over the tube as the fan curve and the radiator resistance were initially given as a static pressure. The CFD program Fluent requires total pressure values however.

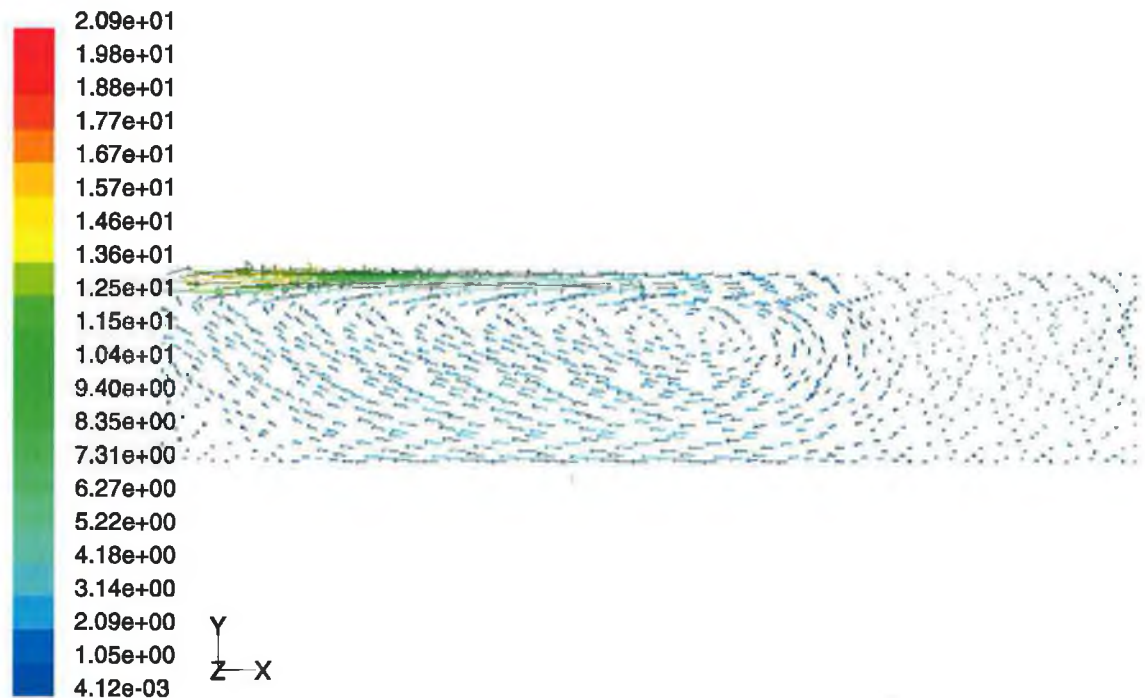
Experimentation on an empty three-dimensional model of a trailer was started after some confidence was gained with small models. The inlet fan boundary condition with the fan curve was used again, and there was a free boundary at the return air outlet of the trailer. The mesh was created using the Gambit pre-processor [87] initially with a node every 100 mm. A more progressive mesh to allow more detail around the inlet and outlet was introduced while keeping the amount of memory and computation time required to a minimum. The copper meshing scheme was finally adapted with a node distance of 10 mm on the inlet and about 50 mm on the outlet.

Different turbulence models have been reviewed, including the K- ϵ model, LES model and the RMS models. It became apparent that the RMS model was the most suitable model for this preliminary experiment as suggested in a publication by Naïma Zertal-Ménia et al. [88] who investigated different CFD models and their

suitability. The analysis performed by Fluent Inc for Thermo King in 1999 [89] used the K- ϵ model however.

The analysis as illustrated below all use the RSM model, using the 'Intensity and Length scale' turbulence model with 50% turbulence on hydraulic diameter of 0.329 m (the inlet dimensions divided by two), which is integrated into the CFD software Fluent.

The results seem to get reasonably close to the results as measured in the simulation environment, but further analysis is needed to verify the correct flow patterns inside the trailer. The CFD results represent three dimensional flow models. This gives a deeper understanding of the overall flow in the trailer, and provides information for additional tests in the simulation environment in order to confirm those flow patterns.



Velocity Vectors Colored By Velocity Magnitude (m/s)

Jun 16, 2004
FLUENT 6.1 (3d, segregated, RSM)

Figure 5-19: Vector plot of the velocity through the mid plane of the trailer

Figure 5-19 illustrates a default vector plot of the mid plane of the trailer. This can be compared to the analysis software created to analyse the flow in the simulation tank. This information could be used to compare the results of the CFD with the results of the experiments. There are however more ways of visualising the flow

which may give greater insight into the flow patterns by producing a more advanced three dimensional picture as can be seen in the following figures.

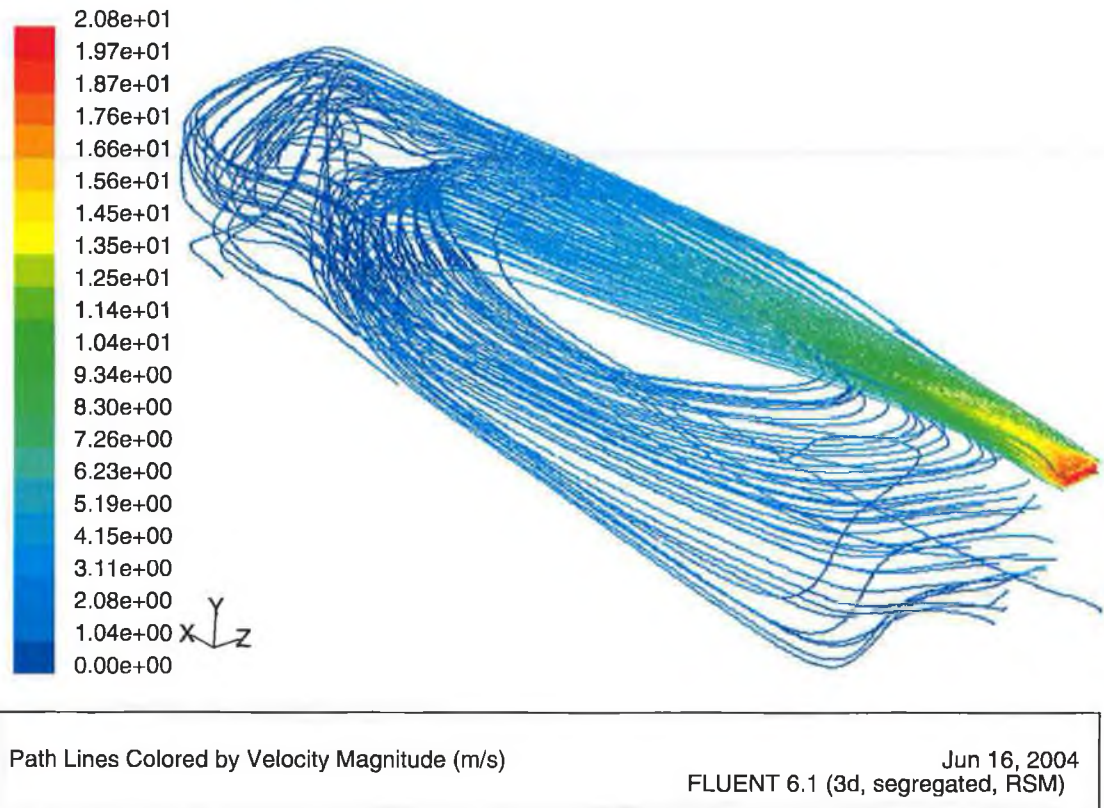
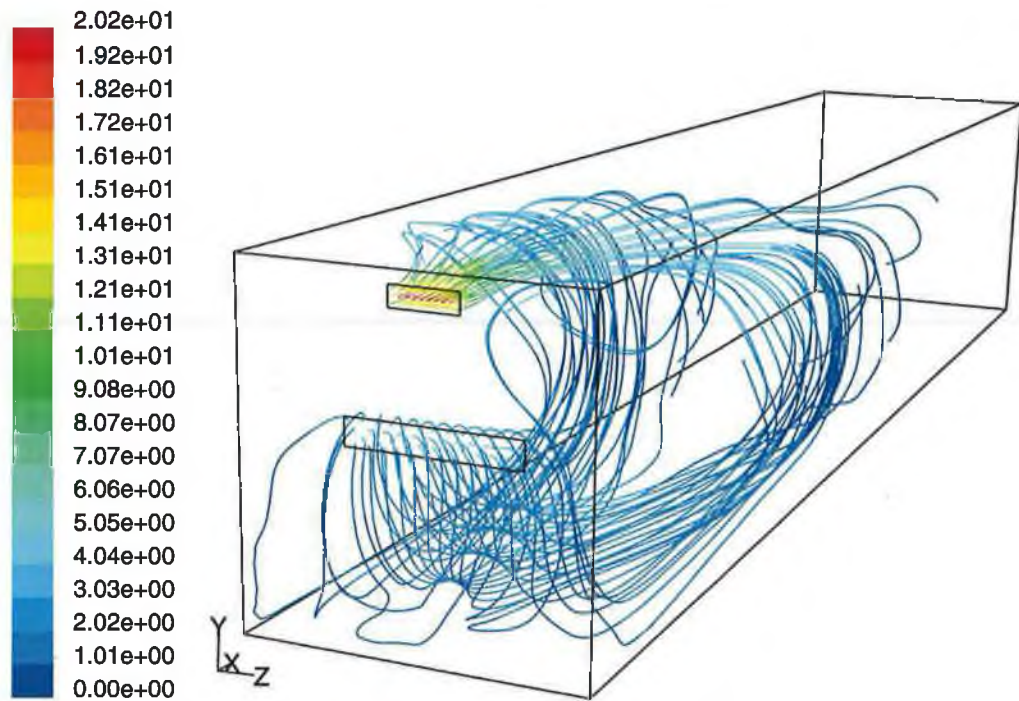


Figure 5-20: Path lines of the flow entering the trailer

The above figure illustrates the route of the flow entering the trailer with the use of path lines. This gives a clear image of the distribution of the flow throughout the trailer, especially when the information is presented in the form of an animation illustrating the flow pattern.

The model predicts that most of the flow goes to about $\frac{3}{4}$ of the length of the trailer, where most of the flow returns back to the front and some continues the path to the back. The flow returning to back is mainly sucked back into the entering flow, as becomes obvious when looking at the small amount of path lines that returns back to the outlet.

Although this information gives a satisfactory representation of the flow, extensive analysis is needed to verify if the information is presented correctly.



Path Lines Colored by Velocity Magnitude (m/s)

May 24, 2004
FLUENT 6.1 (3d, segregated, RSM)

Figure 5-21: Path lines indicating the flow returning to the refrigeration unit

Figure 5-21 shows the three dimensional path lines of the flow returning to the refrigeration unit. Contrasting with Figure 5-20, Figure 5-21 depicts the lines, which originated in the return-air opening of the refrigeration unit and follows them back to their origin.

This visualises the flow going back to the unit providing detail about the origin of the air returning to the refrigeration unit. The figure above in which the air flowing out of the refrigeration unit is visualised doesn't contain information as to how much of the air blown out by the unit circulates through the trailer before the unit sucks it back out.

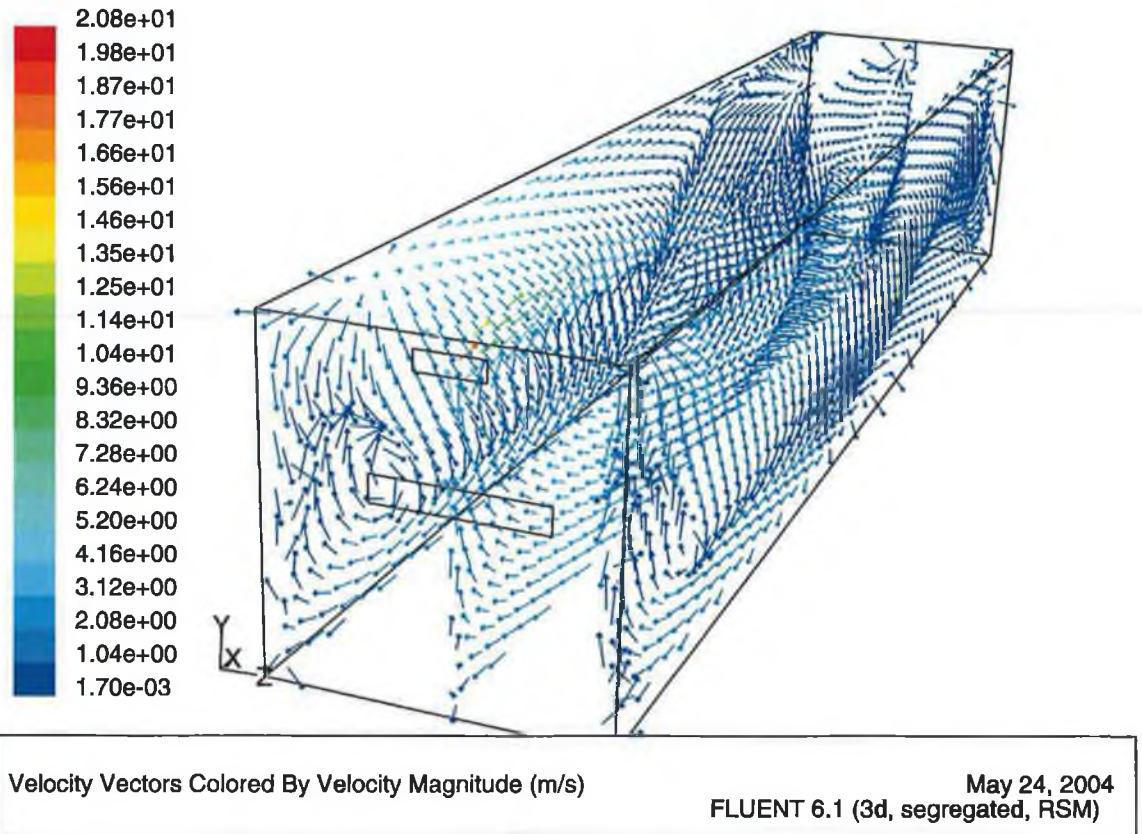


Figure 5-22: Direction of the flow visualised in three different plans

The above result is generated by drawing the path the flow takes from the plane over a short distance, giving information on the direction of the flow taken in three different planes. This gives, as does Figure 5-19, information on the direction of the flow through the highlighted planes, but also information about the direction the flow in those planes travel.

The above examples are just a few illustrations of ways to visualise the flow information produced by the CFD software. The next step is to verify the flow with the experimental results. The best way to approach this is to verify that the flow pattern as illustrated by the path lines is the correct flow direction. The current illumination system used to illuminate the flow in the simulation environment is not powerful enough to provide the information necessary for this analysis. This stopped the development of the CFD models as a means of a thorough verification of the results.

5.6 Additional ways to improve the air flow

Different possibilities to improve the airflow are proposed but not tested due to the time constraints on this project. These methods include:

- Optimal fan exit velocity and direction to improve space air diffusion
- The introduction of directional nozzles on air inlet side
- Varying the location of air outlets
- Advance ducting along the ceiling
- Advanced air return bulkhead

Some of these methods are summarised below.

5.6.1 Optimal air direction and velocity

The easiest and most obvious way to optimise the airflow is to have the optimum velocity and direction of the flow to circulate through the trailer. This test will reflect the basic configuration Thermo King currently uses on the SL-series.

Different measures can be taken to direct the airflow in the trailer. As a starting situation one has the current SL-series configuration, which means one inlet and one outlet.

For example one centralised jet can be utilised, or a centralised jet can be aimed at the sides. Flow going along the side can have a positive influence because of the advantages of the Coanda effect. Directing the flow along the sides will most likely result in a reduced risk of short-circuiting the flow. The air at the top of the trailer will re-circulate with the air from the refrigeration unit preventing a hot spot there.

A way to optimise the direction of the flow is the use of nozzles. Nozzles are an efficient way of directing airflow without causing too much turbulence, but further investigation should be done on this topic.

The optimal exit velocity also has to be established in combination with the direction of the flow. The marketing department or regulations usually dictate the volume of the flow, so the velocity is often the result of the outlet area. Too much heat will be generated when the velocity is too high and will reduce the efficiency of the refrigeration unit. A velocity, which is too low, on the other hand will result in poor airflow and temperature distribution.

An extensive series of tests will have to be conducted in loaded and unloaded situations to establish the correct working of the airflow delivery system after an ideal airflow direction and air velocity is established.

5.6.2 Ducting along the ceiling

A commonly seen improvement to trailers is chutes to guide the airflow from the host unit to the greater length of the trailer. These chutes are usually made of a flexible material, and have holes to let air escape as it travels along the length of the trailer. Thermo King does claim that no chutes are needed although most transporters have them nevertheless installed in their trailer. Chutes make the loading of the trailer much less sensitive and important than a load without this air guidance aid.

The general rule for air chute design is to have at least 1548 cm² of cross sectional area to guide the air, going from 3 to 5 m from the back of the trailer. At least 20% of the air is recommended to bleed off the sides to provide airflow around all of the cargo before reaching the end of the chute and the trailer. These guidelines are issued by the NPLA/RTF [90].

5.6.3 Bulkheads

Air return bulkheads are used in refrigerated trailers to guarantee that the air is able to return to the refrigerating unit without too much restriction. The bulkhead provides space between the cargo and front wall. The cargo would otherwise be loaded against the front wall stopping the air from returning to the unit and stopping the air delivery system from working properly.

The problem with the air return bulkhead is the restriction of space as explained in previous chapters. The space available must be used in an efficient way.

Results so far indicate that a bulkhead with a structure as open as possible will be the best solution, where the top of the bulkhead can be open to provide extra air to return. Experiments so far, however, assumed a proper loaded trailer in combination with the current refrigeration layout. Improperly loaded trailers might need a closed top part of the bulkhead because of a risk of a short circuit if the cargo blocks the air stream blown into the trailer. Additional experiments are needed on this specific topic to make sure the right design decisions are made under perfect and imperfect circumstances.

Chapter 6

Conclusions and Recommendations

This chapter summarizes the major findings of this thesis, extracts conclusions and offers recommendations for further work.

6.1 Conclusions

Reflecting the goals of the study, which required the airflow phenomena within a trailer to be identified, a joint measurement and numerical modelling approach was undertaken.

6.1.1 Experimental test facility

Part of this project focussed on the development of an experimental test facility capable of simulating airflow in a refrigerated trailer.

Requirements of the facility capabilities were:

- i. simulating up to a 16 metre long refrigerated trailer
- ii. simulating different types of refrigeration units
- iii. simulating different loading scenarios
- iv. accurately acquire flow information
- v. possible to operate in a laboratory

These requirements lead towards the development of a one to fifth scaled-model of a refrigerated trailer. The reason for scaling down the trailer was that it will make it easier to operate in a defined space to make changes to the system. The facility was erected from a steel frame, where a combination of glass and perspex were used to define the walls of the facility.

Water was utilised as simulation medium to reduce the required velocity of the fluid and to make measurement of the fluid flow feasible. A centrifugal pump circulates

the water through the system and an ultrasonic flow metre is utilised to measure and to control the flow rate.

Foam blocks were acquired to perform simulations in loaded conditions. The blocks were cut into a shape to represent the cargo loaded on a pallet and strapped into the simulation facility.

6.1.2 Measurement system development

The development of the flow measurement system was the single largest contribution made by this project. This application specific system was custom designed and build to suit the project objectives and the test environment. The measurement system fundamentally consists of three sub systems;

- i. the illumination system used to illuminate the flow;
- ii. the acquisition system that acquires the flow data
- iii. the analysis system to analyse the acquired flow data.

Illumination system

The illumination system is a critical sub-system of the measurement system, its function being to illuminate a narrow cross section of fluid contained within the simulation tank. A very powerful light source is focused to accomplish this task, but creating an adequate light source proved problematic, given the available budget.

A metal sheet with a slit was to be used to focus and aim the light into this thin sheet. Multiple possibilities to create a light sheet were examined, including the use of lasers and high intensive lights. Due to the cost the selected system uses a 400W metal-halide light.

The 400W metal-halide light source, however, while it did not provide sufficient light intensity for this application, it was still possible to get some preliminary results. Advance flow analysis was not possible however and an alternative lighting system was accessed and recommended.

Acquisition system

The acquisition system consists of a high speed camera connected to a personal computer. This high speed camera was specially acquired for this project and is capable of capturing images at a frame rate up to 170 frames per second at the reasonable resolution of 640x480 pixels, or 1280x1024 at a lower frequency.

Analysis and visualisation system

A dedicated software suite was created to analyse the images of the illuminated flow captured by the high-speed camera, and graphically represent the computed result.

This software currently produces a good representation of the flow patterns keeping in mind the low illumination intensity that impacts the quality of the captured image. An improved light sheet will significantly improve the results of the program giving the opportunity to enhance the program code as soon as problems are highlighted.

The program can currently analyse one set of these sequential frames or multiple sets in a single capture or multiple sets of recording to investigate the whole tank. The results can be represented in a vector plot where all the vectors are plotted or a structured vector plot where a limited amount of vectors represent the average of a region. First attempts to make a contour plot have been performed but a higher quality of flow data is required and probably a refined particle identification and tracking algorithm.

6.1.3 Airflow measurement and predictions

Airflow within the trailer

All of the trailer airflow analysis was performed using a one-fifth scaled model of an empty refrigerated trailer. The fluid flow in the scaled model was visualised using a high-speed camera and computer software developed during the course of this project. The experimental program investigated;

- i. the qualitative representation of the flow in the scaled model
- ii. the effect of different outlet flow velocities
- iii. the airflow in a loaded trailer

The first experiment aimed for a qualitative representation of the airflow in the trailer and the effect of an airflow deflector on the outlet of the refrigeration unit. Results identify features of the flow previously unidentified

The second experiment was aimed to discover the effect of different outlet flow velocities. Four sub sequential simulation runs are performed at respectively 12.17,

14.4, 17.88 and 19.86 m/s full size trailer speed. The results suggest that the distance the flow carries into the trailer is approximately linear to the flow velocity.

The third and final aspect is the test program examined a loaded configuration. The software was able to detect a portion of the flow giving a general idea of the flow direction, but lacked the ability to plot a detailed flow picture. The reason for this was the inadequacy of the light sheet used for the experiments and the lack of contrast for the software to analyse the results and to compile it in a vector plot. The main part of the flow follows the same profile as the flow in the empty trailer with the only difference that there is no re-circulation at the back. The flow continues to travel to the back however instead of returning to the refrigeration unit in the front or circulating at the back of the trailer. There is fluid movement all around the cargo.

Simulated flow against real flow

The validity of the experiments in a practical and an experimental form, has to be established to be able to have confidence in the results. This confirmation can be achieved in the form of a airflow test performed in a refrigerated trailer equipped with a Thermo King refrigeration unit and compare these results to the results of the simulation environment under the same circumstances. The validating process was limited to a two-dimensional representation of the airflow in an unloaded trailer.

The simulated flow highly agrees with the flow as measured in the life size refrigerated trailer. The biggest differential was found at the lower speeds as the wind vane anemometer used for the measurement was not able to accurately measure velocities below 0.4-0.6 m/s. The average accuracy above the low velocities was about 15%. This is a very good result keeping in mind the inaccuracy of the wind vane anemometer, and the reduced distance the flow stays attached to the ceiling caused by the turbulence of the centrifugal fan.

6.1.4 Project progress

This project, although it contains a wide variety of expertise, ran very well and only the end experienced some degree of delay due to an underestimated requirement for the light sheet to illuminate the water flow in the simulation environment. This turned out to be a vital component of the whole system.

There was nevertheless an excellent progress made in the development of the software to detect the motion in the captured images and the generation of the first results and the work will be a very good potential base for multiple future projects.

The current project might not have produced as much direct results as hoped or expected, a continuation on this work will definitely have the potential to yield some valuable information on the flow in refrigerated trailers.

Last small point to be mentioned is the project itself and the management. It is nowadays important not only to do the research but to stay within a budget as well managing the cash flow and to make sure the overall project management is executed correctly. The whole project management from writing the proposal, making the budget, doing the research and performing the experiments is part of the project and those entire diverse tasks are performed. The project stayed within budget although an unforeseen extra investment in an illumination method is needed in future continuations of this work.

6.2 Recommendations for future work

6.2.1 Illumination system

The illumination system requires a high intensive light source as for example a pulse laser. A suitable laser was selected and inquiries were made, but this laser was too expensive for the budget allocated to this project, and as a result that although the analysis system is created, only a small part of its potential could be exploited.

The recommendation put forward is to acquire more funding to be able to invest in a medium power pulsed diode laser. This will allow the analysis system to be elevated to the next level and much more of its potential can be exploited.

6.2.2 Software

The high-speed camera functions according to expectation, but effort would be required to synchronise the camera to the illumination system for optimal image acquisition in future project. This should, however, not be a problem as the acquisition frequency of the camera can be utilised to control the illumination system.

The software suite has algorithms to clean the captured images. Regions of pixels representing one particle are identified and replaced by one pixel at the centre of the group. The particle-tracing algorithm has to be reviewed with an improved illumination system and can be enhanced according to information published in the various papers to reduce the number of erroneous vectors. A dynamic code might be created to analyse the general motion of the fluid flow and detect on the change of motion of two frames, the flow velocity and the common direction of the flow.

The overall quality of the program is sufficient enough for initial results and to compare with the airflow in a real trailer. Initial results should allow the flow inside the trailer to be identified and first recommendations for flow improvements can be formulated from the initial results. The results of the program will be of much more value however if an intense and uniform light sheet is made available and the program algorithm is enhanced according to the results.

A user-friendly interface should be developed making the operation of the software easier and more straightforward. Currently Matlab and Fortran executables are used in the program where a lot of parameters have to be given in the call of a function or program. This is both time-consuming and susceptible to error.

All the different modules of the program should be integrated in one easy to use interface where only one program will be used reducing the processing time by cutting out the time needed for the transfer of data between Matlab and the Fortran executable.

This program could ultimately include the capture of the flow and the calibration of the images, where results of the flow analysis can be made available for analysis shortly after the flow is captured. This would allow results to be analysed during the experiments and a phase repeated if needed. An easy to use interface to the analysis software will increase the potential of the software where it could open the way for a possible wider acceptance by other Universities, institutes or Research laboratories.

6.2.3 Airflow improvement recommendations

The velocity of the airflow is one of the major and easiest ways of optimising the refrigeration unit's overall efficiency. Too high an air velocity only costs more energy reducing the efficiency of the unit and only has an arguable advantage on

overall airflow distribution. More tests however are needed to determine the effect of different loading practices on the airflow and to determine the minimum velocity required. Another issue is that possible design changes are needed when changing the air velocity because the same quantity of airflow needs to be guaranteed.

Another improvement on the current airflow system in the Thermo King refrigeration units could probably be to add vanes in the outlet breaking up the vortex. The vortex produced by the fan in the real size trailer scatters the flow reducing its ability to stay attached to the ceiling. The simulation tank does not have this flow disturbance. These vanes could be added in the form of a redesign of the damper blade used to close the air inlet for defrosting as seen on the SB, which is sold by Thermo King in the United States and can be found in truck units.

An extended series of tests are needed to determine if the air deflector as currently used has a positive effect on the direction of the airflow in a loaded refrigerated trailer. This deflector was added to improve the airflow circulation in an empty trailer and improve pull-down temperature differential. The first simulations indicate however that this deflector might have a negative effect on overall flow circulation in loaded conditions. Even airflow and temperature distribution, however in a loaded refrigerated trailer is more crucial than the airflow circulation in an empty trailer.

Reference

- 1 C. Weber, A. Larson, TW. Trach, T. Pham, M. Kristoffersen, R. Hyttel, "Advanced Flow Distribution System for a Refrigerated Trailer", Thermo King internal document, May 2000.
- 2 M.L. Hoang, P. Verboven, J. De Baerdemaeker, B.M. Nicolai; Analysis of the air flow in a cold store by means of computational fluid dynamics; 2000; International Journal of Refrigeration nr. 23.
- 3 N. Zertal-Ménia, J. Moureh, D. Flick; Simplified modelling of air flows in refrigerated vehicles; International Journal of Refrigeration 25 (2002).
- 4 J. Moureh, N. Menia, D. Flick; Numerical and experimental study of airflow in a typical refrigerated truck configuration loaded with pallets; 2002; Computers and electronics in agriculture nr. 34
- 5 W.A. Rogers; Simulation of Air Flow and Heat Transfer in a Refrigerated Trailer; April 1999; Thermo King Corporation and Fluent Inc.
- 6 W.A. Rogers; Simulation of Air Flow and Heat Transfer in a Refrigerated Trailer; Addendum; August 1999; Thermo King Corporation and Fluent Inc.
- 7 J.R. Fontain, F. Boilley, R. Rapp, J.C. Sérieys and J..C. Cunin; Analysis of a three-dimensional ventilation flow: experimental validation on a water scale model of numerical simulations; Numerical Heat Transfer; Part A, 26; 1994.
- 8 G.M. Swanson, M.V. Ott; The story of Frederick McKinley Jones; 1994; Runestone press
- 9 Thermo King University, Transport Temperature Control Systems, 2000, Thermo King Corporation .
- 10 H. Opatova, O. Laguerre, E. Derens, K. Demnerova, J. Moureh, B. Commere; Temperature monitoring and modelling of chilled food in the cold chain; 1999; 20th International Congress of Refrigeration, Sydney 1999.

- 11 P.G. Jolly, C.P. Tso, Y.W. Wong, S.M. Ng; Simulation and measurement on the full-load performance of a refrigeration system in a shipping container; 2000; International Journal of Refrigeration, nr 23 2000.
- 12 D. Flick, G. Alvarez, Ch. Doursat, J. Moureh; Flow and transfer modelling during cooling of fruit and vegetables stored in pallets; 1999; 20th International Congress of Refrigeration, Sydney 1999.
- 13 J. Moureh, O. Languerre, D. Flick, B. Commere; Analysis of use of insulating pallet covers for shipping heat-sensitive foodstuff in ambient condition; 2002; Computers and Electronics in Agriculture 34 (2002) 89-109
- 14 J. Moureh, E. Derens; Numerical modelling of the temperature increase in frozen food packaged in pallets in the distribution chain; 2000; International Journal of Refrigeration 23 (2000) 540-552
- 15 R.Lindqvist; Air distribution design for controlled atmosphere in reefer cargo holds; 1999; 20th International Congress of Refrigeration, Sydney, 1999.
- 16 B. Hunt Ashby; Protecting Perishable Foods During Transport by Truck; 2000; Agricultural Marketing Service, Transportation and Marketing Programs, USDA.
- 17 Perishable Logistics Association/ Refrigerated Transportation Foundation
- 18 J.F. Douglas, J.M. Gasiorek, J.A. Swaffield; 3rd Edition Fluid Mechanics; 1995; Longman Singapore Publishers (Pte) Ltd.; Chapter 9
- 19 White F.M., Fluid Mechanics, 1998, Chapter 5, Mc Graw-Hill
- 20 H. Tennekes, J.L. Lumley; A first course in turbulence; 1972; MIT Press Cambridge (MT)
- 21 J.O. Hinze; Turbulence (2nd edition); 1975; McGraw-Hill New York
- 22 E. Hecht; Physics Calculus; 1996; Brooks/Cole Publishing Company; Chapter 11
- 23 J.F. Douglas, J.M. Gasiorek, J.A. Swaffield; 3rd Edition Fluid Mechanics; 1995; Longman Singapore Publishers (Pte) Ltd.; Chapter 9
- 24 Dr. A. Sleight; An Introduction to Fluid Mechanics; 2001; University of Leeds
- 25 C.A. Wassenbauer; The NASA Lewis Research Center Water Tunnel Facility; NASA Contractor Report 4777; July 1997
- 26 Ch. Blohm and H.C. Kuhlmann; The two-sided lid-driven cavity: experiments on stationary and time-dependent flows; 2000; ZARM "Centre of applied space technology and Microgravity", University of Bremen

- 27 Standard for Laboratory airflow Measurement; ASHREA Standard; 1987.
- 28 How to measure turbulence with hot wire anemometers; Dantec Dynamics A/S; February 2002
- 29 Ch. Blohm and H.C. Kuhlmann; The two-sided lid-driven cavity: experiments on stationary and time-dependent flows; 2000; ZARM "Centre of applied space technology and Microgravity", University of Bremen
- 30 B.Nath, W. Löber, W. Baetz, W. Holzapfel; Laser light sheet imaging of gas flow with laser diodes; 1998; 8th International Symposium on Flow Visualisation, Sorrento, Italy, Sept 1-4 1998.
- 31 K. Stacy, K. Severance, B.A. Childers; Computer-Aided Light Sheet Flow Visualisation Using Photogrammetry; July 1994; NASA Technical Paper 3416
- 32 K. Ness, J. Woods, B.A. Fleck; Jet-Wall Interactions: Investigation into the effects of Turbulent water jets within an enclosure; 2000; University of Alberta
- 33 K.-U. Graw, J. Lengrich; Particle Image Velocity (PIV) on coastal engineering; 2002; First German-Chinese Joint Symposium on Coastal and Ocean Engineering, April 10-12, 2002, Rostock, Germany
- 34 H. Meng; Tackling turbulence with holographic particle image velocimetry (HPIV); 1999; American Institute of Aeronautics and Astronautics, AIAA-99-3755
- 35 M.J. Molezzi, J.C. Dutton; Application of Particle Image Velocimetry in High-Speed Separated Flows; 1993; AIAA Journal Vol. 21, No 3, March 1993
- 36 W.T. Lai, D.C. Bjorkquist, M.P. Abbott, A.A. Naqwi; Video systems for PIV recording; 1998; Meass. Sci. Technology 9, (1998) 297-308.
- 37 N. Tani, M. Mori, K. Hishida, M. Maeda; Development of Fiber-Bundle-Image-Guided PIV; Department of System Design Engineering, Kohoku-ku, Yokohama. Japan
- 38 Y. Kawaguchi, T. Segawa, Z. Feng, P. Li; Experimental study on drag-reducing channel flow with surfactant additives - spatial structure of turbulence investigated by PIV system; 2002; International Journal of Heat and Fluid Flow 23 (2002) 700-709

- 39 F.H. Post, T. van Walsum; Fluid flow visualization; 1993; Focus on Scientific Visualization, H. Hagen, H. Müller, G.M. Nielson (eds.), Springer Verlag, Berlin, 1993.
- 40 Ch. Blohm and H.C. Kuhlmann; The two-sided lid-driven cavity: experiments on stationary and time-dependent flows; 2000; ZARM “Centre of applied space technology and Microgravity”, University of Bremen
- 41 T.A. Clarke, R.N. Franklin, M.J. Sullivan, J.A. Stasiek; An Image Processing System for Real-Time 2-D and 3-D Tracking of TLC Particles; Northampton Square, Technical University of Gdansk.
- 42 K. Kerenyi, S. Stein, J. Sterling Jones; Advanced Flow Visualisation Techniques for the Federal Highway Administration Hydraulics Research Laboratory; 2001; ASCE 2001
- 43 C.A. Wassenbauer; The NASA Lewis Research Center Water Tunnel Facility; NASA Contractor Report 4777; July 1997
- 44 W. C. de Leeuw, H.G. Pagendarm, Frits H. Post, B. Walter; Visual Simulation of Experimental Oil-Flow Visualization by Spot Noise Images from Numerical Flow Simulation; 1995; Delft University of Technology Netherlands
- 45 W. Merzkirch; *Flow Visualization (2nd edition)*; 1987; Academic Press
- 46 J.J. van Wijk; “Spot noise – texture synthesis for data visualization”; 1991; T.W. Sederberg, editor. Computer Graphics (SIGGRAPH '91 Proceedings), volume 25, pages 263–272.
- 47 Y. Li; Motion Tracking in Active Vision System; B.S.E.E., 2001, University of Louisville.
- 48 J. Yamato; Tracking moving object by Stereo Vision Head with Vergence for Humanoid Robot; May 1998; Massachusetts Institute of Technology, University of Tokyo.
- 49 S. Wong, S. Vassiliadis, S. Cotofana; A Sum of Absolute Differences Implementation in FPGA Hardware; June 2002; Delft University of Technology.
- 50 Okamoto K, Hassan Y A, Schmidi WD; Algorithm improvement in particle tracking velocimetry; 1995; Exp. Fluids, vol 19, pp342-347
- 51 M.J. Molezzi, J.C. Dutton; Application of Particles Image Velocimetry in High-Speed Separated Flows; 1993; AIAA Journal, Vol. 31, No. 3, March 1993

- 52 K. Stacy, K. Severance, B.A. Childers; Computer-Aided Light Sheet Flow Visualization Using Photo-grammetry; July 1994; NASA
- 53 M. Stellmacher, K. Obermayer; A new particle tracking algorithm based on deterministic annealing and alternative distance measures; 1999; Experiments in fluids
- 54 J. Kompenhans, R. Höcker; Application of Particle Image Velocimetry to High Speed Flows; 1998; Von Kármán Institute Lecture Series 1998-06, Von Kármán Inst. Brussels, March 1988, pp 67-83.
- 55 R. Höcker, J. Kompenhans; Application of Particle Image Velocimetry of Transonic Flows; Proceedings; 1990; Fifth International Symposium on Applications of Laser Techniques to Fluid Mechanics, Springer-Verlag Berlinn, 1990, pp 415-434
- 56 M.E. Post, L.P. Goss, L.F. Brainard; Two-Colour Particle-Imaging Velocimetry in a Turbine Cascade; Jan 1991; AIAA 29th Aerospace Science Meeting, AIAA Paper 91-0274
- 57 M.J. Moluzzi, J.C. Dutton; Application of Particle Image Velocimetry in High-Speed Separated Flows; 1993; AIAA Journal, Vol. 31, No. 3, March 1993
- 58 G.M. Quénot, J. Pakleza, T.A. Kowalewski; Particle image velocimetry with optical flow; Experiments in Fluids 25 (1998)
- 59 W. Weng, G. Liao, W. Fan; An improved cross-correlation method for (digital) particle image velocimetry; State Key Laboratory of Fire Science, University of Science and Technology of China
- 60 Kazuo Ohmi, Hang-Yu Li; Particle tracking velocimetry using a discrete relaxation method; Osaka Sangyo University
- 61 Georges Quénot; Synchronous Orthogonal Dynamic Programming for Particle Image Velocimetry
- 62 Dmitry Chetverikov; Applying Feature Tracking to Particle Image Velocimetry; 2002; Computer and Automation Research Institute, Budapest, Hungary
- 63 S.J. Baek, S.J. Lee; A new 2d particle tracking algorithm using match probability; 1996; Exp. Fluids 22 23-32

- 64 Hyoung-Bum Kim and Sang-Joon Lee; Performance improvement of two-frame particle tracking velocimetry using a hybrid adaptive scheme; 2002; Measurement Science and Technology
- 65 M. Stellmacher, K. Obermayer; A new particle tracking algorithm based on deterministic annealing and alternative distance measures; 1999; Experiments in fluids
- 66 S. Gold, A. Rangarajan, S. Pappu and E. Mjolsness; Learning with pre-knowledge: Clustering with point and graph matching distance measures; 1996; Neural computation, 8:787-804.
- 67 S. Gold, A. Rangarajan, C. Lu, S. Pappu and E. Mjolsness; New algorithms for 2D and 3D point matching: Pose estimation and correspondence; 1998; Pattern recognition, 31(8): 1019-1031.
- 68 S. Gold, E. Mjolsness and A. Rangarajan; Clustering with a domain-specific distance measure; 1994; Advances in Neural Information Processing Systems, 6:96-103.
- 69 S. Gold, C.P. Lu, A. Rangarajan. S. Pappu and E. Mjolsness; New algorithms for 2D and 3D point matching; 1995; Advances in Neural Information Processing Systems, 7:957-964.
- 70 A. Rangarajan, S. Gold and E. Mjolsness; A novel optimising network architecture with applications; 1996, Neural Computation, 8:1041-1060.
- 71 Hui Meng; Tracking Turbulence with Holographic Particle Image Velocimetry (HPIV); 1999; AIAA
- 72 R. Kreпки, Ye Pu, Hui Meng, K. Obermayer; A new algorithm for the interrogation of 3D holographic PTV data based on deterministic annealing and expectation minimization optimisation; 2000; Experiments in Fluids
- 73 W.A. Rogers; Simulation of Air Flow and Heat Transfer in a Refrigerated Trailer; April 1999; Thermo King Corporation and Fluent Inc.
- 74 W.A. Rogers; Simulation of Air Flow and Heat Transfer in a Refrigerated Trailer; Addendum; August 1999; Thermo King Corporation and Fluent Inc.
- 75 Ducts Design; Chapter 32; ASHREA Handbook, Fundamentals 1993
- 76 Space Air Diffusion; Chapter 31; ASHREA Handbook, Fundamentals 1993

- 77 R.R. Lindqvist; Air distribution design for controlled atmosphere in reefer cargo holds; 1999; 20th International Congress of Refrigeration, Sydney, 1999.
- 78 J.R. Fontaine, R. Rapp, H. Koskela, R. Niemelä; A numerical approach to design air diffusers is given in the paper "Evaluation of CFD-modelling methods for air diffusers; 2002; Room vent 2002, Copenhagen, 2002.
- 79 J.F. Douglas, J.M. Gasiorek, J.A. Swaffield, Fluid Mechanics 3rd Edition, Chapter 1995, 23.3, Longman Singapore Publishers
- 80 White F.M., Fluid Mechanics, 1998, Appendix A (p691), Mc Graw-Hill
- 81 J.F. Douglas, J.M. Gasiorek, J.A. Swaffield; 3rd Edition Fluid Mechanics; 1995; Longman Singapore Publishers
- 82 S. Eisenberg, Dr. W. Reckers, B. Wieneke; Visualization and piv measurements of high-speed flows and other phenomena with novel ultra-high-speed ccd camera; 2002; CIMNE, Barcelona, Spain 2002
- 83 Ch. Blohm and H.C. Kuhlmann; The two-sided lid-driven cavity: experiments on stationary and time-dependent flows; 2000; ZARM "Centre of applied space technology and Microgravity", University of Bremen
- 84 S.J. Baek, S.J. Lee; A new 2d particle tracking algorithm using match probability; 1996; Exp. Fluids 22 23-32
- 85 H.G. Pagendarm, H. Sobieczky; Dedicated analysis and visualization technology for large discrete data sets; 1995; 7th International Symposium on Flow Visualization, Seattle, WA, Sept. 11-14, 1995
- 86 FLUENT 5 User's Guide Volume 1, pg. 6-46 – 6-48
- 87 Gambit 1.1 modelling guide, May 1998, Fluent Inc,
- 88 Naïma Zertal-Ménia, Jean Moureh, Denis Flick; Modélisation simplifiée des coulements d'air dans un véhicule frigorifique; 2002; International Journal of Refrigeration 25 (2002) 660-672
- 89 Rogers W.A., Simulation of Air Flow and Heat Transfer in a Refrigerated Trailer; Addendum, 1999, Thermo King Corporation and Fluent Inc.
- 90 Perishable Logistics Association/ Refrigerated Transportation Foundation

Bibliography

- Adrian J.R., Yao C.-S., Pulsed Laser Technique Application to Liquid and Gaseous Flows and the Scattering Power of Seed Materials, 1985, Applied Optics, Vol. 24, No. 1, 1985
- ASHREA Handbook, Fundamentals 1993, Space Air Diffusion, 1993, Chapter 32; ASHREA Handbook, Fundamentals 1993
- ASHREA Handbook, Fundamentals 1993 , Ducts Design, 1993, Chapter 32; ASHREA Handbook, Fundamentals 1993
- ASHREA Standard, Standard for Laboratory air-flow Measurement, 1987, ASHREA Standard 1987
- Astro Flight Inc., Understanding scale speed, , <http://www.astroflight.com/>, Astro Flight Inc.
- Bleier, F.P., Fan Handbook, Selection, Application, and Design, 1997, McGraw-Hill
- Blohm Ch., Kuhlmann H.C., The two-sided lid-driven cavity: experiments on stationary and time-dependent flows, 2000, ZARM "Centre of applied space technology and Microgravity", University of Bremen
- Chen J.-D., Wada N., Visualization of immiscible displacement in a three-dimensional transparent porous medium, 1986, Exp. Fluids 4, 336-338
- Chetverikov D., Applying Feature Tracking to Particle Image Velocimetry, 2002, Computer and Automation Research Institute, Budapest, Hungary
- Dantec Dynamics A/S, How to measure turbulence with hot wire anemometers, 2002, Dantec Dynamics A/S
- Dossat R.J., Horan T.J., Principles of Refrigeration, 2001, Prentice Hall

- Finn D.P., Brennan S.L. , Sensitivity analysis using CFD of air distribution in transport refrigeration containers, 2003, International Congress of Refrigeration 2003, Washington, D.C.
- Flick D., Alvarez G., Doursat CH., Moureh J., Flow and transfer modelling during cooling of fruit and vegetables stored in pallets, 1999, 20th International Congress of Refrigeration, Sydney 1999
- Fontain J.R., Boilley F., Rapp R., Sérieys J.C. and Cunin J.C. , Analysis of a three-dimensional ventilation flow: experimental validation on a water scale model of numerical simulations, 1994, Numerical Heat Transfer; Part A, 26
- Gad-El-Hak M., Fluid Dynamics from the Beginning to the Third Millennium, 1998, Int. J. Engng, Vol. 14, No. 3.
- Graw K.-U., Lengricht J., Particle Image Velocimetry (PIV) in coastal engineering, 2002, First German-Chinese Joint Symposium on Coastal and Ocean Engineering April 10-12, 2002, Rostock, Germany
- Hecht E., Optics, 1984, Sec.ed., Addison-Wesley
- Hoang M.L., Verboven P., Baerdemaeker J. De, Nicolaï B.M., Analysis of the air flow in a cold store by means of computational fluid dynamics, 2000, International Journal of Refrigeration nr. 23.
- Hunt Ashby B. , Protecting Perishable Foods During Transport by Truck, 2000, Agricultural Marketing Service, Transportation and Marketing Programs, USDA
- Jähne B., Digital Image Processing, 2002, Springer
- Jain A.J., Fundamentals of Digital Image Processing, 1989, Prentice-Hall, Inc.
- Jolly P.G., Tso C.P., Wong Y.W., Ng S.M., Simulation and measurement on the full-load performance of a refrigeration system in a shipping container, 2000, International Journal of Refrigeration number 23.
- Kawaguchi Y.,Segawa T., Feng Z., Li P. , Experimental study on drag-reducing channel flow with surfactant additives - spatial structure of turbulence investigated by PIV system, 2002, International Journal of Heat and Fluid Flow 23 (2002) 700-709

- Keane R.D., Adrian J.R., Optimization of Particle Image Velocimeters Part 1 - Double Pulsed Systems, 1990, University of Illinois, Measurement Science and Technology, Vol 1, 1990
- Keane R.D., Adrian J.R., Optimization of Particle Image Velocimeters Part 2 - Multiple Pulsed Systems, 1991, University of Illinois, Measurement Science and Technology, Vol 2, 1991
- Kim H.B., Lee S.J., Performance improvement of two-frame particle tracking velocimetry using a hybrid adaptive scheme, 2002, Measurement Science and Technology, 13 (2002)
- Krepki R., Pu Y., Meng H., Obermayer K., A new algorithm for the interrogation of 3D holographic PTV data based on deterministic annealing and expectation minimization optimization, 2000, Experiments in Fluids [Suppl.] S99-S107
- Lai W.T., Bjorkquist D.C., Abbott M.P., Naqwi A.A., Video systems for PIV recording, 1998, Measurement in Science and Technology, Vol. 9, March 1998
- Li Y. , Motion Tracking in Active Vision System, 2001, University of Louisville, B.S.E.E.
- Lindqvist R., Air distribution design for controlled atmosphere in reefer cargo holds, 1999, 20th International Congress of Refrigeration, Sydney, 1999.
- Meng H., Tackling turbulence with holographic particle image velocimetry (HPIV), , Laser Flow Diagnostics Laboratory, Kansas State University
- Molezzi M.J., Dutton, J.C., Applications of On-Line Particle Image Velocimetry to High Speed Flows, 1993, Florida A&M University and Florida State University, SPIE Vol 2052, 1993
- Molezzi, M.J., Application of Particle Image Velocimetry in High Speed Separated Flows, 1993, Ph.D. Thesis University of Illinois, Urbana-Champaign., 1993
- Moureh J., Derens E., Numerical modelling of the temperature increase in frozen food packaged in pallets in the distribution chain, 2000, International Journal of refrigeration
- Moureh J., Flick D., Wall air-jet characteristics and airflow patterns within a slot ventilated enclosure, 2003, International Journal of Thermal Sciences

- Moureh J., Laguerre O., Flick D., Commere B., Analysis of use of insulating pallets covers for shipping heat-sensitive foodstuffs in ambient conditions, 2002, Computers and electronics in agriculture
- Nixon M., Aguado A., Feature Extration & Image Processing, 2002, Newnes
- Ohmi K., Li H.Y., Particle tracking velocimetry using a discrete relaxation method, 2001, Osaka Sangyo University
- Opatova H., Laguerre O., Derens E., Demnerova K., Moureh J., Commere B., Temperature monitoring and modelling of chilled food in the cold chain, 1999, 20th International Congress of Refrigeration, Sydney 1999
- Post F.H., Walsum T. van, Fluid flow visualization, 1993, Focus on Scientific Visualization, H. Hagen, H. Müller, G.M. Nielson (eds.), Spring Verlag, Berlin, 1993.
- Prenel J.P., Porcar R., G. Diemunsch, 3D flow visualization by means of laser beams sweeps., 1987, Flow visualization IV, Springer, Berlin (1987)
- Prenel J.P., Porcar R., Rhassouli A.El., Three-dimensional flow analysis by means of sequential and volumic laser sheet illumination, 1989, Exp. Fluids 7, 133-137
- Quénot G., Synchronous Orthogonal Dynamic Programming for Particle Image Velocimetry, 2000, 9th International Symposium on Flow Visualisation 2000
- Quénot G.M., Pakleza J., Kowalewski T.A., Particle image velocimetry with optical flow, 1998, Experiments in Fluids 25 (1998)
- Rockwel D., Magness C., Towfighi J., Akin O., Corcoran T., High Image Density Particle Image Velocimetry Using Laser Scanning Techniques, 1993, Experiments in Fluids, 14, 1993
- Rogers W.A., Simulation of Air Flow and Heat Transfer in a Refrigerated Trailer; Addendum, 1999, Thermo King Corporation and Fluent Inc.
- Rogers W.A. , Simulation of Air Flow and Heat Transfer in a Refrigerated Trailer, 1999, Thermo King Corporation and Fluent Inc.
- Ruck B., A New Laser-Optical Method for Visualization and Real-Time Vectorization of Flow Fields, 1995, ASME Conference, Hilton Head, SC, 1995

- Shlien D.J., Inexpensive method of generation of a good quality laser light sheet for flow visualization, 1987, *Exp. Fluids* bf 5, 356-358
- Stellmacher M., Obermayer K. , A new particle tracking algorithm based on deterministic annealing and alternative distance measures, 1999, *Experiments in fluids* 1999
- Swanson G.M. , Ott M.V. , The story of Frederick McKinley Jones, 1994, Runestone Press
- Tao B., Mailkiel E., Katz J., Analysis Tools for Holographic Particle Image Velocimetry, 1999, 3rd International Workshop on Particle Image Velocimetry
- Thermo King University, Transport Temperature Control Systems, 2000, Thermo King Corporation
- Wassenbauer, C.A. , The NASA Lewis Research Center Water Tunnel Facility, 1997, Contractor Report 4777, NASA
- White F.M., *Fluid Mechanics*, 1998, Mc Graw-Hill
- Weng W., Liao G., Fan W., An improved cross-correlation method for (digital) particle image velocimetry, , State Key Laboratory of Fire Science, University of Science and Technology of China
- Westerweel J., *Digital Particle Image Velocimetry - Theory and Application -*, 1993, Delft University Press
- Wong S., Vassiliadis S., Cotofana S., A Sum of Absolute Differences Implementation in FPGA Hardware D, 2002, Delft University of Technology.
- Yamato J., Tracking moving object by Stereo Vision Head with Vergence for Humanoid Robo, 1998, Massachusetts Institute of Technology, University of Tokyo
- Yu H., Liao C.; Liang H.-M., Scale model study of airflow performance in a ceiling slot-ventilated enclosure: Isothermal condition, 2003, *Building and Environment*
- Zertal-Ménia N., Moureh N., Flick D., Simplified modelling of air flows in refrigerated vehicles, 2002, *International Journal of Refrigeration* 25 (2002).

Appendix

Appendix A	Digital appendix	A-1
Appendix B	Overview of the programs written	B-1
Appendix C	Seeding particles	C-1
Appendix D	Pictures of the simulation test rig	D-1

Appendix A Digital appendix

A.1 Drawings

The drawings of the simulation facility are enclosed on a compact disk and stored in the TIFF format with multiple pages. The drawings describing the assembly are:

1. tank-complete.tif
2. tank-frame.tif
3. tank-half.tif
4. trailer_inside_empty.tif
5. unit-assy-01.tif

The drawings describing the parts are:

6. beam-drawing.tif
7. bulkhead.tif
8. cargo_block.tif
9. clamp-strip.tif
10. clampstrip-assy.tif
11. corner-profile.tif
12. dubbel-bottom.tif
13. glass-cover.tif
14. glass-dubble-bottom.tif
15. glass-front-back.tif
16. glass-side.tif
17. glass-top-bottom.tif
18. liner-a2-drawing.tif
19. seperator-assy.tif
20. seperator-mat.tif

21. sheet-drawing.tif
22. tank-outlet.tif
23. top-cover.tif
24. unit-baseplate-drawing.tif
25. unit-baseplate-drw.tif
26. water-collector.tif
27. water-release.tif
28. water-sheet-end.tif
29. water-sheet.tif
30. wt-glash17.tif
31. wt-glash18.tif
32. wt-glash19.tif
33. wt-strips.tif

A.2 Software suit source code

The source code van de software developed during the course of this project can be found on the enclosed compact disk. The computation code is written in Fortran 66, where the overall program management and visualisation code is written Matlab.

The Fortran code is edited with the Compaq Fortran 90 Visual Studio software suite, this explains the fast numbers of files for one program. The Matlab code is created and run using the Mathworks Matlab software.

Fortran 66 code:

1. clean.dep Part of the clean module (to clean and prepare the image)
2. clean.dsp Part of the clean module (to clean and prepare the image)
3. clean.dsw Part of the clean module (to clean and prepare the image)
4. clean.exe The clean module executable (to clean/prepare the image)

5. clean.for	The clean module Fortran base code
6. clean.opt	Part of the clean module (to clean and prepare the image)
7. clean.plg	Part of the clean module (to clean and prepare the image)
8. cleanV12.for	An older version of the clean module
9. structure.exe	Executable of the module to structure and average the data for a vector plot
10. structure.for	Source code of the module to structure and average the data for a vector plot
11. track.dsp	Part of the tracking module, tracking the particles
12. track.dsw	Part of the tracking module, tracking the particles
13. track.exe	The track module executable
14. track.for	The tracking module Fortran source code
15. track.opt	Part of the tracking module, tracking the particles
16. track.plg	Part of the tracking module, tracking the particles

Matlab code:

1. cleanimage.m Part of the clean module, running the clean executable
2. cleanup.m Matlab code to structure and clean the results for a structured vector/contour plot
3. contour_plot.m Matlab module to create the contour plots
4. imageoverlay.m Matlab code to overlay multiple frames to examine the particle movement
5. mginput.m Matlab module to read mouse input on the screen
6. plot_result.m Matlab module to plot the results in a vector plot
7. run_batch.m Matlab module capable of automatic performing multiple analysis of the different movie streams
8. run_batch_corr.m Module same as above but with correcting option to only partly analyse the frames in case of disruption in the image (for example a reflection at the top)
9. run_fortran.m Matlab module to analyse a movie file and prepare the frames for analysis using the clean executable
10. run_track.m Matlab module processing the prepared frames to be analysed using the track executable
11. run_track_corr.m Matlab module as above but capable of partly analysing a frame in case part of the frame is disrupted
12. run_track_overlay.m Matlab module to analyse and overlay subsequently frames using the track executable
13. script.m Script to test the cleanimage and cleanup scripts
14. sum_tank.m Matlab module compiling the resulting data of multiple regions into one full vector plot of the simulation facility
15. sum_tank_corr.m Matlab module as above with corrected algorithm

Result data files (matrix stacks of Matlab containing the results):

1. full tank real 20hz pixels.mat
2. full tank real 25hz pixels.mat
3. full tank real 35hz pixels.mat
4. full tank real 45hz pixels.mat

Working directory files (temporary files needed for computation):

1. data.dat
2. data1.dat
3. data2.dat
4. data3.dat
5. data4.dat
6. result.dat
7. struct.dat

A.3 Captured flow data

The enclosed compact disk contains some movie files made with the high-speed camera during the course of this project and used for the analysis as discussed in his thesis. Only a small amount of the vast number of recordings is included because of the size of the individual files. The files as included can only be reviewed with a movie player capable of reducing the frame rate since the files are captured at a high speed.

The movies included are:

1. pos 1 4000us 99fps 20hz.avi
2. pos 1 4000us 99fps 25hz.avi
3. pos 1 4000us 99fps 35hz.avi
4. pos 1 4000us 99fps 45hz.avi
5. pos 2 4000us 99fps 20hz.avi
6. pos 2 4000us 99fps 25hz.avi
7. pos 2 4000us 99fps 35hz.avi
8. pos 2 4000us 99fps 45hz.avi
9. pos 3 4000us 99fps 20hz.avi
10. pos 3 4000us 99fps 25hz.avi
11. pos 3 4000us 99fps 35hz.avi
12. pos 3 4000us 99fps 45hz.avi
13. pos 4 4000us 99fps 20hz.avi
14. pos 4 4000us 99fps 25hz.avi
15. pos 4 4000us 99fps 35hz.avi
16. pos 4 4000us 99fps 45hz.avi
17. pos 5 4000us 99fps 20hz.avi
18. pos 5 4000us 99fps 25hz.avi
19. pos 5 4000us 99fps 35hz.avi
20. pos 5 4000us 99fps 45hz.avi

Appendix B Overview of the programs written

Track.exe

Track is the main program for the motion detection. It reads the data from three data files data1.dat to data3.dat as the three frames and returns the vectors detected in a file result.dat after processing it. See the program code for a description of the parameters used in this program.

Run_track.m

Run_track is a Matlab program to control the program track.exe. It reads the movie file and writes the needed frames to the data files. The data imported back into Matlab after track has calculated the flow data.

Run_batch.m

Run_batch is a Matlab program that runs "run_track" a few times with different sub sequential frames of the same movie file to get a denser vector field.

Sum_tank.m

Sum_tank basically runs "run_batch" a few times over in which "run_batch" every time takes a new movie for analysis. Run_batch corrects the position of the resulting vectors with the offset in the length direction on which the movie is made and so gets a vector plot of the whole trailer after the program is finished.

Structure.exe

Structure divides the whole trailer up in blocks and calculates the average value of the vectors in a certain block and puts one vector in the middle. This will give a more structured and organised vector plot if the vectors are plotted.

Plot_result.m

Plot result writes all the vectors to a file. The program 'structure' then structures the results and 'plot result' import the results. It then plots the vectors in a vector plot and adds arrows and labels to identify the magnitude of the vector plots.

Contour_plot.m

Contour converts the simplified vectors (result from plot_result) to make a simple contour plot, which identifies velocity with the use of colours. The result of the current programs and the program contour itself is not yet developed to a level to give a good representation of the flow, but is created as an example of the possibilities.

Appendix C Seeding particles

ZARM [91] has carried out a study on the suitability of different seeding particles in a research project for "lid driven cavity flow". The result can be found in Table C-1 below:

<i>material/ powder</i>	<i>producer/ agent</i>	<i>designation</i>	<i>approx. mean density [g/cc]</i>	<i>approx. mean diameter [μm]</i>	<i>shape</i>	<i>comment</i>	<i>valuation</i>
Bronze	Merck	Aluminium flakes	2.70	60	flakes	Flow vis.	satisfactory, high density
TiO ₂	Merck	Iriodin 111	3.1	10	flakes	Flow vis.	satisfactory, too small, high density
TiO ₂	Merck	Iriodin 215	3.2	35	flakes	Flow vis.	satisfactory, high density
Polyetheretherketone PEEK	Vitrex	PEEK 150PF	1.32	80	round	Flow vis.	good, high density
Embossing powder	Heindesian	Sternenstaub, white	1.4	150	round	Flow vis.	satisfactory, too large, high density
Polyamide 12 PA	Dantec	PSP-5	1.03	5	round	LDV	good
Polyamide 12 PA	Dantec	PSP-50	1.03	50	round	Flow vis.	good
Polyamide 12 PA	Crea Nova	Vestosint 1118	1.016	28	round	flow vis., LDV	good
Polyamide 12 PA	Crea Nova	Vestosint 2070	1.016	5	round	LDV	excellent
Polyamide 12 PA	Crea Nova	Vestosint 2157	1.016	57	round	Flow vis.	excellent
Polymethylmethacrylat	Lehmann & Voss	Elvacite 2013	1.15	100	round	Flow vis.	satisfactory, too large

<i>material/ powder</i>	<i>producer/ agent</i>	<i>designation</i>	<i>approx. mean density [g/cc]</i>	<i>approx. mean diameter [μm]</i>	<i>shape</i>	<i>comment</i>	<i>valuation</i>
PMMA							
Polyester	IGP	PES 5009	1.26	55	round	Flow vis.	good
Polyester	Relius	533-0060	1.19	43	round	Flow vis.	excellent density and reflection
Polystyrene	BPM		1.06	100	nearly round	flow vis.	good reflection, satisfactory shape
Polyimide	H.P. Polymer	P84	1.4	60	round	flow vis.	good, yellow powder
Polybenzimidazole PBI	Hoechst- Celanese	Celazole	1.3	90	round	flow vis.	excellent
Hollow spheres, grey	Omya	Fillite SG	0.7	100	spherical	flow vis.	satisfactory, too light, too large, good reflection
Hollow spheres	Potters	Spherical 110P8	1.1	8	spherical	LDV	Good
Hollow spheres, silver coated	Potters	SH400S33	1.4	11	spherical	LDV, flow vis.	excellent, although high density
ELC - temperature sensitive liquid crystals	Japan Capsular Products	RM3032, RW3035, RX3040	1.0	25	round	flow vis., LDV	better for thermal applications
TLC - temperature sensitive liquid crystals	Hallcrest	BM/R35C5W/ S-40	1.02	20	round	flow vis., LDV	better for thermal applications , silicone oil may destroy LC

Table C-1: Properties of various seeding materials

Appendix D Pictures of the simulation test rig

This appendix contains a collection of pictures of the test rig in two locations. The first location is at the facility of Thermo King Europe in Galway, the second location is the engineering workshop in the Galway Mayo Institute of technology, where the project was continued.

D.1 Location Thermo King Europe



Figure D-1: Tank with initial laser test set-up

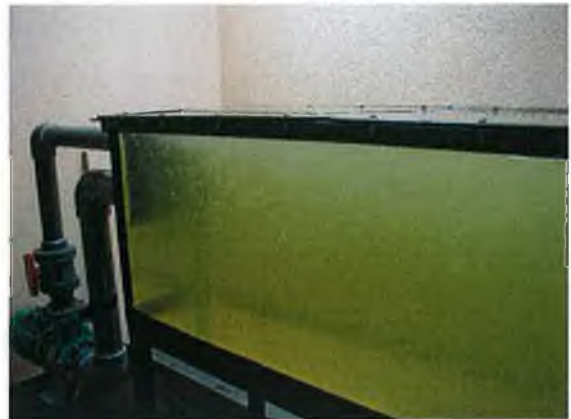


Figure D-2: initial test run with air circulation

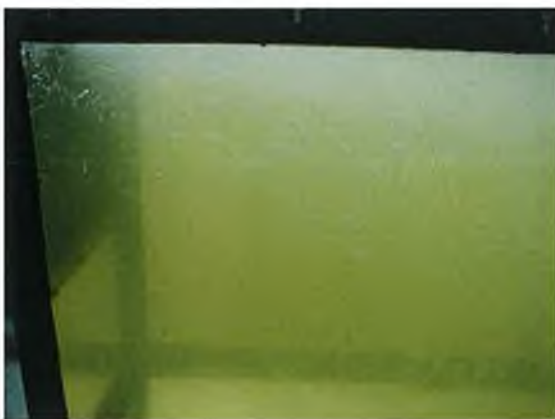


Figure D-3: Air bubbles circulating through the tank in initial test runs



Figure D-4: The attachment of the pump to the tank and the speed drive



Figure D-5: Simulation tank after the build is completed

D.2 Location Galway Mayo Institute of Technology



Figure D-6: The simulation tank set-up



Figure D-7: A side view of the tank



Figure D-8: The height-speed camera



Figure D-9: The water pump assembly



Figure D-10: The controller for the laser as used in the project following up

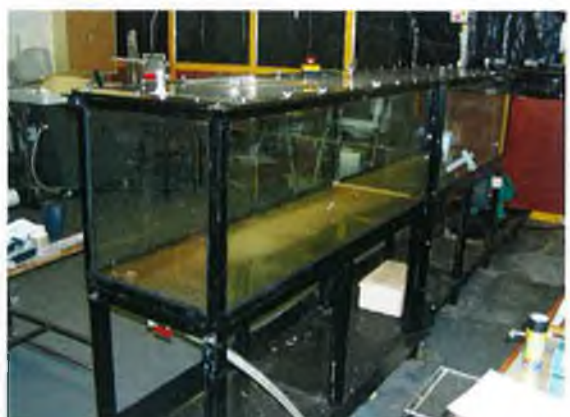


Figure D-11: The back of the water tank



Figure D-12: The inside of the water tank



Figure D-13: Close-up of the bulkhead assembly



Figure D-14: The laser as used in the follow-up project

91 Ch. Blohm and H.C. Kuhlmann; The two-sided lid-driven cavity: experiments on stationary and time-dependent flows; 2000; ZARM "Centre of applied space technology and Microgravity", University of Bremen